Contract NAS9-14294
DRL No. T-974
Line Item No. 4
DRD No. MA-183T
Beckman No. FR-2679-102

NASA CR-
144508

FINAL REPORT

CARBON DIOXIDE SENSOR

September 1975

Prepared for:

National Aeronautics and Space Administration
Lyndon B. Johnson Space Center
Advanced Systems Procurement Section
Houston, Texas 77058

Beckman® INSTRUMENTS, INC.
ADVANCED TECHNOLOGY OPERATIONS
ANAHEIM, CALIFORNIA 92806

ABSTRACT

Analytical techniques for measuring CO_2 were evaluated and rated for use with the Advanced Extravehicular Mobility Unit. An infrared absorption concept using a dual-wavelength monochromator was selected for investigation.

A breadboard carbon dioxide sensor (CDS) was assembled and tested. The CDS performance showed the capability of measuring CO_2 over the range of 0 to 4.0 kPa (0 to 30 mmHg) P_{CO_2}.

The volume and weight of a flight configured CDS should be acceptable. It is recommended that development continue to complete the design of a flight prototype.

CONTENTS

PARAGRAPH		PAGE
ABSTRACT		iii
SUMMARY		vii
TEST RESULTS		ix
CONCLUSIONS		xi
RECOMMENDATIONS		xiii
1.0	INTRODUCTION	1
2.0	CONCEPT STUDY PHASE	3
2.1	Purpose and Scope of Task	3
2.2	Results Obtained	3
2.2.1	Evaluation of the Concepts	3
2.2.2	System Comparison and Ranking	7
2.2.3	Recommended Optimum Concept	8
3.0	DESIGN PHASE	11
3.1	Purpose and Scope of Task	11
3.2	Overall Results Obtained	11
3.3	System Description	12
3.3.1	Functional Description	12
3.3.2	Dynamic Range, Minimum Resolvable Signal, Noise Equivalent Power	16
3.3.3	System Error Analysis	18
3.4	Electronic Design	19
3.4.1	Preamplifier	19
3.4.2	Post Amplifier	23
3.4.3	Demodulator/Filter	25
3.4.4	Difference Circuitry	25
3.4.5	Source Driver	27
3.4.6	Electronics Summary	30
3.5	Optical Design	31
3.5.1	Advantages of Monochromators over Filter System	31
3.5.2	Monochromator Design for the CDS	31
3.5.3	Optical Design for Sampling Volume, Source Optics, and Source	35
3.5.4	Optical Design for Detectors and Detector Optics	37
3.5.5	Spectral Energy Transfer	41
3.5.6	Source	42
3.5.6.1	Candidate Sources	42
3.5.6.2	Source Testing for Concept Study	45
3.5.6.3	Source Selection	48
3.5.6.4	Source Development Problems and Solutions	50
3.5.7	Detector	53
3.5.7.1	Detector Selection	53
3.6	Mechanical Design	57
3.6.1	Optical Mounting	58
3.6.2	Housing Design	58
3.6.3	Sample Flow	59

CONTENTS (Continued)

PARAGRAPH		PAGE
3.6.4	Structural Analysis	59
3.6.5	Non-Metallic Materials	60
3.6.6	Size and Weight	61
3.7	Quality Assurance	63
3.8	Reliability and Safety	63
4.0	FABRICATION PHASE	65
4.1	Purpose and Scope of Task	65
4.2	Results Obtained	65
5.0	TEST PHASE	67
5.1	Purpose and Scope	67
5.2	Description of Test Specimen	67
5.3	Test Philosophy	67
5.4	General Test Requirements and Methods	68
5.4.1	Environment	68
5.4.2	Adjustments and Repair	68
5.4.3	Measurement and Test Equipment	71
5.5	Testing	71
5.5.1	List of Tests	71
5.5.2	Procedures	71
5.5.2.1	Range	71
5.5.2.2	Accuracy	71
5.5.2.3	Response	78
5.5.2.4	Specificity	78
5.5.2.5	Switch Setting	80
5.5.2.6	Power	85
5.5.2.7	Voltage	85
5.5.2.8	Operating Ambient	87
5.6	Discussion of Test Results	89
5.6.1	Accuracy Test	89
5.6.2	Specificity	91
5.6.3	Operating Ambient Temperature	92
5.6.4	Pressure	92
6.0	HARDWARE AND DOCUMENTATION DELIVERY	95
6.1	Purpose and Scope of Task	95
6.2	Results	95

Appendix A - Test Data
Appendix B - Design Notes
Appendix C - Detector Performance Data Sheets

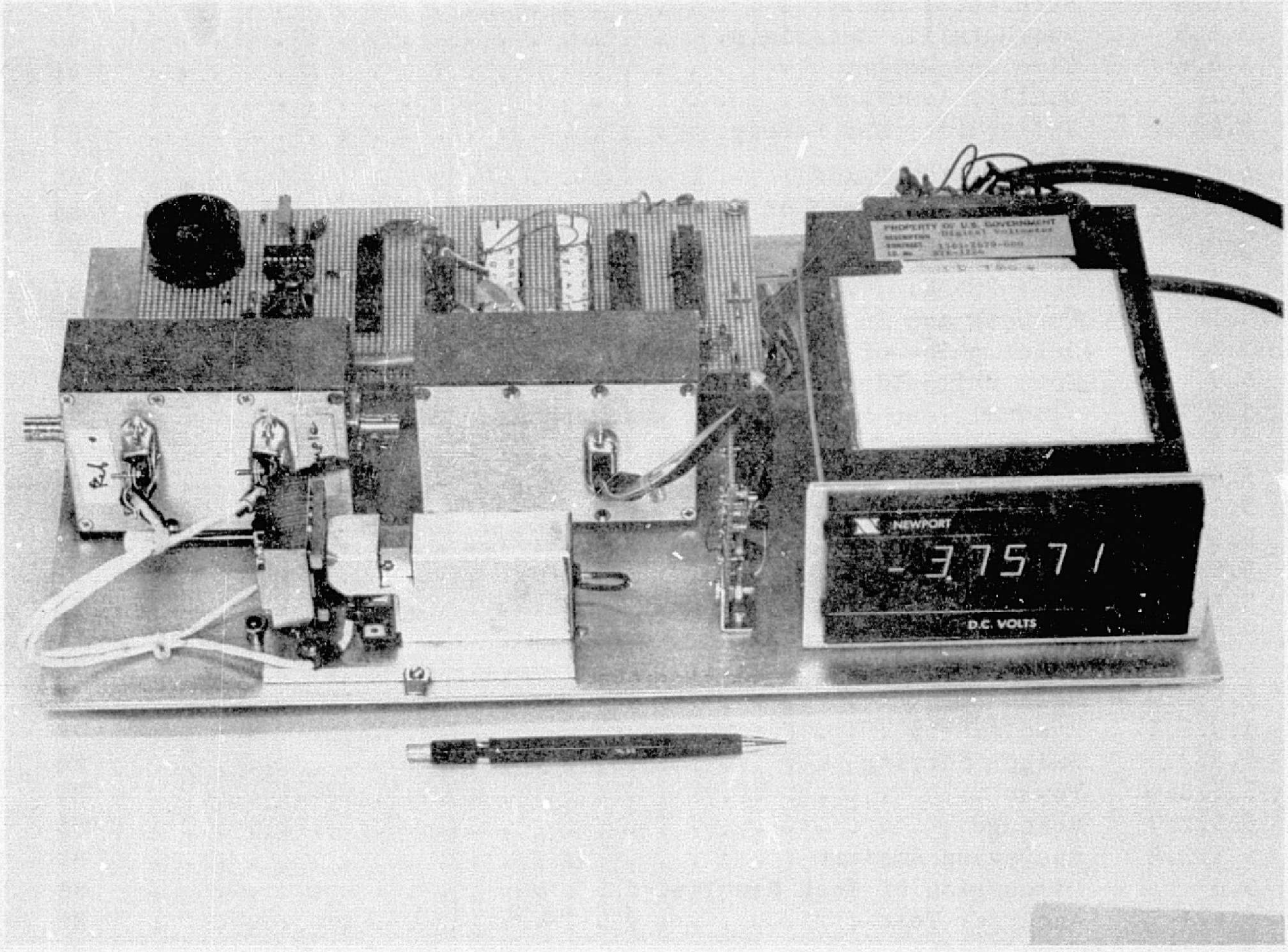

Breadboard Carbon Dioxide Sensor

SUMMARY

The program objective was the design, development, and testing of a Carbon Dioxide Sensor (CDS) for use in the Advanced EMU (Extravehicular Mobility Unit).

The scope of the CDS Program was limited to the development of a selected measurement principle and the fabrication and testing of a breadboard adequate to demonstrate the principle. The CDS breadboard was delivered to NASA at the end of the program.

The CDS Program consisted of three major phases:

- Concept Study Phase
- Design and Fabrication Phase
- Testing Phase

Concept Study Phase

The objectives of the Concept Study Phase were:

1. An investigation into all possible CO_2 measurement techniques.
2. A detailed evaluation of the best concepts that would satisfy the requirements and program technical objectives.
3. A ranking of these concepts based on imposed criteria.
4. A recommendation of the optimum concept to be designed, tested, and delivered to NASA.

Based on an extensive review of CO_2 analytical techniques, it was concluded that infrared absorption using a dual-wavelength monochromator was the most promising technique.

Design and Fabrication Phase

In this phase the main emphasis was on demonstrating that the monochromator could be made small enough to properly interface with the spacesuit. Certain

critical circuits of the signal processing electronics were designed for flight use. Other circuit needs were met with laboratory equipment or existing vendor hardware. The resulting hardware was largely breadboard in arrangement but suitable for testing against the main performance requirements.

Test Phase Results

Our test results show that all performance requirements necessary to demonstrate CO_2 measurement feasibility were met.

Our investigation showed that the selected approach is capable of development to flight hardware. The ultimate weight of the Sensor is estimated to be 85 grams. The design goal for weight cannot be met. No difficulty should be encountered in deploying the sensing element in the spacesuit without interference with the wearer. Inherent with infrared measurements of CO_2, both temperature and pressure compensation are required. This can be accomplished for the normal operating range.

It is expected that the useful life goal of 15 years can be met.

Recommendation

Based on the test results of the breadboard and our analysis of flight hardware requirements, Beckman recommends that development work be continued to provide flight-qualified hardware.

TEST RESULTS

PRIMARY PERFORMANCE REQUIREMENTS*	DEMONSTRATED PERFORMANCE
RANGE	
"The CDS shall be capable of measuring Carbon Dioxide partial pressure between 0.20 and 4.0 kPa (1.5 and 30 mmHg)."	• The CDS can measure CO_2 over the range of 0.20 to 4.0 kPa (1.5 to 30 mmHg) partial pressure. (Para. 5.5.2.1.)
ACCURACY	
"Accuracy shall be ±5 percent of full scale or better at normal operating conditions."	• Over the range of 0 to 30 mmHg P_{CO_2}, the accuracy is within ±5% for normal operating conditions. At 1.3 kPa P_{CO_2} (10 mmHg) o. less, the accuracy is within ±1% of full scale. (Para. 5.5.2.2.)
RESPONSE	
"Time for a 63 percent response to a step change in CO_2 partial pressure from 0.33 to 3.3 kPa (2.5 to 25 mmHg) shall not exceed one minute at normal operating conditions."	• Response time is practically instantaneous and depends on the rate at which the gas concentration changes in the sample path. A response of less than two seconds was measured for the breadboard unit. (Para. 5.5.2.3.)
SPECIFICITY	
"The CDS shall be specific for CO_2 with no more than 0.5 percent change in either zero or span occurring due to exposure to oxygen, nitrogen, or water vapor at any concentration, or any combination. The zero or span shall not change more than 0.5 percent as a result of exposure to trace contaminants normally found in a closed ecological system."	• Variations in oxygen and/or nitrogen concentration had no measurable effect on the sensor response. Water vapor (100% relative humidity) changed the output less than 0.5%. (Para. 5.5.2.4.)

*As defined in Statement of Work

PRIMARY PERFORMANCE REQUIREMENTS	DEMONSTRATED PERFORMANCE
SIZE	
"The CDS shall be designed for minimum volume. The sensing element shall be a size capable of being mounted in the oral nasal area of a spacesuit. Design objective shall be twenty cubic centimeters volume or less for combined sensing element and electronics. The remote electronics, if applicable, shall be less than forty cubic centimeters."	• The sensing element has a volume of approximately 89.9 cm^3 (5.5 $in.^3$) with an envelope of 87 x 40 x 25 mm (3.4 x 1.6 x 1 in.). (Para. 3.8.6.)
WEIGHT	
"Design objective for sensing element weight shall be thirty-two grams or less."	• The weight of the breadboard sensing element is 120 grams. (Para. 3.8.6.)
SWITCH SETTING	
"The switch shall close when the average inspired carbon dioxide level reaches 1.33 ±.57 kPa (10.0 ±2.0 mmHg) as indicated by the telemetry output."	• The coefficient of variation of the measurement at 1.33 kPa (10 mm) is only 2% (.2 mm). The signal-to-noise ratio at the alarm point is 20 to 1, providing a capability to alarm well within the ±2 mmHg allowable range. (Para. 5.5.2.5.)
POWER	
"Power consumption of the CDS shall be less than three watts."	• Power consumption for the breadboard totals 2.5 W, exclusive of the commercial ratio meter. The power consumption for the electronics for the preamplifier to the difference circuitry is less than 50 mW. (Para. 5.5.2.6.)
OPERATING AMBIENT	
"Pressure : 21 to 128 kPa (3.1 psia to 18.5 psia)."	• The CDS can operate over the pressure range of 21 to 128 kPa (3.1 to 18.5 psia).
"Temperature: 4.4° to 43°C (40° to 110°F)."	• Over the temperature range of 4.4° to 43°C there is minor variation in the CDS output. Further testing of this parameter should be conducted with a flight configured system. (Para. 5.5.2.8.)

CONCLUSIONS

The conclusions presented here are addressed to each requirement of the end item (CDS) specification. They are presented in two groups. The first are those based on test results and observations made with the breadboard system. The second group are extrapolations from the test data as to the capability of this measurement principle to meet the flight hardware specification.

- The dual-wavelength monochromator measuring concept selected by NASA for our investigation is capable of development to flight hardware.
- The sensing element can be mounted in the oral nasal area of the spacesuit.
- The CDS can make measurements over the desired range of 0.20 to 4.0 kPa (1.5 to 30 mmHg) P_{CO_2}.
- An accuracy of readout of better than ±5% of full scale was achieved for the normal operating pressure range.
- No special sampling means are needed. Adequate sampling can be achieved by forced convective and diffusion transport.
- The inherent speed of response of the CDS is too rapid and must be slowed down to preclude false alarms. This can easily be accomplished mechanically.
- The CDS is sufficiently specific to CO_2 to prevent erroneous read-out from interference by any gases or trace contaminants likely to be present in normal use.
- The weight objective of 32 grams for the sensing element cannot be met. A flight unit is expected to weigh about 85 grams.
- The CDS can operate to provide a continuous output and control an alarm switch within the desired range of 1.33 ±.27 kPa (10.0 ±2.0 mmHg) P_{CO_2}.
- The CDS can be operated from a battery pack. Voltage regulation is needed but tolerances are loose compared to the state of the art.
- A flight prototype CDS is needed for verification of performance under all operating ambient conditions.

- The major item for improvement to achieve maximum performance is the source.

Extrapolations to Flight Hardware

- Using high reliability electronic components, there appears to be nothing to preclude achieving a useful life of 15 years for the CDS.
- There are no hazards associated with the operation of the CDS.
- The CDS can be designed to consume approximately 3 watts of power.
- The CDS can be configured to prevent interference of the output by water vapor or foreign matter.
- The CDS is inherently rugged. It should be easy to package it to meet the non-operating and storage ambient conditions.

RECOMMENDATIONS

The performance of the breadboard verifies the suitability of the monochromator principle for a CDS. The performance can be improved with a flight prototype. The continued development of the dual-wavelength monochromator for use with the Advanced EMU is recommended.

This development program would accomplish the following specific objectives:

1. Develop and/or obtain a source with an emissivity approaching 0.8 for use with the monochromator.
2. Refine the optical design based on the source obtained to minimize the volume and weight of the sensing element.
3. Study the mounting interface requirements and design, and provide a means of mounting the sensing element and backpack electronics.
4. Finalize the electronic design: (a) to provide the output required for readout, (b) for operation of a TBD switch at the alarm point, and (c) for conditioning signals for the telemetry bus (if required).
5. Provide temperature and pressure compensation for the CDS.
6. Study the trade-offs for packaging the electronics--viz., discrete components versus integrated circuits--and select the most practical approach to provide the packaging density needed to stay within the allowable backpack volume.
7. Advance the design of the detector to integrate the amplifier with the detector chip, resulting in reduced volume and enhanced performance.
8. Perform development tests as required to support the design effort.
9. Perform qualification tests on the completed CDS flight prototype to verify the design.

1.0 INTRODUCTION

It is desirable to have a Carbon Dioxide Sensor (CDS) for the Advanced Extravehicular Mobility Unit (EMU) with a useful life of 100 mission cycles over a period of 15 years. Presently available sensors have a useful life of only approximately one year. This program was undertaken to evaluate all known analytical techniques for measuring carbon dioxide and to select and verify an optimum concept for support of the long-term EMU Program. The scope of the CDS Program was limited to the development of the selected measurement principle and the fabrication and testing of a breadboard system adequate to demonstrate the principle.

The CDS Program was conducted in three parts. First was a concept study. A comprehensive trade-off analysis was made and recommendations were submitted to NASA for the selection of a specific technique to be investigated. Second, a design was evolved in which special emphasis was placed on demonstrating that the sensing element could be sized to fit into a spacesuit. In the electronics, design attention was directed primarily to circuit performance, with assemblies arranged for the convenience of circuit testing and debugging rather than being sized for minimum volume. Third, the assembled hardware was tested to determine compliance with the specifications and to identify any problem areas.

This report summarizes the work done in each part of the program in accordance with the tasks delineated in the Statement of Work, and presents our conclusions and recommendations.

2.0 CONCEPT STUDY PHASE (SOW Paragraph 3.2.1)

2.1 Purpose and Scope of Task

The impetus for the current CDS Program was the need for an improved carbon dioxide sensor that would meet the requirements of the Advanced Extravehicular Mobility Unit. The Portable Life Support System (PLSS) CO_2 Sensor for the lunar missions used an electrochemical technique that inherently has a relatively short storage life and long response time, and thus falls short of certain CDS requirements. Consequently, the concept study phase emphasized an investigation of all other potential techniques rather than concentration on further refinements of the electrochemical sensor. The electrochemical sensor was, however, included among those techniques studied and evaluated in detail since it does have a history of successful performance on the Apollo program.

The best concepts that would satisfy the requirements and program technical objectives were ranked based on criteria from the contract Statement of Work. An optimum concept was recommended for development and delivery to NASA.

2.2 Results Obtained

2.2.1 Evaluation of the Concepts

As shown in Figure 2-1, Beckman first performed a literature search of nearly 500 references that described potential CO_2 measurement techniques. Sixteen techniques were selected for further investigation and ranking against the selection criteria.

Beckman presented the results of this investigation on July 24, 1974, at NASA-JSC. At that time, four techniques/sensors were selected by NASA-JSC for further in-depth studies:

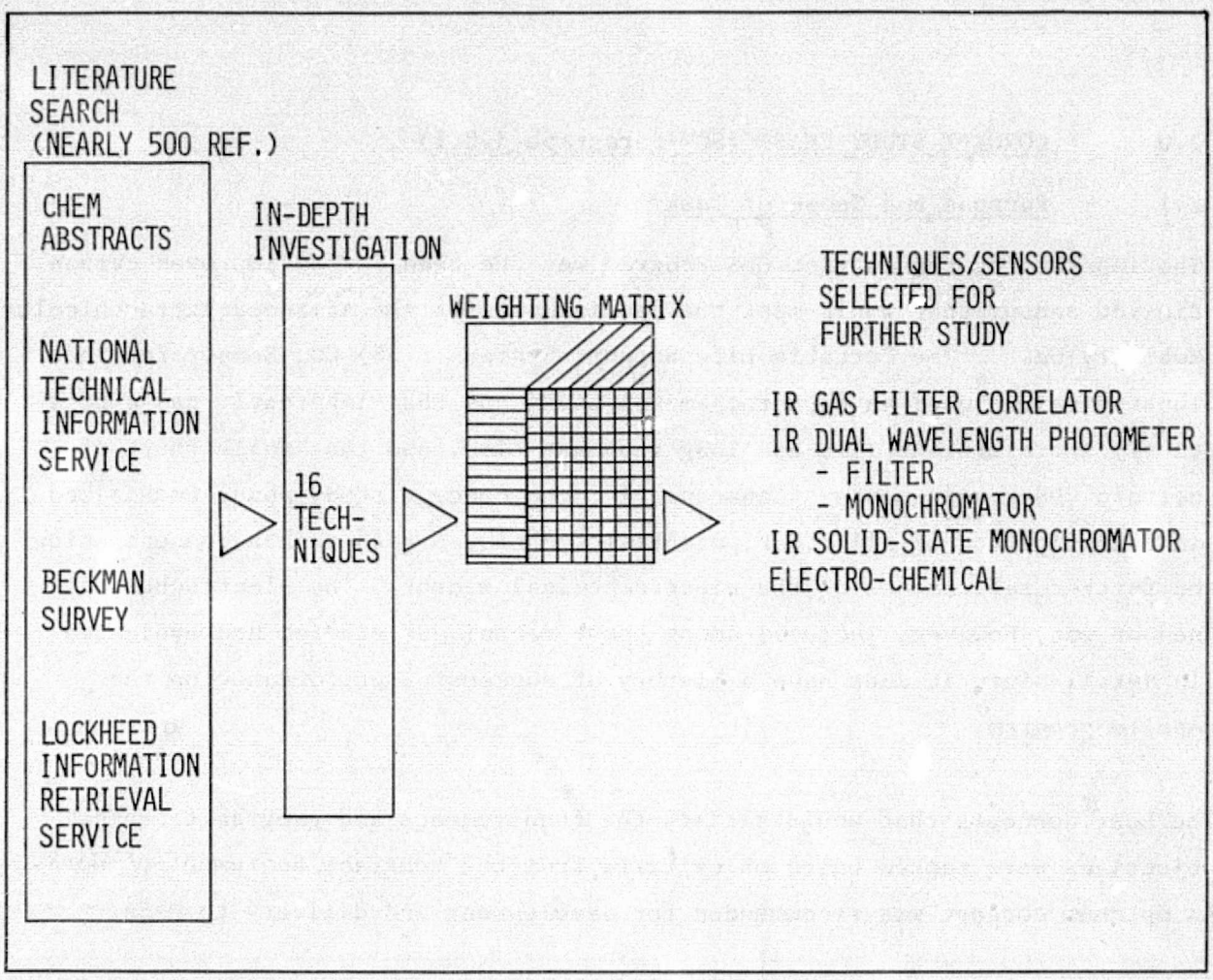

Figure 2-1. Literature Search

1. Gas Filter Correlator
2. Dual-Wavelength Photometer (Filter)
3. Solid-State Monochromator
4. Electrochemical Sensor

Beckman investigated these four techniques in detail, plus a variation of the Dual-Wavelength Photometer that uses a monochromator instead of filters. The investigation included a study of manufacturer's data, component and system level analyses, testing, and evaluation and ranking of the concepts based on the following requirements, as defined in the SOW:

a. Performance (compliance with all the requirements of the SOW)

- Measurement Range: 0.20 to 4.0 kPa P_{CO_2} (1.5 to 30 mmHg).
- Accuracy: ±5% of full scale or better at normal operating conditions.
- Response: <1 minute.
- Specificity: <0.5% change due to oxygen, nitrogen, water, and trace contaminants.
- Power: <3 W.
- Size: <20 cm^3.
- Weight: <32 grams.

b. Reliability

c. Maintenance and Servicing

d. Expected Life

e. Size (volume and envelope)

f. Weight

g. Cost

h. Development Risk

i. Development Lead Time

j. Impact to EMU

It is significant that each of the candidate techniques measures CO_2 by the absorption of IR energy in the 4.25 μm spectral band. Thus, a fundamental first consideration was determining the specific absorption characteristics of each technique and the effect on system parameters. This led to a definition of system constraints for each technique.

Further, since each technique requires an IR source and an IR detector, it was then possible to establish source and detector requirements for each technique based on the specific absorption characteristics. All potential sources and detectors were evaluated against these requirements to establish candidates for later evaluation as system components. The sources and detectors were ranked on the basis of breadboard tests and manufacturer's data. The different possible measurement techniques were then analyzed, such as dc and ac systems, and the consequent effect upon system components was evaluated. A preferred system and preferred components were established.

The four IR concepts were then evaluated using the preferred measurement techniques and using preferred components. The pros and cons for each concept were established.

The evaluation then extended to the ranking of the four IR concepts and the electrochemical concept, and concluded with a recommended concept to be designed, fabricated, and tested in the subsequent program phases. The overall evaluation sequence is shown in Figure 2-2.

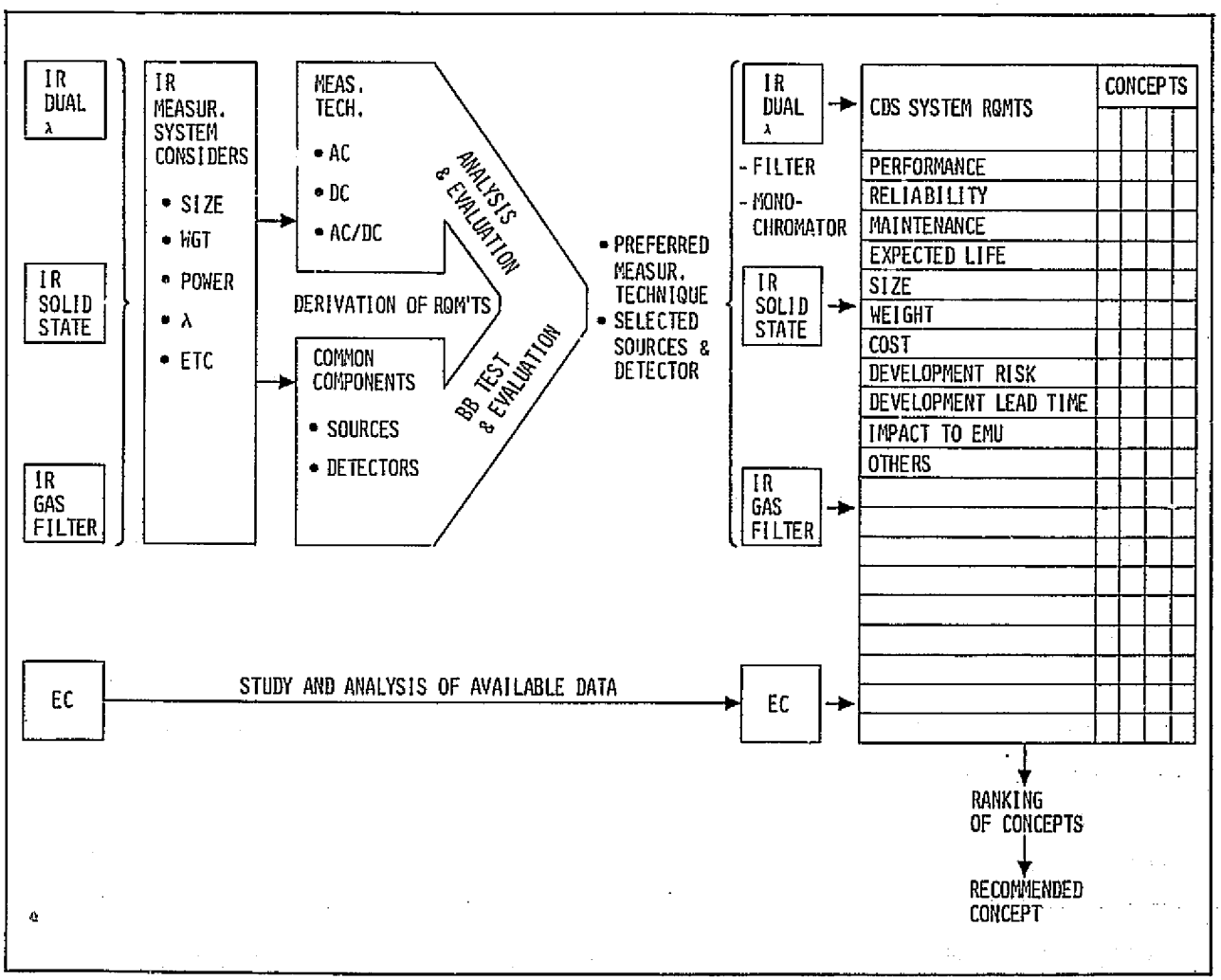

Figure 2-2. Concept Evaluation Sequence

2.2.2 System Comparison and Ranking

The five concepts evaluated were compared with each other using criteria and weighting factors established by NASA-JSC. These comparison criteria and weighting factors are shown in Table 2-1.

TABLE 2-1. COMPARISON CRITERIA AND WEIGHTING FACTORS

Criteria	Weighting*	Maximum Rating
Low Power Requirements	1	10
Low Mechanical Complexity	2	20
Low Electronics Complexity	2	20
High Reliability	3	30
Low Maintenance	2	20
Long Life Expectancy	2	20
Small Volume and Envelope	1	10
Light Weight	2	20
Low Cost	1	10
Low Development Risk	3	30
Short Development Lead Time	1	10
Minimal Impact on PLSS	1	10
Specificity to CO_2	3	30
Susceptibility to Contaminants	3	30
		270

*From NASA-JSC

A panel of three engineers independently scored each system. Differences were then reconciled to arrive at a consensus. A summary of comparison scores is shown in Table 2-2. Based on the supplied comparison criteria and weighting factors, the five concepts received the following scores:

Electrochemical Sensor	217 points
IR Dual-Wavelength Photometer (Monochromator)	209 points
IR Dual-Wavelength Photometer (Filters)	201 points
IR Gas Filter Correlator	171 points
IR Solid-State Monochromator	170 points

TABLE 2-2. SUMMARY OF COMPARISON SCORES

Criteria List*	Weighting Factor	Electrochemical--pH	IR Gas Filtering	IR SS Monochromator	IR Dual Wavelength Photometer (Filter)	IR Dual Wavelength Photometer (Monochromator)
Low Power Requirements	1	9	7	8	7	7
Low Mechanical Complexity	2	18	12	10	14	16
Low Electronic Complexity	2	16	10	8	14	14
High Reliability	3	18	15	20	24	24
Low Maintenance	2	10	12	14	18	18
Long Life Expectancy	2	14	18	18	18	18
Small Size Volume and Envelope	1	9	8	7	8	7
Light Weight	2	18	16	12	16	14
Low Cost	1	8	6	4	6	6
Low Development Risk	3	22	22	16	24	27
Short Development Lead Time	1	9	6	5	7	9
Minimal Impact on EMU	1	9	7	6	7	7
Specificity to CO_2	3	30	22	22	18	22
Susceptibility to Contaminants	3	27	20	20	20	20
		217	171	170	201	209

*Criteria List and Weighting Factors Supplied by NASA

There are certain important aspects in the evaluation of the concepts, however, that do not appear in the comparison criteria and that will be discussed in the next subsection.

2.2.3 Recommended Optimum Concept

From the relative rankings of the five approaches studied, based solely on the raw scores, it might be concluded that the Electrochemical Sensor was the logical choice for further development. However, there is a factor implicitly included in the rankings that affected some of the relative ratings in favor of the Electrochemical Sensor. This factor is the *seeming* ability of the Electrochemical Sensor to meet all CDS requirements contained in the contract

Statement of Work. The lack of pressure dependence, for example, makes it possible for the Electrochemical Sensor to easily meet the specified accuracy over the entire pressure range of 21 to 128 kPa (3.1 to 18 psia). No IR sensor can do this without very precise pressure compensation, or for a relatively limited pressure range without pressure compensation. The inclusion of pressure compensation in the IR sensors automatically reduces their reliability. From a practical standpoint, however, *the better IR approaches should provide a more reliable alarm point under normal CDS operating conditions (without pressure compensation) than has been obtained to date with the existing (proven) electrochemical design.* Furthermore, the limited useful life of the electrochemical sensor causes a significant maintenance problem for a long-term application. Consequently, the slightly better ranking of the electrochemical approach based on the raw scores must be adjusted to reflect the impact of additional significant factors.

The Gas Filter Correlation approach was downgraded because of a predicted relatively large filter thermal coefficient, and because the correlation filter sealing is critical. Filters were downgraded compared to a conventional monochromator because they lack ease of modification based upon experimental results. The solid-state monochromator is perhaps the most interesting because of its novelty. However, it has a higher development risk and theoretical rather than proven reliability.

With such factors being considered to modify the ranking based on the raw scores, it was concluded that the final ranking, in order of preference, should be:

1. Dual-Wavelength Photometer using a Monochromator
2. Electrochemical Sensor
3. Solid-State Monochromator
4. Dual-Wavelength Photometer using Two Filters
5. Gas Correlation Filter

3.0 DESIGN PHASE (SOW Paragraph 3.2.2)

3.1 Purpose and Scope of Task

The design effort was limited to providing hardware that would be adequate to demonstrate the selected measurement principle. A major concern was to show that the sensing element, if development continued to flight hardware, could be reduced in size to fit within or near the spacesuit helmet. Electronics packaging was of little concern in view of the available techniques for minimizing volume requirements. The primary effort in this area was directed at maximum control of electronic error contribution, control of noise, and high reliability. As the actual suit/helmet interface requirements were not established at the time of the design phase, only a limited amount of effort was spent in considering possible locations and mounting means for the sensing element.

Consideration was given to the choice of non-metallic materials and a list of those used was submitted to NASA. This was presented at the time the design was reviewed, which concluded the design phase. At that time the methods and processes to be used in fabricating the breadboard CDS were also described.

As the scope of the overall effort was limited to designing hardware "adequate to demonstrate the selected measurement principle," it should be noted that further development effort is required in all areas to fully optimize the performance of the CDS.

3.2 Overall Results Obtained

A major success was achieved in the design of the Dual-Wavelength Monochromator, which closely approaches in size and performance a flight type unit. It is readily apparent that this sensing element can be developed to flight hardware and can meet the suit/helmet interface requirements. Another significant point was proven with the inclusion of a dual detector within the monochromator

housing. The detector assembly, provided by Molectron, Inc., was a prerequisite to obtaining the small sensor volume. The preamplifier used with the detectors has discrete components, and a further size reduction is possible when the functional chips are integrated with the detector. How the monochromator, which is the key element of the CDS, is related to the rest of the system is shown in the functional block diagram, Figure 3-1.

3.3 System Description

3.3.1 Functional Description

The basic components of the system (Figure 3-1) are the source of infrared energy, the monochromator, the detectors, and the associated electronics. The details and features of these components are covered in the following subsections on electronic, optical, and mechanical design. The overall function of the system is based on the absorption of infrared energy at 4.25 μm by CO_2. The infrared energy is generated by a resistive heating element modulated at 10 Hz. The energy is passed through a sample cell, where the presence of CO_2 attenuates it at 4.25 μm. On entering the monochromator, the spectrum is diffracted into the two wavelengths of interest. The reference wavelength is at 4.0 μm where no absorption occurs from either CO_2 or any of the other gases likely to be present. The comparative signals from the pyroelectric detectors are then processed to provide an output proportional to the concentration of CO_2.

The helmet sensor assembly contains a modulated source, a monochromator, a sample cell, and a dual hybrid detector assembly. Each hybrid detector assembly contains a pyroelectric detector and a field-effect transistor (FET) assembly consisting of one dual FET and one feedback resistor for each detector. The electrical interface between the helmet sensor unit and the backpack electronic unit is a cable containing a 10-Hz modulation signal to drive the source, signals for the hybrid detector assembly, and bipolar voltage to operate the FETs. Although the signal levels at the output of the FETs are quite small, the impedance level is also sufficiently low to allow coupling the small signal to the preamplifiers located in the backpack

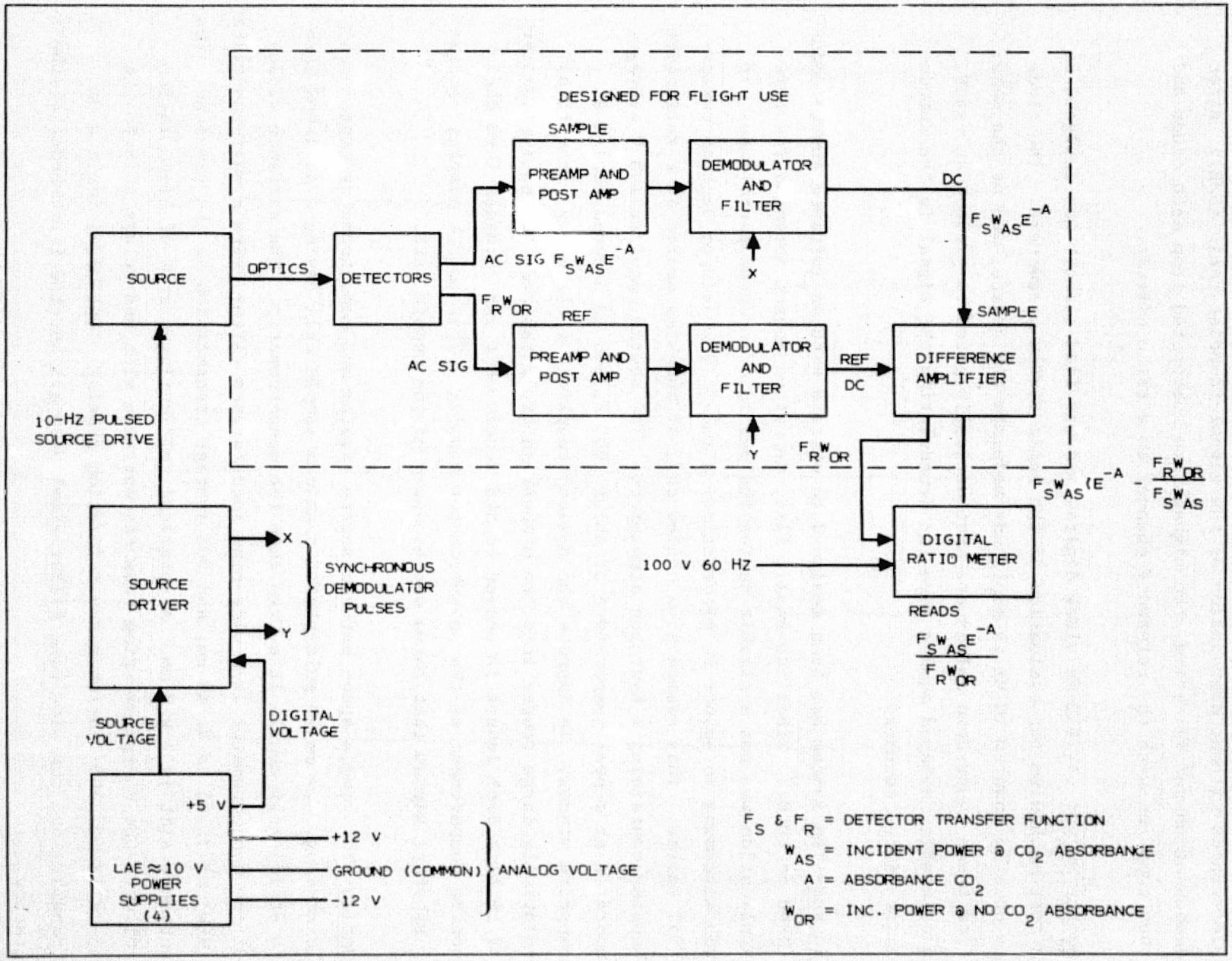

Figure 3-1. CDS System Block Diagram

electronics without degradation of the signal-to-noise ratio (SNR). After demodulation and filtering, the signals are subtracted from each other and then compared with the reference channel in a ratio circuit.

Source Driver--A 2650-Hz clock digitally-controlled circuit was designed as a test mechanism for evaluation of the basic system parameters. The clock is counted down to 10 Hz to amplitude modulate the source, and at the same time these count-down pulses are systematically gated to produce an exact, predictable, delayed square wave for demodulating the signal in the demodulator filter network.

Source--The system has been designed to operate with an infrared source modulated at 10 Hz. Since the small, flat, deposited source intended for this application was not available during the period of program performance, it was necessary to select an alternative--a recently developed Beckman commercial source. This source is a coiled-coil of tungsten sealed in a reflective housing containing a hydrogen atmosphere. The source requires 1.8 W average, operates at a peak temperature of about 1000 K, and is located behind a sapphire window. To improve the optical coupling of the energy from this relatively large source into the monochromator, a tapered, reflective adapter of 24.6-mm path length is sealed to the source unit and threaded into the source compartment of the monochromator housing. This source adapter carries a sapphire window that forms one boundary of the sample path.

Optics--The sample space between source adapter and monochromator contains a 12-mm-long, 4.7 mm ID gold-plated aluminum sample cell having a polished bore to efficiently couple IR energy into the monochromator. The entrance window of the monochromator is a wide-band interference filter, with a half-bandwidth (HBW) of 3.365 to 4.743 μm, and 90% average transmission in the passband. The entrance slit is 1 x 3 mm. A spherical collimating mirror of 80-mm radius collects the energy emerging from the entrance slit and relays it onto the 13- x 13-mm, 300-line/mm plane reflection grating. Optimized for a 4-μm transmission, the wide-band filter eliminates all but the first order of the grating.

Dispersed energy reflected from the grating is collected by the collimating mirror and focused through the anti-reflection coated exit lenses onto the two pyroelectric detector elements. These detector elements are precisely located at focal points for reference (4.0 μm) and CO_2 sensing (4.25 μm) wavelength, respectively. A sapphire window provides a seal over the exit lenses.

To prevent any change in CO_2 level in the optical path, other than in the sampling area, the monochromator housing has been leak tested, provided with a small Ascarite-filled capsule to remove residual CO_2, purged with dry N_2, and sealed.

Detector Assembly--The detector assembly consists of two pyroelectric detectors hermetically sealed in a TO-5 can and covered by a sapphire window. The assembly is mounted in a glass-epoxy shielded can along with two dual junction FETs (J-FETs) and the current feedback resistors. Everything is placed in one housing in order to provide the lowest shunt capacity across the detector.

The J-FETs are a special Siliconix device chosen for their low leakage characteristics (0.1 pA). One detector is inverted for proper signal processing in the difference circuit (see "Difference Circuitry" on following page).

Preamplifier--The preamplifier is a FET input operational amplifier designed for a low SNR by proper FET selection, high feedback resistors, and component layout and orientation (part of detector assembly).

The basic formulation for the SNR was given in the design and development program presentation, IR-2679-101.

Post Amplifier--The post amplifier is a noninverting current amplifier with a front end zero network designed for thermal detector pole cancellation.

The gain factor of this section is designed to deliver a 10-V peak-to-peak (p-p) signal to the demodulation circuitry. It is at the output of the

demodulator circuitry that the equalization of the reference and sample signals takes place for proper system ratioing at 0 mmHg P_{CO_2}.

Demodulator and Filter--The demodulator is an ac-coupled half-wave FET demodulator triggered by the source delayed gated circuitry to synchronously demodulate the reference and sample signal. A dc signal related to changes in the peak-to-peak value of the ac input is thus obtained.

Difference Circuitry--The difference circuitry is actually the sum of the reference and sample signals (one being inverted because of the detector circuitry inversion), which results in a difference of reference to sample signals. An additional output amplifier is added to the reference channel to give similar 10-Hz attenuation as the difference side.

Ratio--The ratio circuitry is an off-the-shelf digital ratio panel meter purchased from Newport Labs. It has ±0.05% accuracy full scale.

3.3.2 Dynamic Range, Minimum Resolvable Signal, Noise Equivalent Power

At 1.3 kPa (10 mmHg) P_{CO_2} the attenuation through the sample cell is 0.6. It is expected that if the cell should become occluded due to water vapor, the signal would be reduced further by 0.5. For a 1% resolution signal the smallest resolvable signal to the detector would be:

$$\underline{P}_d = \bar{N}_\lambda \cdot T_C \cdot R \cdot \varepsilon_\lambda^o$$

where

$\bar{N}_\lambda$ = 9×10^{-3} $W \cdot cm^{-2} \cdot sr^{-1} \cdot \mu m^{-1}$ (calculated)

$\underline{P}_d$ = lowest signal at detector, $W \cdot cm^{-2} \cdot sr^{-1} \cdot \mu m^{-1}$

T_C = attenuation through sample cell: 0.6 x 0.5 = 0.3

ε_λ^o = optical throughput

R = resolution (0.01)

For a pulsed source:

$$\underline{P}_d = (9 \times 10^{-3})(0.3)(1.76 \times 10^{-5})(0.01)$$

$$\boxed{\underline{P}_d = 4.7 \times 10^{-10} \text{ W}}$$

The calculation above sets the noise equivalent power (NEP) requirement for the system at 4.7×10^{-10} W. Note that this is a minimum requirement that does not allow a full 1% resolution from 1.2 to 4.0 kPa P_{CO_2} (9 to 30 mmHg). (Presumably better resolution would not be required outside the alarm range.)

If an emissivity of 0.4 is assumed for this calculation,

$$NEP_P = \epsilon_P \underline{P}_d = (0.4)(4.7 \times 10^{-10}) \text{ W.}$$

$$\boxed{NEP_P = 1.88 \times 10^{-10} \text{ W}}$$ Pulsed Source Detector Requirement

For a fixed source:

$$\epsilon_F = 0.98 \text{ (emissivity of the fixed source)}$$

$$NEP_F = 2\pi \epsilon_F P_d$$

$$\boxed{NEP_F = 2.9 \times 10^{-9} \text{ W}}$$ Fixed Source

The basic SNR requirement was presented in detail in the preliminary Design and Development Program Presentation (IR-2679-101) related to the NEP.

It was shown that the main noise contributors were: shot noise from the gate current ($i_N^2 = 2_q I_g$, where I_g is gate leakage current), shot noise from offset contributions, and Johnson noise from feedback resistor.

The resultant noise equivalent power shows our detector must be in the 1×10^{-10} W region. The Molectron data show for detector No. 1: 3.9×10^{-10}, and for detector No. 2: 3.2×10^{-10}, which is a factor of two off the figures with the 0.4 assumption for emissivity.

With this and a 60% optics throughput, we expect a SNR of 100. Data taken to date (10 Hz demodulated filtered) show a 0.1 to 0.3% noise figure, which is within calculated values, assuming the signal modulation is of a reasonable magnitude.*

3.3.3 System Error Analysis

The system error analysis approach of the Design and Development Program Presentation (DDPP) is still valid relating back to the 79% modulation figure generated from the Concept Study Guide Report of October 9, 1974.

Of the four system approaches analyzed in the DDPP, approach #4 (difference to a ratio) still has the prime advantage due to the large signal modulation. If after further testing the modulation factor is considerably less, then a closer look should be taken at the second choice of a pure ratio output.

The four basic approaches are given along with their related results (Table 3-1) for referencing (taken from the Design and Development Program Presentation, IR-2679-101):

1. Difference method
2. Difference with AGC (sum) method
3. Ratio method
4. Difference-to-ratio method

*Signal modulation: change in sample signal at maximum mm P_{CO_2} concentration ratioed to sample signal at 0 mm P_{CO_2} concentration.

TABLE 3-1. SOURCE POWER ERROR VARIATION

Circuitry Approach	kPa P_{CO_2}	Voltage Error for 1% Error		Best Low Absorb	Best High Absorb	Best 10 mmHg P_{CO_2}	Most Linear Band (1% Full Scale)
		% of Reading	% of Full Scale				
Difference Method	.13	20	0.666				
	1.3	2.5	1.78				
	4.0	1.26	1.26				
Difference With AGC (Sum) Method	.13	2.11	0.070	2			
	1.3	5.9	4.008				
	4.0	0.7249	0.7249		2		
Ratio Method	.13	1.0	0.033	1			
	1.3	1.0	0.712			1	2
	4.0	1.0	1.0				
Difference-to-Ratio Method	.13	19.03	0.6301				
	1.3	1.5	1.06			2	1
	4.0	0.266	0.266		1		

3.4 Electronic Design

The presentation in this subsection will be to first discuss each individual electronic subsystem--considering requirements, approach, problems experienced, changes, and basic breadboard operation--and then to evaluate the electronic system evaluation, summing up the design goals along with the overall system performance. It will be pointed out where potential development problems are and where further work is needed in order to perfect the final flight hardware.

3.4.1 Preamplifier

The preamplifier (Figure 3-2, Print No. 554741) combines the detector assembly with two stages of amplification. The first stage is a dual differential coupled FET that amplifies the signal and, in turn, delivers this signal to AR1, which provides sufficient open-loop gain to establish a feedback factor of at least 40 dB at the chopping frequency. The next stage of amplification is accomplished by AR2 and its associated components. The feedback network

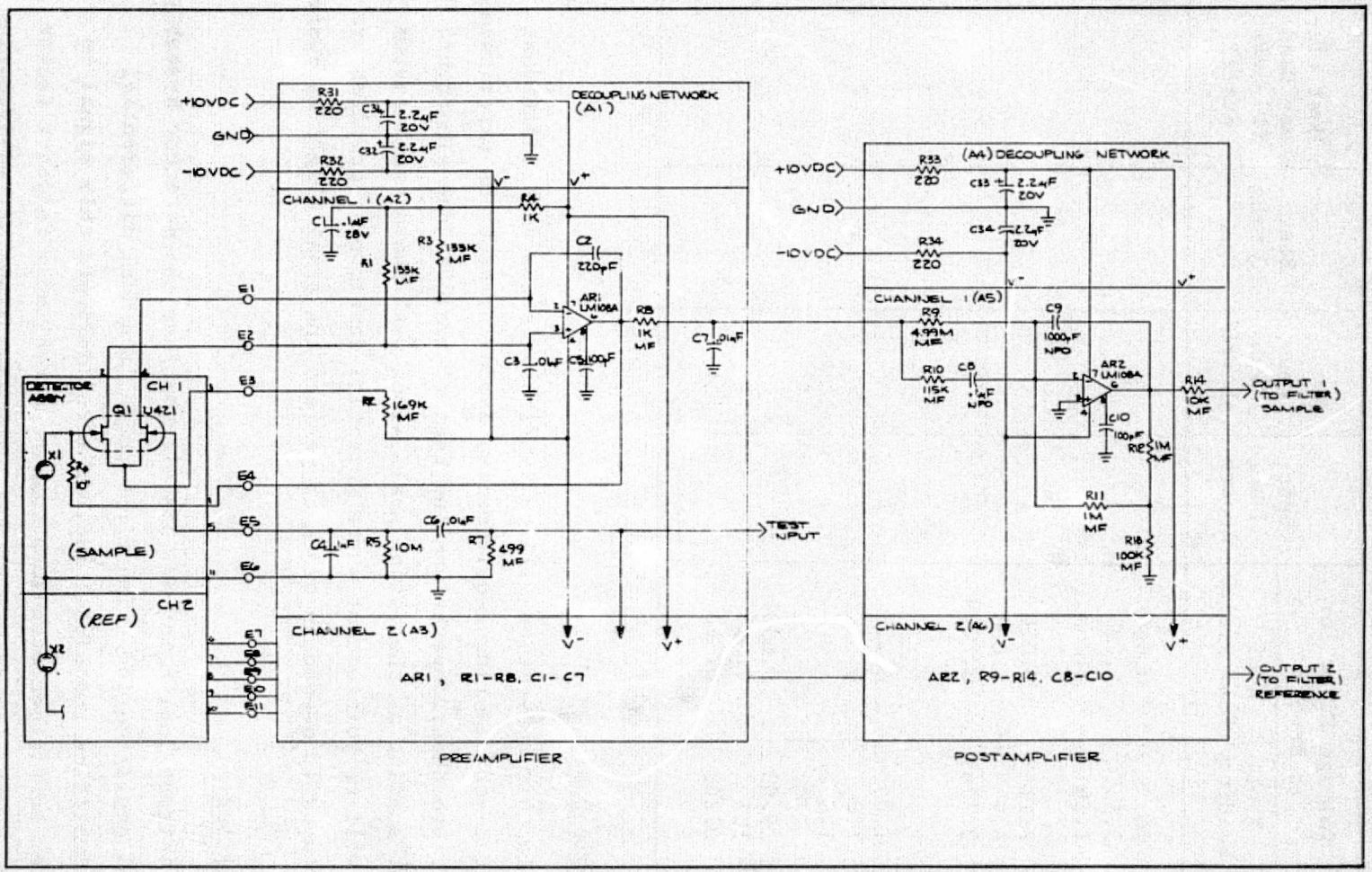

Figure 3-2. Detector Amplifier, Schematic Diagram

provides a bandpass configuration centered about 10 Hz. There are two identical signal processing channels.

The derived requirements of Table 3-2 for the preamplifier are based on the following set of assumptions:

- Under the most ideal conditions of maximum signal level and a source emissivity of 1, a cell transmission of 1, and no water absorption, etc., the voltage to the demodulator shall be 10 V p-p.
- The minimum expected signal assumes 50% transmission due to water vapor and a source emissivity of 0.4.
- The NEP requirement for the detector/preamplifier is based on a requirement of 1% signal resolution at the minimum expected signal level.
- The optical throughput of the system is 1.76×10^{-5} $cm^2 \cdot sr^{-1}$.

TABLE 3-2. DERIVED REQUIREMENTS OF PREAMPLIFIER AND POST AMPLIFIER

• Minimum expected signal (T_D = 750 K)	- 1.88×10^{-8} W (average value
• Maximum expected signal	- 1.67×10^{-6} W (peak value)
• Input to demodulator	- 10 V p-p
• NEP	- 1.88×10^{-10} W
• Preamplifier/detector gain	- 1.1×10^{5} V/W
• Post amplifier gain	- 54.4

A FET operational amplifier operating in the current mode with a 10^{11}-ohm feedback resistor will give the required bandwidth. Stray capacitance across the feedback element gives rise to undesirable phase shift, and this must be kept small in order to achieve the required bandwidth and reduce undesirable memory effects.

The preamplifier circuit measures the detector current rather than the detector voltage. Measuring the detector voltage is avoided because of the unknown

source impedance, which enters directly into the gain expression. The voltage responsivity of the detector is affected by not well understood thermal variations of the detector capacitance and by the relatively unpredictable wiring and transistor input capacitance. The pyroelectric detector is a current source whose responsivity rises with frequency, flattening off above the thermal time constant. Thus, the circuit is not affected by thermal variations of the detector capacitance, nor by the capacitance of the wiring and the input transistor.

The circuit for the CDS detector preamplifier is a dual FET followed by a monolithic operational amplifier. Current from the detector is amplified in accordance with equation (1). The amplifier operates as a current amplifier, with the output connected to the inverting input through R_f (10^{11} ohm). In this way, the input to the amplifier is maintained to within a few millivolts of ground.

$$\frac{e_o(j\omega)}{P_D(j\omega)} = \frac{R_O j\omega\tau_T}{(1+j\omega\tau_T)} \frac{R_f}{(1+j\omega R_f C_s} \qquad (1)$$

where

P_D = incident detector power, watts
R_O = current responsivity, amperes/watt
τ_T = detector thermal time constant, seconds
R_f = feedback resistor, ohms
C_s = stray capacitance, farads
ω = $2\pi F$, hertz

The long time constant pole at $1/\tau_T$ radian per second will be canceled by the network shown following the preamplifier. Phase lead provided by this network results in zero phase shift to the modulated signal at 10 Hz.

The dual FET and the 10^{11}-ohm resistor are mounted on the same substrate as the detector chip. This stabilizes the circuit from mechanical vibration to minimize microphonic noise.

Although discrete components were used in the breadboard, they are mounted close together to provide a relatively low impedance interface. This low impedance (less than 300 K ohms) is important in terms of desensitizing the preamplifier and detector from microphonic or spurious outputs resulting from mechanical vibration. The major emphasis in the design of the preamplifier is directed toward low noise performance. This task is made difficult by the high impedance of the detector, which results in two simultaneous requirements that are somewhat conflicting--low voltage noise and low current noise. Low current noise is more basic and, consequently, a U421 J-FET from Siliconix has been chosen for the input device.

3.4.2 Post Amplifier

The post amplifier (refer to previous Figure 3-2, Print No. 554741) provides the gain necessary to raise the preamplifier output voltage to 10 V p-p at the demodulator input. A maximum gain of 50 is required. In addition, high-pass and low-pass filtering is provided to minimize the noise bandwidth at the carrier frequency. The transfer function of the post amplifier is given by equation (2).

The capacitance values have been restricted to a maximum value of 0.1 μF to reduce circuit packaging density.

The overall response of the detector preamplifier/post amplifier is flat in the region of 10 Hz and, therefore, will have zero phase shift. This aids in reducing the sensitivity of amplitude variations due to minor component variations that determine the modulation frequency.

$$\frac{e_o(j\omega)}{e_i(j\omega)} = \frac{R_T}{R_9} \frac{[1+j\omega(R_9+R_{10})C_8]}{(1+j\omega R_{10}C_8)(1+j\omega R_T C_9)} \qquad (2)$$

where

$$R_T = R_{11} + R_{12} + R_{11}R_{12}/R_{13}$$

$$\omega = 2\pi F, \text{ hertz}$$

By design, the zero of transmission at $\tau = (R_9 + R_{10})C_8$ is set equal to the pole resulting from the detector thermal time constant, τ_T. The remaining design constraints are tabulated in Table 3-3.

TABLE 3-3. DESIGN REQUIREMENTS FOR POST AMPLIFIER

• $(R_9 + R_{10})C_8$	=	Detector thermal time constant, τ_T
• $R_{10}C_8$	=	R_TC_9
• $\mathrm{Re}\left(\frac{e_o}{e_1}\right)\omega_c'$	=	50
• $(\phi)_{\omega_c}$	=	0 for preamplifier and post amplifier in combination

As the breadboard detector was not yet available, testing to verify calculations was started using a simulated pyroelectric detector. Tests covered were:

- Power Consumption
- Offset
- Frequency Response
- Transient Response
- Linearity
- Noise (Preamplifier only)
- Gain (Post amplifier only)

It was found that the preamplifier gain was down by a factor of 30% at 10 Hz, which was later attributed to excessive capacitance across the feedback resistor.

During the preliminary test setup an excessive amount of 60-Hz ripple was picked up. This was alleviated once we received the detector assembly from Molectron. With the detector, the testing was completed satisfactorily. Test results were in agreement with calculated values.

3.4.3 Demodulator/Filter (Figure 3-3, Print No. 554746)

The signals are capacitive-coupled into the demodulator circuitry which consists of a J-FET switch triggered by an exact delayed square-wave pulse originating in the source driver circuit. The result is a half-wave rectified signal coupled into the filter network.

Referring to the design notes, Appendix B, it can be seen that an output of 32% of signal peak value was calculated with a 0.3% 10-Hz ripple component. Relating this to a half-wave 5-V peak value input, an output of 1.6 Vdc with a 5-mV 10-Hz ripple component should be achieved.

Test data from Appendix A shows that for an input signal of 3 V peak-to-peak (1.5 V peak input) an output of 0.4762 Vdc (from page "2" of the "retake" section, Appendix A) with a 1.30-mV ac ripple was obtained. This is 31.7% of signal peak value with a ripple component of 0.2729% of the peak value.

Relating the calculated value to the tested value shows a correlation that gives a high confidence level in the design and performance of this signal processing approach.

Temperature testing over a 40°C range shows a 30 mV change in output. This is equal to 0.071%/°C. This can be minimized by proper care in the selection of the temperature coefficient of components.

Further testing and evaluation are needed relating to signal demodulation phase shifting temperature effects to ensure that this is the optimum approach for the final flight configuration.

3.4.4 Difference Circuitry

The function of the difference circuit is twofold. In the sample channel side the sample signal voltage is subtracted from the signal output voltage of the reference side. The reference channel side simply inverts the reference signal.

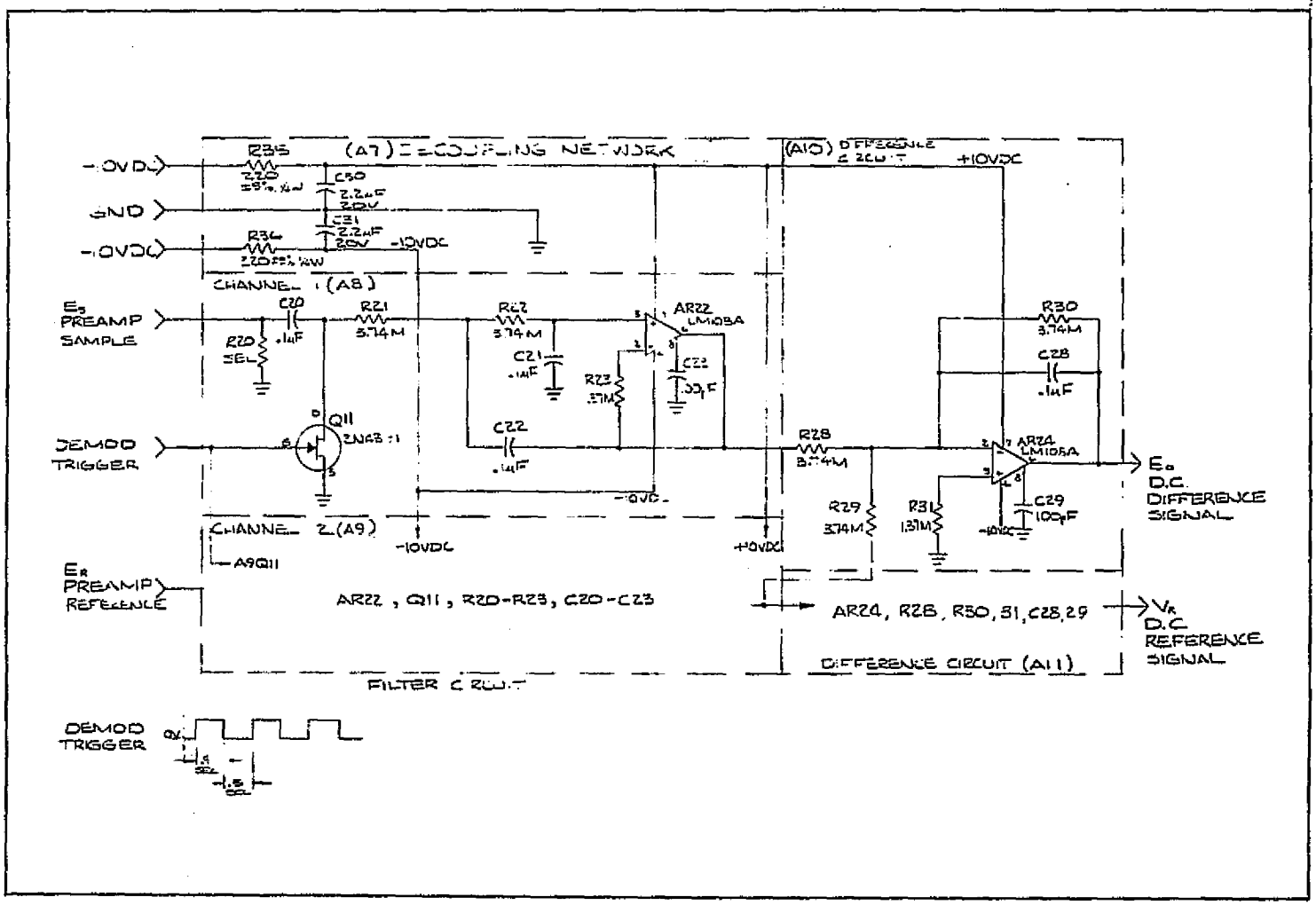

Figure 3-3. Filter and Difference Circuit, Schematic Diagram

The second function is attenuation. A pole formed by the feedback capacitor and resistor further attenuates the 10-Hz ripple from the filter circuit by a factor of 20. The total attenuation for the 10 Hz from the filter and the difference circuitry is greater than 76 dB.

The Newport Labs ratio meter is an off-the-shelf item and will not be discussed as a part of this report except to mention that its accuracy is such as to attribute negligible errors to our system.

3.4.5 Source Driver (Figures 3-4, 3-5)

The basic requirements for this circuit are:

- To supply a modulated voltage for the source.
- To supply a delayed signal capable of demodulating the post amplifier signal synchronously in the reference and sample channels.

Since the CDS is basically an evaluation unit, it was of prime importance to be able to control the demodulator delay pulse to a precise degree. To accomplish this, a circuit for breadboard use only was designed. With it, the pulse can be varied by 1.40-degree increments over the entire 360-degree cycle. This makes it possible to evaluate system (source to demodulator/filter) signal with regard to phase, temperature, and amplitude variations independent of the method of pulsing the source.

Pulses from a 2.56-kHz oscillator are counted down for the 10-Hz source modulation signal. At the same time, the count-down pulses are gated by an adjustable strapping block to give the desired delay in turning on and off the demodulator pulse for the reference and sample signals. The use of the strapping clock to select the gating is shown in Figure 3-4. This method proved very successful because both the modulated source and the demodulation pulse are slaved to the same clock network, which gives an accurate time base for system evaluation.

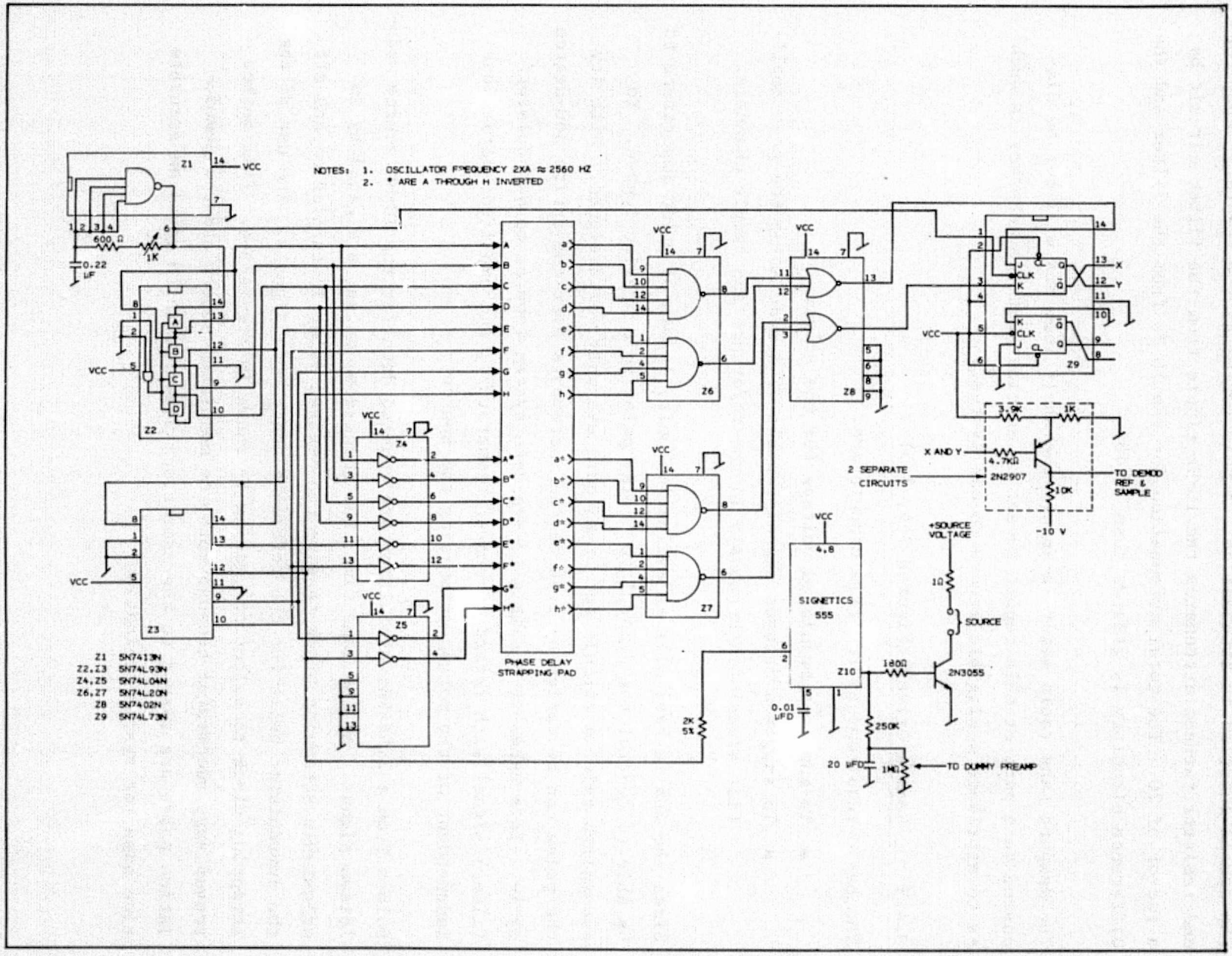

Figure 3-4. Source Timing Circuitry

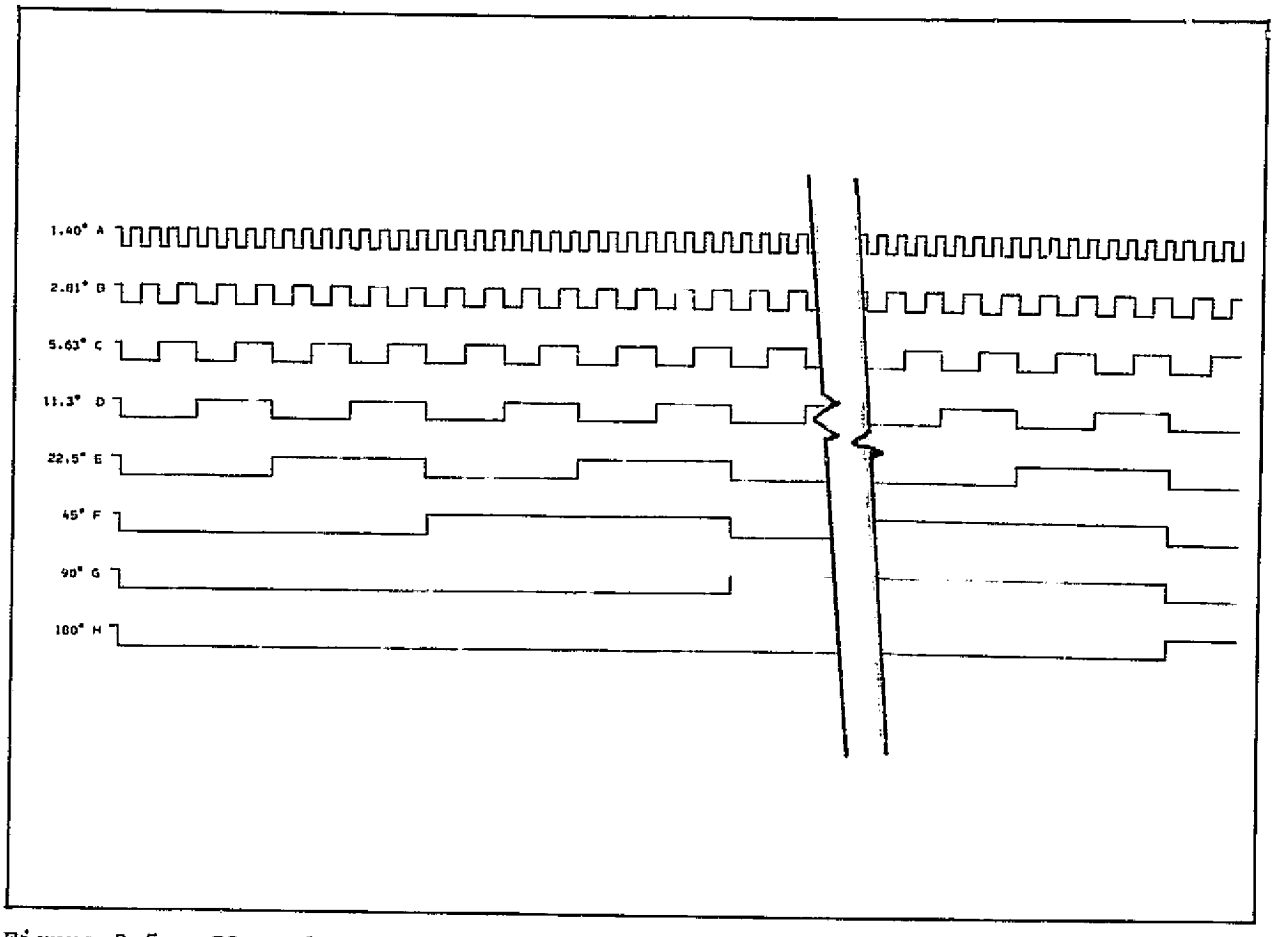

Figure 3-5. CO_2 Helmet Source Timing Chart

3.4.6 Electronics Summary

The electronics design fulfills the basic design requirements. With the exception of an apparent 30% overall system gain drop from calculated values when using the simulated detector, which was attributed to excessive capacitance across the preamplifier feedback resistor,* the calculated-to-performance characteristics of noise, phase shift, gain (excluding preamplifier), and ripple were surprisingly accurate. However, there are still some unknown effects and design approaches to be considered. Some further testing should be performed on the electronics relating to temperature effects with the various assemblies. Some calculations have been performed relating temperature to the two most important parameters: amplitude and phase.

It appears from the work that has been done that one of the main concerns would be amplitude change as a function of phase shifts. Temperature effects relating phase to amplitude can substantially be reduced, since we use a ratio-type system, by selecting parts (channel-to-channel) that track.

Some problems and new designs to be looked into outside of temperature phase are:

- The compensation of emissivity changes of source with temperature (reference channel feedback is one possible approach).
- A flight method for modulating the source.
- A method for phase delaying the source pulse for demodulation circuitry.
- Completion of the design and fabrication of the ratioing method and output scaling amplifier.
- The performance of more elaborate worst-case analyses relating to tolerances and temperature effects.

*It was not verified that we actually had this gain deterioration in the final perfected detector assembly.

3.5 Optical Design

3.5.1 Advantages of Monochromators over Filter Systems

Monochromator optical systems can be dimensionally scaled down to the small volumes that are feasible for filter systems. Such physically small monochromators offer important spectral and photometric advantages over filter systems, namely:

- Monochromators can give much higher wavelength accuracy and repeatability than can filters.
- Monochromators can give much higher wavelength repeatability between other instruments of the same design than can filters.
- Monochromators can produce either controlled or the ideal triangular or trapezoidal spectral band shapes for all their wavelengths, whereas filters cannot.
- Monochromators are spectrally self-calibrating, whereas each filter must be individually calibrated with a monochromator.
- Monochromators usually have better stray light rejection than filters.
- A single monochromator can generally define either several or a large number of wavelengths more economically than can an equivalent multiple-filter optical system.

3.5.2 Monochromator Design for the CDS

The monochromator optical design used for the CDS is shown in Figures 3-6, 3-7, and 3.8. It is an Ebert-type monochromator using a single fixed grating for wavelength dispersion. This type of monochromator gives excellent spectral image quality for its fast f/3.5 relative aperture. Its optical design is very simple since only two optical components are required, a 300-line/mm commercial grating blazed at 3.5 μm and a spherical collimating mirror with an 80-mm radius of curvature. The effective monochromator focal length is only 40 mm, but this is sufficient to separate the 4.00- and 4.25-μm spectral images by 4.87 mm.

The monochromator entrance slit is an opening 1 mm wide by 3 mm high. The 1-mm slit width gives the monochromator a roughly 0.102-μm spectral bandwidth at 4.00 and 4.25 μm. The individual dimensions and locations for the exit slit openings

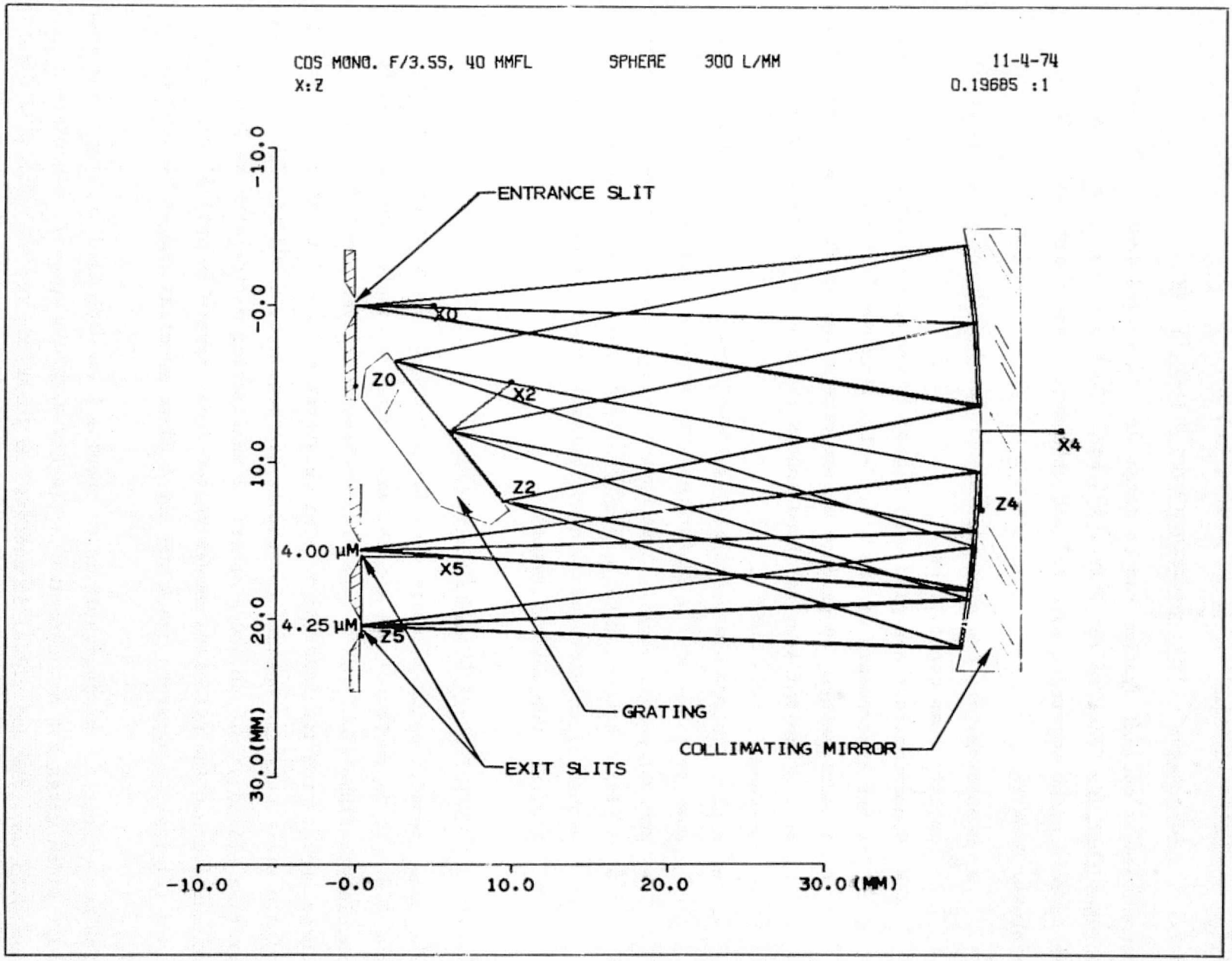

Figure 3-6. Monochromator Ray Trace (Top View)

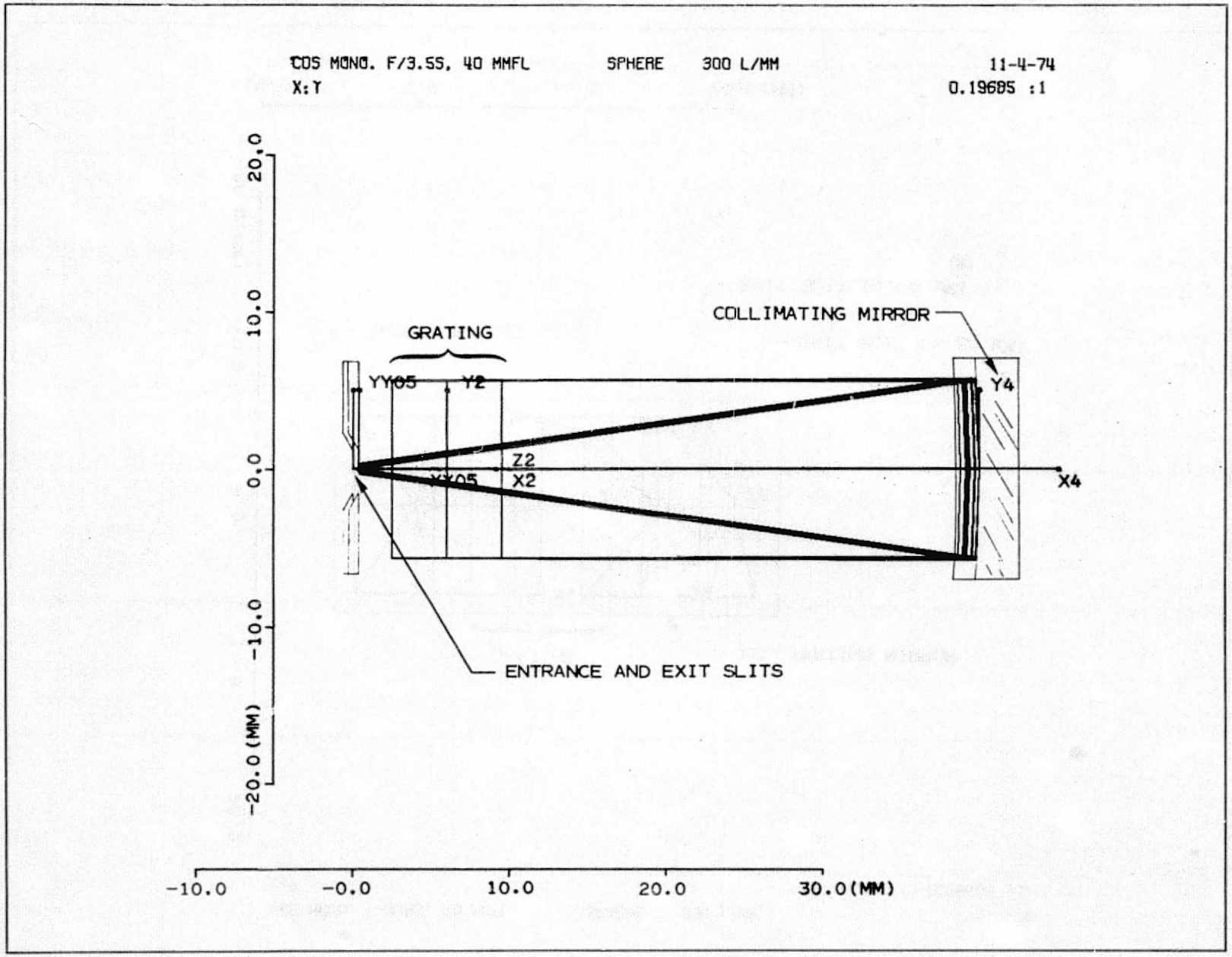

Figure 3-7. Monochromator Ray Trace (Side View

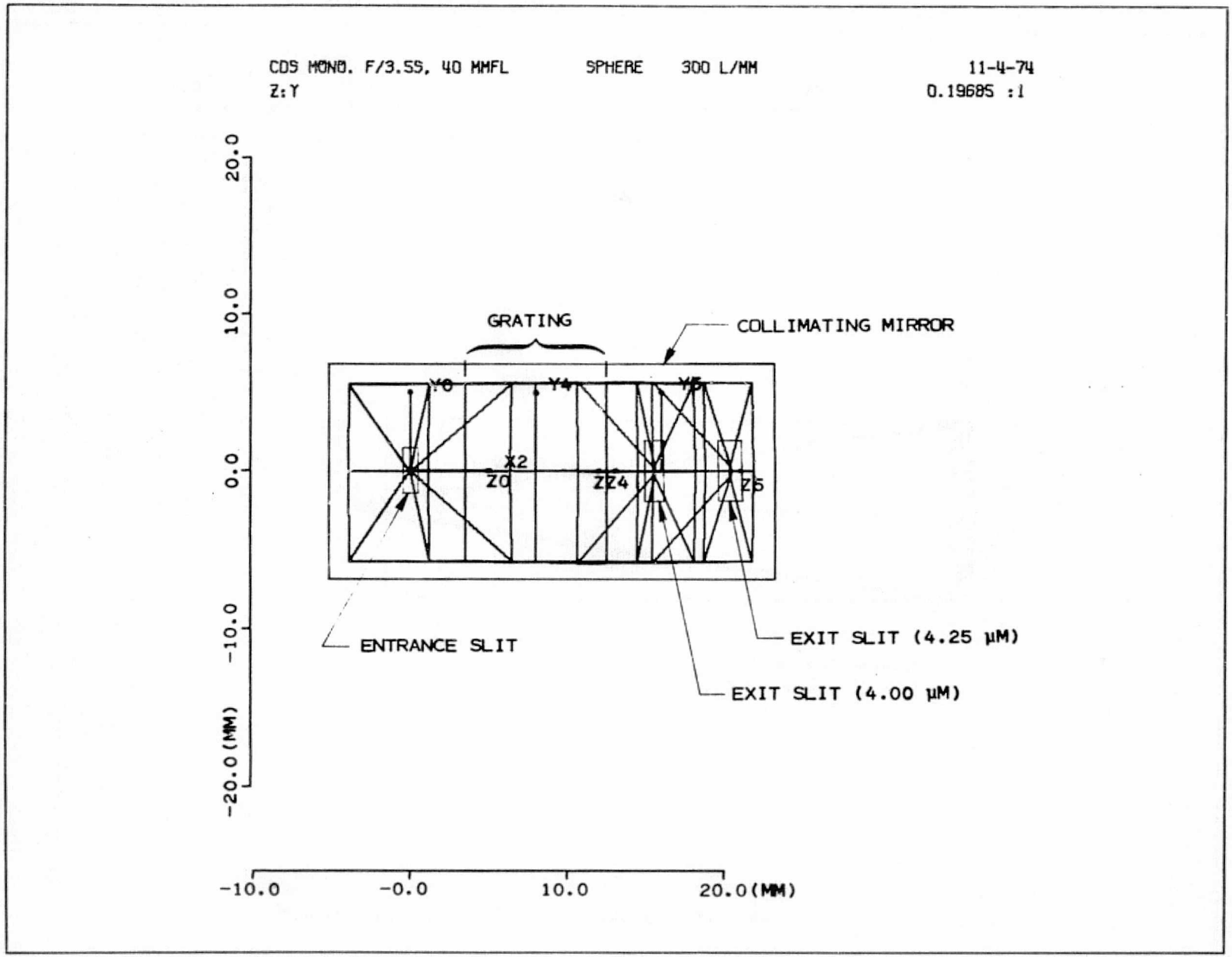

Figure 3-8. Monochromator Ray Trace (Front View)

for the 4.0- and 4.25-μm spectral images were defined by accurate computer ray traces for the spectral images of the 1- x 3-mm entrance slit at these two wavelengths.

Figures 3-6, 3-7, and 3-8 are accurate computer ray-trace plots of the top, side, and front views of the monochromator for two families of nine rays, each starting from the center of the entrance slit. The two families represent 4.0 and 4.25 μm, respectively. Both families intercept the full grating surface which is 11.42 mm square, in an identical uniform nine-point array. This makes the grating the optical stop of the monochromator optical system.

Figure 3-9 defines the monochromator spectral image locations and characteristics, showing eight families of 100-ray point-spread spot diagrams for 4.0 and 4.25 μm. Each family of 100 rays starts from a single point at the entrance slit and intercepts the 11.42-mm square grating area in an identical uniform 100-point square array. Four different starting points are used on the entrance slit; the two opposite sides of the slit at its top and center were used at the two wavelengths to create these eight spot diagrams. The locations and shapes of the two exit slits are illustrated in Figure 3-9 by the dashed lines. The optical aberrations for each of these eight spectral images are seen to be much less than 10% of the exit slit width. This means that these are very good quality images for this application.

3.5.3 Optical Design for Sampling Volume, Source Optics, and Source

The sampling volume for the CO_2 gas analysis is located in front of the monochromator entrance slit, as shown in Figure 3-10 and 3-11. The breath sample is confined to a 12-mm optical path length on one side by a germanium window near the monochromator entrance slit and on the other side by a germanium focusing lens. (This focusing lens could not be used with the compromise commercial source in the breadboard assembly--see paragraph 3.3.1).

The germanium focusing lens is designed to optically couple the illumination from a small 1-mm square radiant source to the monochromator with the maximum possible efficiency. The source lens is a germanium plano-convex lens with a 14-mm radius of curvature on its convex surface.

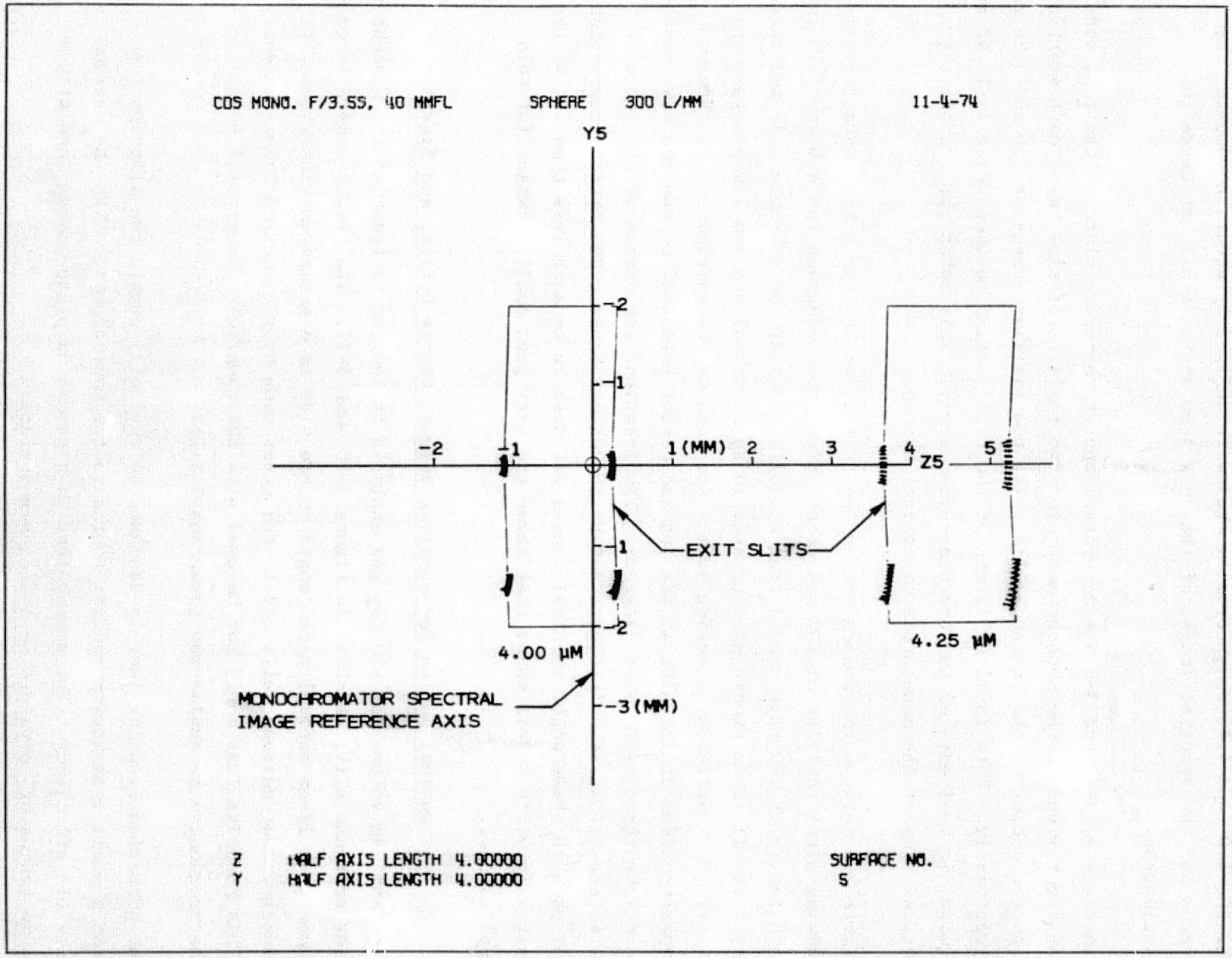

Figure 3-9. 100-Ray Point Spread Spectral Images for Monochromator

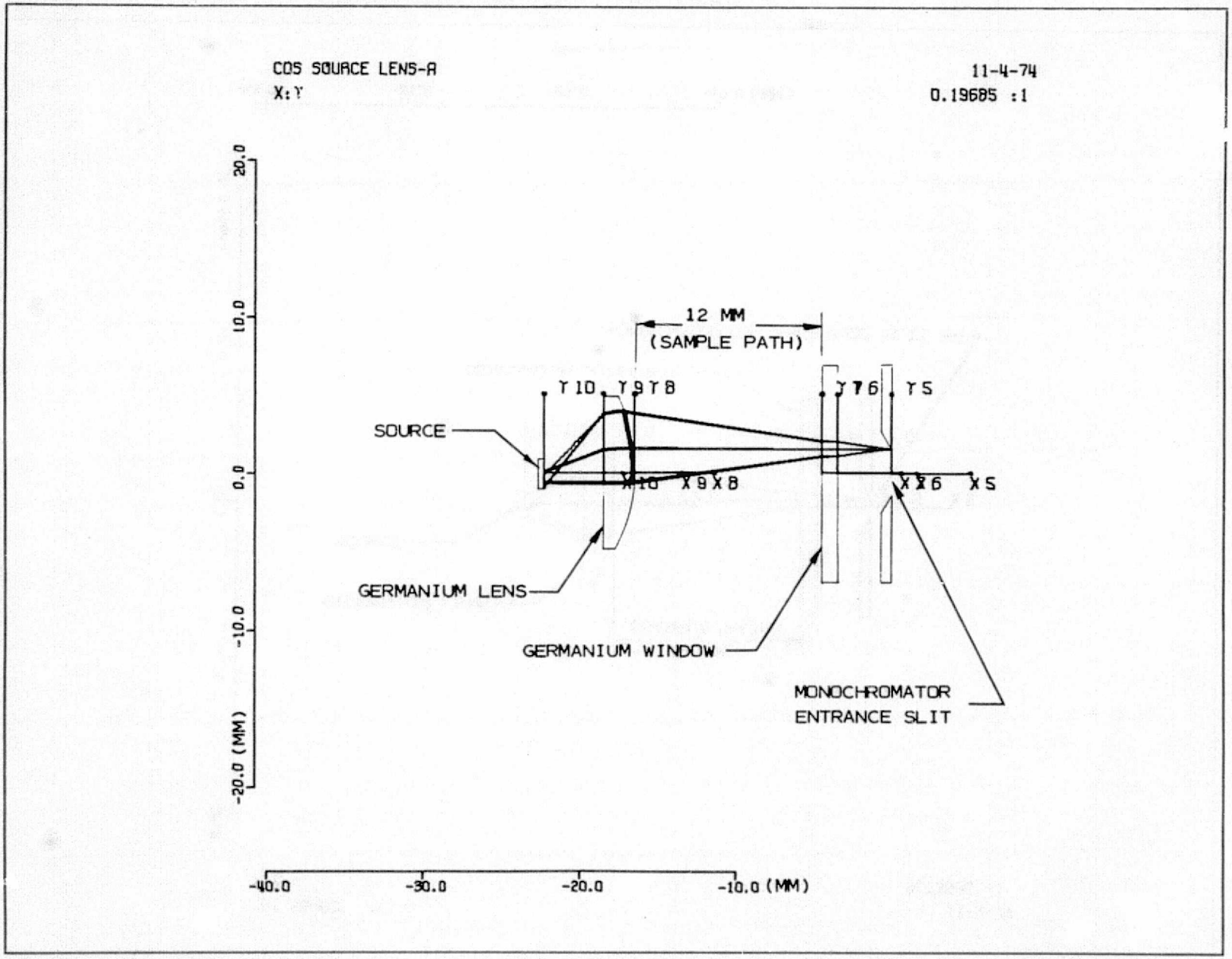

Figure 3-10. Source and Sample Optics Ray Trace (Top View)

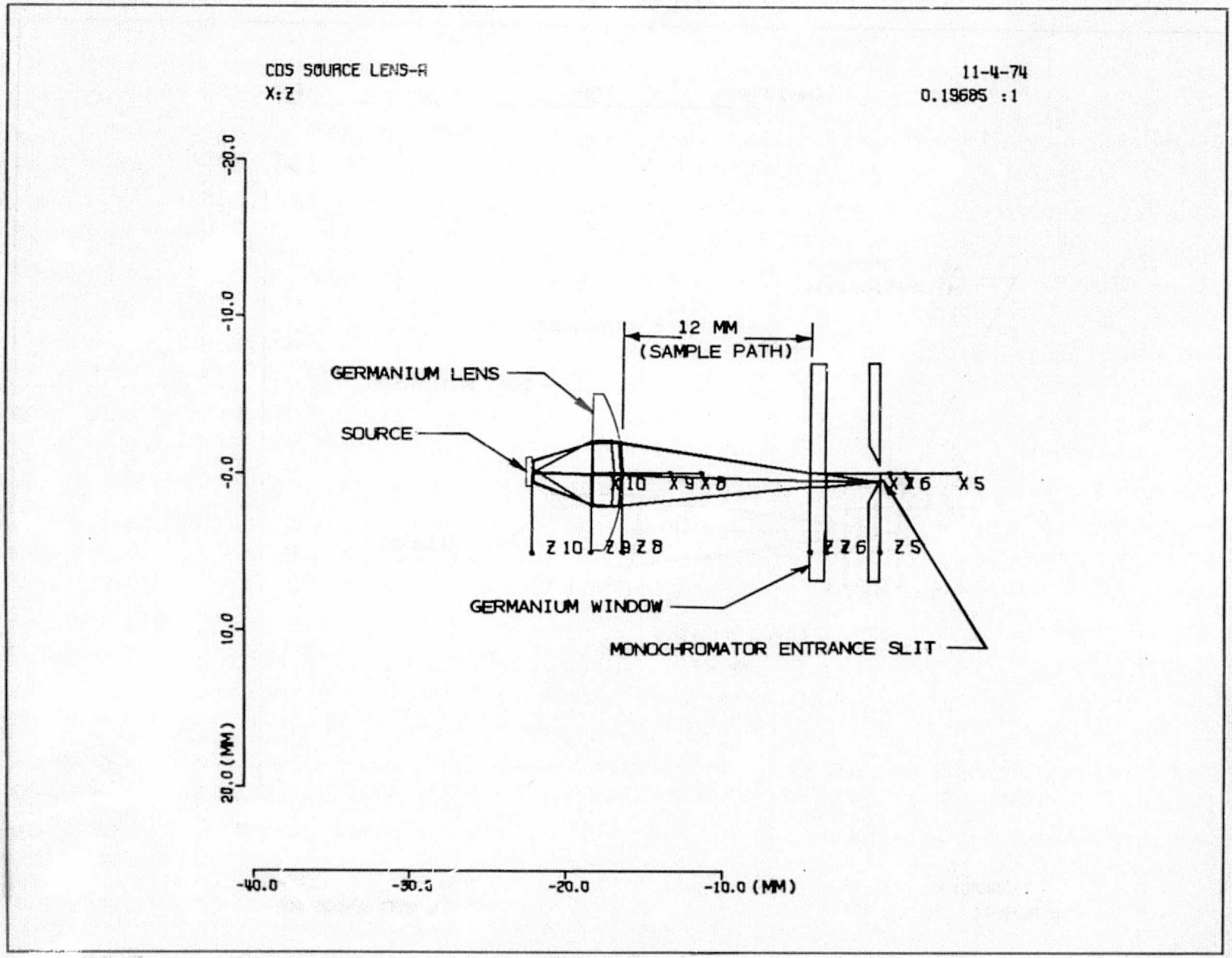

Figure 3-11. Source and Sample Optics Ray Trace (Side View)

Figures 3-10 and 3-11 are accurate computer ray-trace plots of the top and side views, respectively, of the source, source lens, sampling volume, window, and monochromator entrance slit. These ray traces show one family of nine rays that starts from one corner of the entrance slit and intercepts the grating surface in a uniform nine-point square area. This family of nine rays is shown here ray traced through the sampling volume, the source lens, and finally to the source. It is demonstrated here, and can be shown as well for all other entrance slit starting points, that all rays fall within a source area less than 1 mm square. Thus, the source is not required to be larger than 1 mm square.

3.5.4 Optical Design for Detectors and Detector Optics

Separate detectors are used to sense the 4.00- and 4.25-μm wavelengths. Figure 3-12 shows where these detectors are located relative to the monochromator, as well as optics that are needed to properly illuminate the detectors. It is an accurate computer ray-trace top view plot of the detector optics, which follow the two monochromator exit slits for 4.0 and 4.25 μm, respectively. Two sets of nine rays are used in this ray trace for each of the two wavelengths. Each set of nine rays for the same wavelength has ray starting points on the opposite edges of the grating, and the rays intercept the full exit slit area in a uniform nine-point array. Therefore, the sets of rays that are shown in Figure 3-10 are the true boundary rays of the monochromator for the two wavelengths.

A germanium plano-convex lens follows each exit slit. These lenses are coated for maximum transmittance in the 4.00- to 4.25-μm wavelength ranges. The convex surface of the lens has a 15.0-mm radius of curvature.

Each of the two lenses has been designed to image the grating surface on its respective detector surface. The images of the grating are slightly less than 1 mm square and match the 1-mm square area of the detector very closely.

The grating is the optical stop of the monochromator, so if it is completely imaged on the detector by rays that also fully fill the slit areas, then the

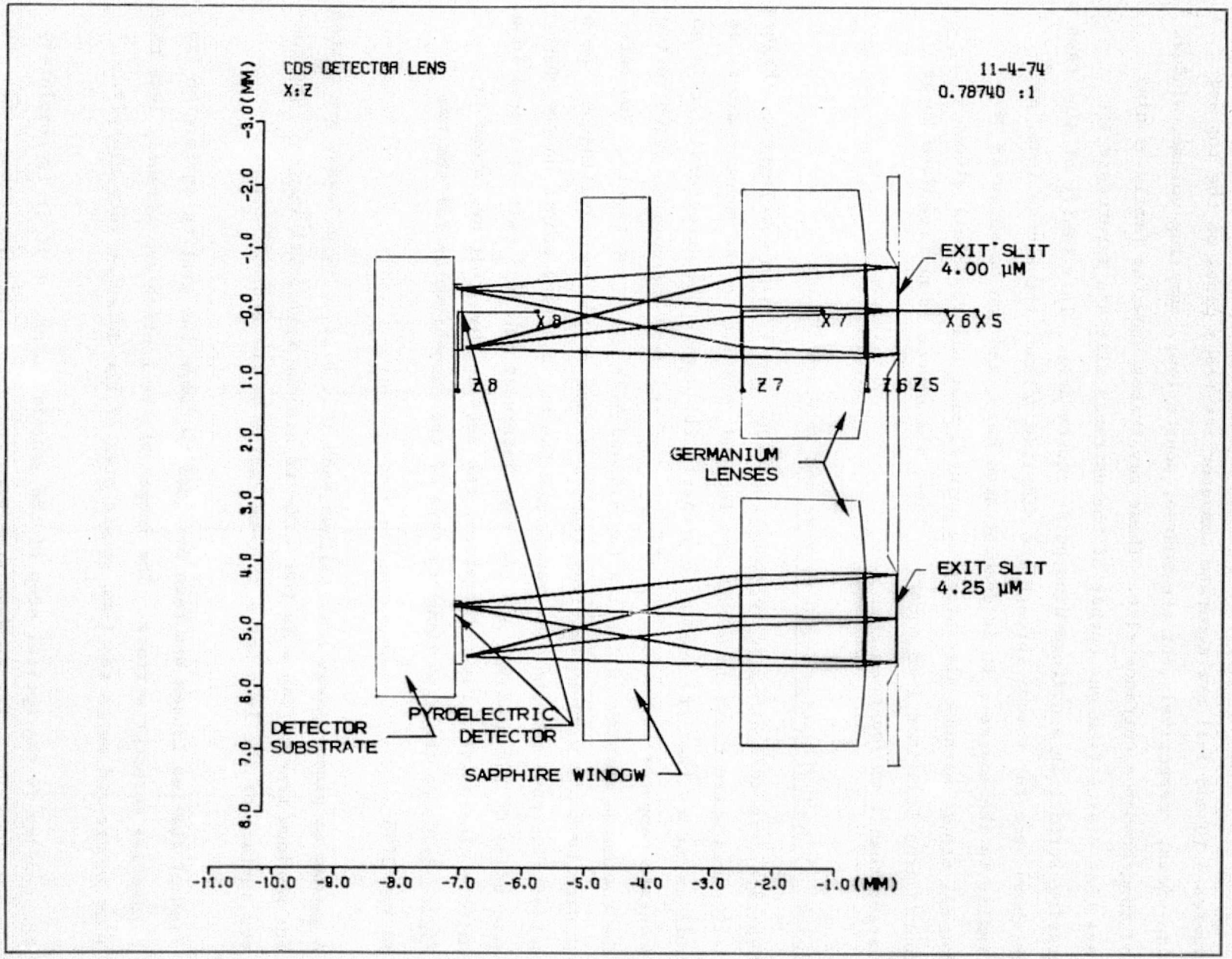

Figure 3-12. Detector Optics Ray Trace (Top View)

monochromator throughput, or radiant transfer, is maximized. Further, when the detector area is the same size or slightly larger than the grating image, then the detector receives a minimum amount of stray light from outside the grating. This is an important stray light reduction feature.

The two detectors are pyroelectric detectors, 1 mm square, mounted on a common substrate, with their spacing defined by the ray trace shown in Figure 3-12.

The pyroelectric detectors must be sealed in a dry inert atmosphere. Therefore, a sapphire window is used to seal the detector in a TO-5 can. Although this sapphire window is illustrated in Figure 3-12, it was not a part of this particular ray trace.

3.5.5 Spectral Energy Transfer

The spectral energy falling on each of the detectors may be determined by equation (3):

$$P_\lambda = \frac{N_\lambda (\Delta\lambda) A_S A_g T_\lambda \tau}{F^2} \text{ (W)} \qquad (3)$$

where

N_λ = Spectral radiance of the source
= 6×10^{-2} W·cm^2·sr·μm for a 700 K true blackbody source at 4 μm

$(\Delta\lambda)$ = Spectral bandwidth
= 0.051 μm

A_S = Entrance slit area
= (0.1 cm x 0.3 cm)
= 0.03 cm^2

A_g = Grating area
= (1.14 cm)^2
= 1.3 cm^2

F = Monochromator focal length
= 4 cm

τ = Chopper period

= 0.5

T_λ = Spectral transmittance of the complete optical system for all coated lenses and windows

= 0.4

Then, substituting the coefficients for 4 μm,

$$P = \frac{6 \times 10^{-2} \times 0.051 \times 0.03 \times 1.3 \times 0.5 \times 0.4}{(4)^2} \text{ W}$$

$$= 1.46 \times 10^{-6} \text{ W}$$

The signal-to-noise ratio (SNR) is defined thus:

$$(SNR)_\lambda = \frac{P_\lambda}{(NEP)_\lambda}$$

where $(NEP)_\lambda$ is the noise equivalent power for the detector. The poorest performing of the two pyroelectric detectors had an $(NEP)_\lambda = 3.9 \times 10^{-10}$ W at the 10-Hz operating frequency, so:

$$(SNR)_\lambda = \frac{1.48 \times 10^{-6}}{3.9 \times 10^{-10}} = 3820$$

for this detector.

This SNR is computed for a true blackbody source. It must be derated by the true emissivity of the real source and the modulation efficiency of the source.

3.5.6 Source

3.5.6.1 Candidate Sources

The source represents a major portion of the remaining effort where significant design and progress must be made to proceed to the flight hardware. It largely controls the total amount of power to be consumed, directly affects the SNR, and is a latent hazard.

Obtaining an adequate source proved to be a very time-consuming and difficult task. The only deviations from the theoretical design of the breadboard CDS were the result of problems associated with the source. At the outset, we expected to use either one of Beckman's several off-the-shelf sources or a commercially available one. However, the source we finally used was a modification of a newly developed commercial Beckman source.

During the concept study, the available sources were evaluated against the basic requirements listed below:

- Extremely small
- Long life >> 1000 hours
- Ac or dc mode
- Adequate energy at 4.0 to 4.5 μm
- Available or require only small development effort
- Low power < 1 W
- High resistivity-high efficiency power conversion
- High emissivity

It was decided to use a pulsed modulation source in preference to mechanical chopping to enhance reliability, reduce complexity, and obtain the advantages of ac signal processing. Ten hertz was chosen as a nominal modulating frequency, based on previous experience with sources. Pulsing at higher frequencies would result in reduced output signals, because there is insufficient time for the filament to cool to almost zero emission.

The types of sources investigated were:

- Injection laser diodes
- Commercially available incandescent sources
- Beckman developed flat blackbody source
- Barnes developed flat platinum source
- Beckman developed Kanthal wire filament
- Beckman developed tungsten-rhenium filament

Injection Laser Diode — The small size of light emitting diodes (LED) would make them extremely attractive for the CDS. However, the output wavelengths of the LEDs are only in the near infrared to approximately 900 nm, which precludes their use. There are injection laser diodes available with output wavelengths up to 8.5 μm. Of these, the PbS crystal diode with output at 4.3 μm looked attractive as has been described in the literature. Personnel at RCA and the Lincoln Laboratory at the Massachusetts Institute of Technology were contacted for state-of-the-art developments. Unfortunately, these diodes only lase at liquid helium temperature, as was suspected, and cannot be considered for the CDS.

Commercial Sources — Commercially available sources were evaluated as to their suitability for the CDS. This search did not produce a source that passed the basic requirements. Size and power consumption (< 1 W) could not be met. None of the commercial sources were therefore selected for flight application in the CDS.

Flat Blackbody — The construction of the Beckman proprietary blackbody source is as follows: An alumina substrate, as well as the resistance terminations, are first silk screened with low resistance conductive leads. These are then vitrified in a high temperature furnace. The resistance elements are then screened and the unit again fired. The result is a monolithic alumina structure with the conductors and the resistance elements integral with that substrate. The emissivity of the structure can be improved by the addition of overcoats of glass frit and carbon.

Sources of this type operating at levels between 15 and 20 W have been used in commercial instruments for approximately five years. The reliability has been excellent and scaling down to 1 W is feasible. However, the thermal mass is too large to operate in a pulsed mode at 10 Hz.

Flat Platinum Source — This source was developed by Barnes Engineering in 1970 for a Miniature Carbon Dioxide Sensor and seems to have the required characteristics. The source consists of a selected, smooth mica substrate with platinum

evaporated on the front surface and gold on the back surface. Time constants of 50-70 ms reportedly have been measured for this source. Barnes was contacted for more information. Unfortunately, no further work after the initial contract had been performed and the exact manufacturing procedures were not available. This source was ruled out as a candidate because more work would have to be performed, especially with respect to manufacturing technique, and it could not be obtained in time for use on our breadboard.

Filament Sources — Beckman has extensive experience in thermal source design and performance from the company's commercial nondispersive infrared instruments and from the development program of submarine nondispersive gas analyzers. These sources consist of filament coils wound with Kanthal or tungsten-rhenium wire. Of the various sources investigated, it seemed that one of this type would be more likely to meet our needs. Several of these sources were specifically manufactured and tested for this application.

3.5.6.2 Source Testing for Concept Study

The objective of the source testing was to determine whether the desired source characteristics could be obtained with the proposed Kanthal and tungsten-rhenium sources. Specifically, the following tests were performed:

- Verification of peak wavelength (750 K, 4.0 μm) versus input power.
- Frequency response of the filament sources (0 to 100 Hz).
- Power consumption verification (~1 W).

The filaments manufactured and tested were coiled Kanthal A-1 wire (0.0025 mm diameter) and tungsten rhenium coiled (0.038 mm diameter).

Peak Wavelength Test — The filaments were first assembled and sealed in a source block with a sapphire window. The source was then evacuated and backfilled with 700 torr of helium. Helium was used because of its high thermal conductivity. The source was then placed in a Beckman IR 20 Infrared Spectrophotometer, dc power was applied to the filament, and the radiation versus wavelength was measured. From published blackbody curves, a filament temperature of about

750 K is needed to provide maximum radiation at about 3.9 μm. Voltage and currents were measured to heat the source to 750 K.

Typical values for the tungsten-rhenium filament are:

Voltage	Current	Wavelength Maximum (μm)
10	-	3.7
9	-	3.75
7	360 mA	3.8
6	340	3.85
5	318	3.92
4	285	4.08

Frequency Response — The source was then assembled in a test system with a PbSe (lead selenide) detector that had been tested using a chopper-type system to prove that the detector and electronics had a response time of less than 1 ms. (Response times of 0.1 s are expected for the sources.) A square-wave potential was applied to the source filament starting with a frequency of 1 Hz. The voltage applied was set at the value determined to produce about 750 K filament temperature. The pulsing frequency was increased in steps (usually 1, 2, 4, 8, and 16 Hz) and the detector response for constant source potential was determined. Relative response versus frequency for the sources is shown in the graphs of Figure 3-13.

Source Emission — A second series of tests was performed to determine source output at each frequency when the applied potential was adjusted so the maximum filament temperature remained constant. The applied potential, the current drawn, and the emission characteristics are shown below.

Tungsten-Rhenium

Frequency (Hz)	Voltage	Average Current (mA)	Detector Amplitude
2	8	450	21
10	8.7	500	20
16	-	-	18

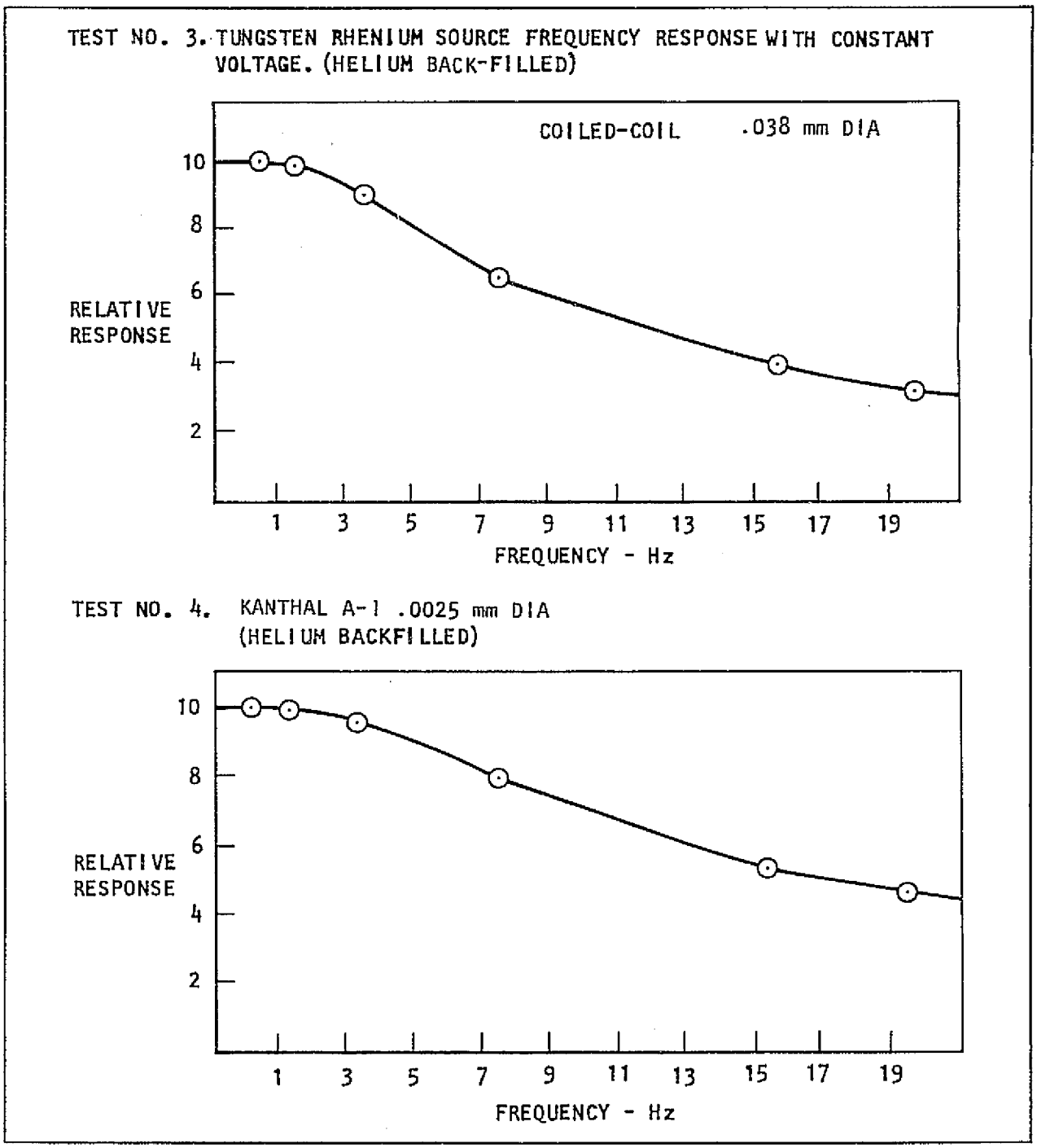

Figure 3-13. Frequency Vs. Relative Response for Sources in Tests #3 and 4

Kanthal

Frequency (Hz)	Voltage	Average Current (mA)	Detector Amplitude
1	10	200	19
4	10	200	19
10	10	200	19
16	11	210	18
100	13.5	240	9

It is seen from this data that the response starts to fall off above 10 Hz. The tungsten assembly also showed evidence of a tungsten-type film building up on the window. The typical waveforms over the range of pulsing frequencies are shown in Figure 3-14.

3.5.6.3 Source Selection

As a result of our investigation of all the available sources, it was concluded that either the Kanthal or the tungsten-rhenium would be suitable for the CDS system. The Beckman flat blackbody and the Barnes flat platinum sources could be considered as remote possibilities.

After receiving approval from NASA to proceed with the design of the dual-wavelength monochromator, the source energy requirements were reviewed. With details of the optical design available, and with detector responsivity, NEP, and a target SNR, the radiating surface area of the source that must be focused into the monochromator was determined. From our analysis it became apparent that the radiating surface area of the available sources was insufficient to provide the energy throughput needed. It was then decided that we should obtain a flat platinum source similar to the one Barnes had used.

As stated earlier, Barnes had not continued development of their source and could not guarantee delivery of one to us. We undertook the design of a source patterned after the Barnes unit. It consists of a vacuum deposited film on a mica substrate. A resistor grid pattern is photoetched to give a heating element of about 50 ohms resistance. The mica chip is suspended with four gold wires in

Waveforms of Source Output Versus Pulse Frequency

(Kanthal A-1, 18 turns)

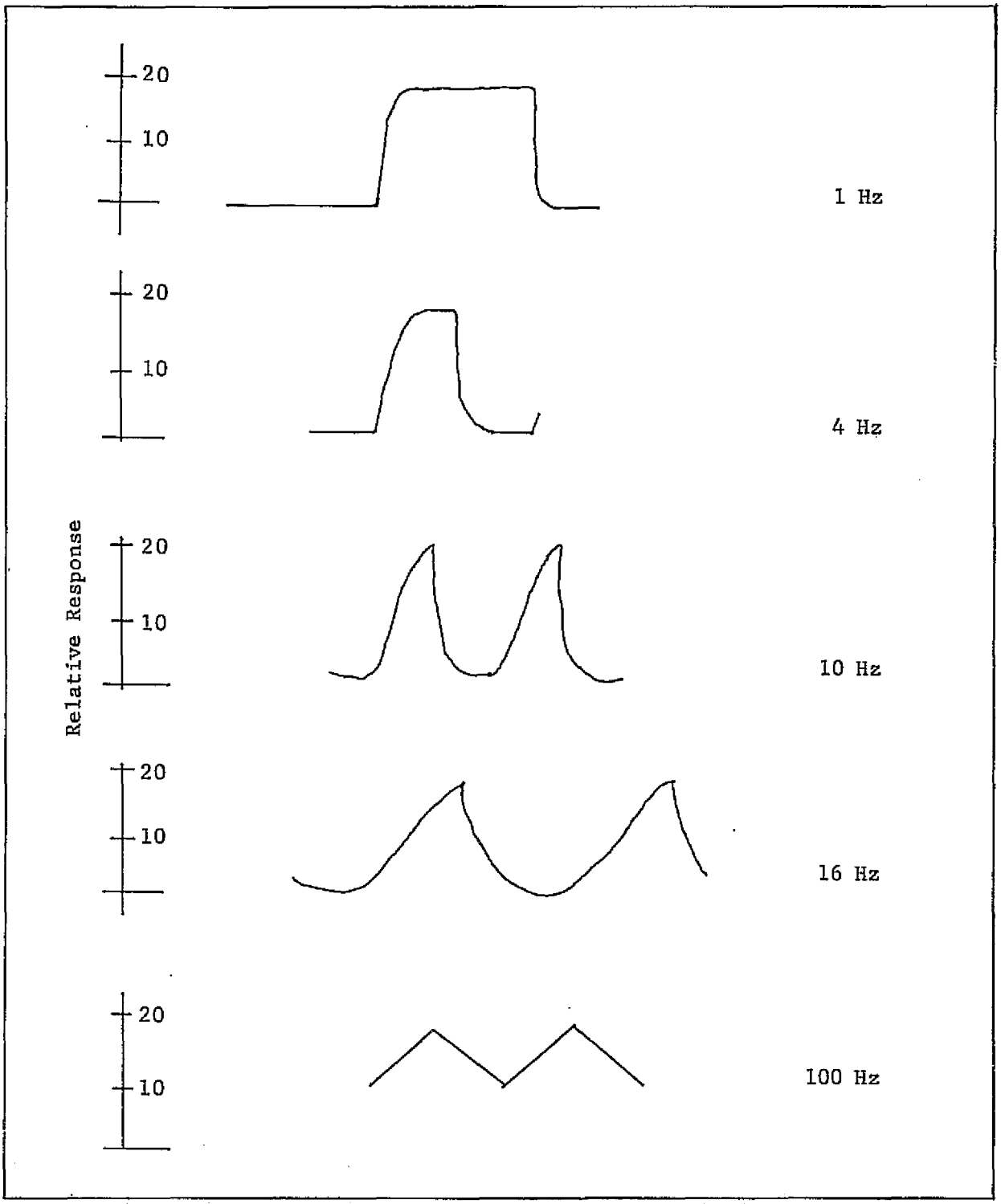

Figure 3-14. Relative Responses for Source in Test #6

a TO-5 size cup. The grid pattern is shown in Figure 3-15. The completed assembly is shown in Figure 3-16.

In making the source assembly, it was necessary to work with several vendors. This proved to be very time consuming and few assemblies were finalized for testing. Because the vendor responsible for depositing the film was unable to achieve satisfactory adherence with platinum, nichrome was substituted. Five nichrome sources were tested. They were not sufficiently durable to last for more than a few hours and had poor emissivity. The nichrome tended to lift from the mica and curl on the edges with thermal cycling. Without additional test pieces it is difficult to say whether this is primarily due to poor adhesion or destruction from differences in the thermal coefficient of expansion. It was found that satisfactory heating and cooling could be obtained at 10-Hz cycling to produce acceptable modulation, but useful life was limited.

As it had not been planned to develop a completely new source for our breadboard, our inability to assemble a satisfactory one in a limited time required a re-examination of available commercial units. Fortunately, a newly developed source was available that was relatively small and had relatively low power requirements. The size and weight are too gross for ultimate use but, since the energy output is satisfactory, a compromise was made for its use with the breadboard. This source consists of a compound wound helical coil of tungsten that is viewed end on. The coil is mounted in a parabolic reflector with a sapphire window. A hydrogen atmosphere is used to increase the rate of cooling. The unit is fabricated from a brass block and uses about 1.5 W.

3.5.6.4 Source Development Problems and Solutions

The fundamental problem with the source is to obtain a greater radiating surface area that can be focused into the monochromator. The flat configuration offers an obviously attractive solution to this problem. However, there are three primary problems identified with the flat source we attempted to develop: poor adhesion of the film to the mica, low emissivity, and fragility of the gold lead wires. We are confident that these problems can be solved if specific development effort is directed to them.

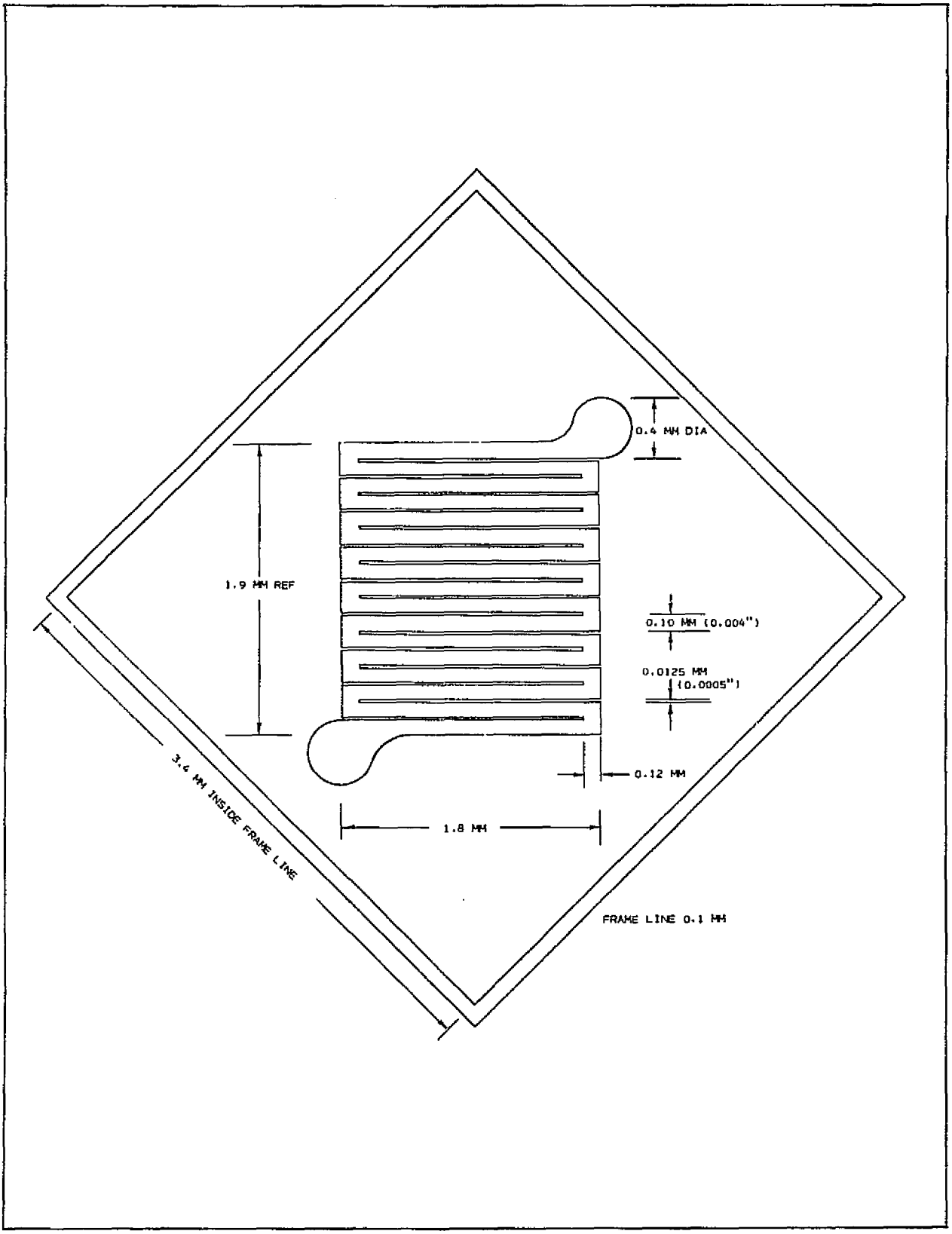

Figure 3-15. Source-Resistive Grid Pattern

Figure 3-16. Assembled Source

If the resistive film cannot be made to withstand the thermal cycling, an alternative configuration that would offer an enlarged area could be tried. Several possibilities for this have been envisioned. The gold lead wires that were used were one mil in diameter. This size was chosen to minimize the conductive heat loss from the resistive grid. It is likely that a two-mil wire could be used satisfactorily to give adequate strength without significantly increasing the power consumption. Low emissivity is a problem common to most resistive heating element sources. Both platinum and nichrome are particularly poor in this respect. Coatings are required to raise the emissivity from about 0.1 to the 0.7 to 0.8 level that is necessary to efficiently use the power applied. High temperature paints and carbon black deposits have been used for this purpose. A new technique, called the dark mirror, offers the possibility of increasing the emissivity without substantially affecting the thermal mass. An investigation of these alternatives should result in a source that will meet the requirements of the CDS system.

3.5.7 Detector

3.5.7.1 Detector Selection

Sensitivity, speed of response, spectral bandpass, and noise equivalent power (NEP) are key factors in detector selection. Of the four primary parameters, spectral response--the manner in which signal varies with wavelength--appears most basic. In the region of 4 μm, only the thermal detectors have the required uniformity in energy absorption and responsivity. Thermistor bolometers, thermopiles, and pyroelectric detectors fall into this category. Restrictions in electrical power and a wide operating temperature range make the implementation of thermistors and thermopiles difficult. Both require some form of electronic chopping in addition to the source modulator to eliminate electronic offset and drift with respect to temperature. Pyroelectric detectors, although not as sensitive as thermopiles, offer several important advantages over the other types of thermal detectors. They do not require an external bias supply, cooling, or electronic chopping.

The choice was based on the smaller thermal coefficient of sensitivity exhibited by pyroelectric detectors (manufacturers' data) compared to that of thermistors. The transfer characteristics analysis indicates that thermistors have a thermal coefficient of 1%/°C, which is about five times that of the chosen pyroelectric detectors.

Various types of materials were considered for the pyroelectric detectors. These included triglycene sulfate (TGS) (doped and undoped), strontium barium niboate (SBN), and lithium tantalate ($LiTaO_3$). These materials are grouped roughly according to their Curie temperature--the Curie temperature of TGS being the lowest, with a value of 45-50°C. $LiTaO_3$ has a Curie temperature of about 500°C, while SBN has a Curie temperature of about 130°C. Since temperature in the Backpack can exceed 50°C, TGS has been ruled out as a candidate for pyroelectric detectors. $LiTaO_3$ has several advantages over SBN. It is less susceptible to shock and vibration damage, it has lower loss tangent noise, and it is somewhat easier to handle than the other materials. Therefore, $LiTaO_3$ was selected as the candidate material for the detectors. The design parameters sought for the pyroelectric detectors are listed in Table 3-4.

*TABLE 3-4. DESIGN REQUIREMENTS FOR THE DETECTOR ELEMENT**

Specification	Value	Units
Wavelength	4 to 4.3	μm
Element Size	1.5 x 1.5	mm
Current Responsivity	1.1×10^{-6}	A/W
Absorption Coefficient	0.9	-
Temperature Range	-40 to +75	°C
Temperature Coefficient of Current Responsivity	0.2	%/°C
Detector Capacitance	20	pF
Thermal Time Constant	0.5	s
Chopping Frequency	10	Hz

*Laser Precision

Table 3-5 is a comparison of the current responsivity of the two candidate devices.

TABLE 3-5. PYROELECTRIC DETECTOR COMPARISON. The devices shown are discrete elements in a TO-5 transistor case.

Parameter	Laser Precision KT-4130	Molectron P1-13
Active Area	0.07 cm^2	0.07 cm^2
Thermal Time Constant	4.0 ms	0.5 s
Current Responsivity	1.2×10^{-6} A/W	1.1×10^{-6} A/W
Capacitance	88 pF	54 pF

Table 3-6 is a comparison of voltage responsivity at a chopping frequency of 10 Hz ($\omega\tau$ = 62.83 r/s).

TABLE 3-6. VOLTAGE RESPONSIVITY OF CANDIDATE DEVICES

Device	C_D pF	τ_T S	$j\omega\tau_T/(1+j\omega\tau_T)$	R_o A/W	$(R_i)_\lambda$ A/W	$(R_V)_\lambda$ V/W
KT-4130	88	40×10^{-3}	0.929	1.2×10^{-6}	1.1×10^{-6}	199
P1-13	54	0.5	1	1.1×10^{-6}	1.1×10^{-6}	324

Equation (4) is used to calculate $(R_V)_\lambda$

$$R_V(j\omega) = R_o \frac{\tau_T}{(1+j\omega\tau_T)C_D} \qquad R_i(j\omega) = R_o \frac{j\omega\tau_T}{(1+j\omega\tau_T)} \qquad (4)$$

where

R_o = current responsivity
C_d = detector capacitance
τ_T = thermal time constant
R_i = current responsivity versus frequency

The two detectors differ in only one significant regard. The Molectron device has a much larger thermal time constant. This should lead to more predictable performance at 10 Hz, or lower, chopping frequency.

Our experience with Molectron detectors has been quite good. Because of chopping at 10 Hz, we chose Molectron for improvements in several areas:

- Smaller area, hence less capacitance and greater responsivity;
- Detectors are coated to enhance absorption;
- Less reactive noise current.

3.5.7.2 Detector Assembly

The detector assembly is housed in a standard TO-5 transistor case. It is a hermetically sealed unit containing a sapphire window at one end and eight hermetically sealed leads extending through the base. The inside of the can contains two pyroelectric detectors with the dimensions shown in Figure 3-17. They are located on 4.98-mm centers. These detectors are represented as a current source shunted by a capacitor. Along with the two detectors are two (dual) FETs. They are selected for low gate-to-drain leakage current and low noise at the chopper frequency of about 10 Hz. The FETs and the resistors connected to the gates of the FETs form the input stage of the preamplifier and feedback networks, respectively. The sapphire window was chosen for its ease of fabrication and high transmission at 4.3 μm. The FETs and feedback resistors are integrated with the detector chips to provide the least amount of shunt capacity across the detector.

Having these high impedance components close to the detector chip has the further advantage of reducing extraneous noise produced by vibration, i.e., decreasing the possibility of having a microphonic assembly. The two dual FETs are selected from a family of low noise devices manufactured by Siliconix. The type selected is a U421. It has the following current characteristic: I_{GS} = 0.1 pA. The TO-5 housing containing the two pyroelectric detectors and FETs is mounted on a glass epoxy printed circuit board that is then interconnected with the preamplifier assembly.

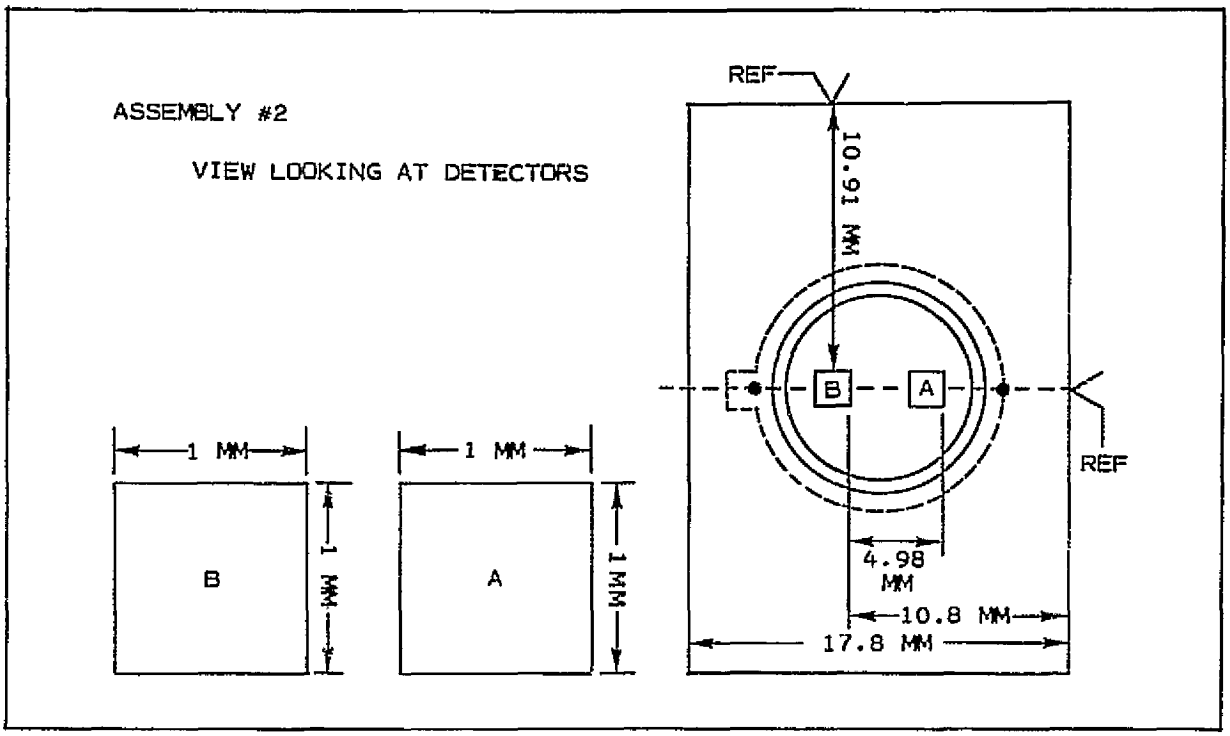

Figure 3-17. The Two Pyroelectric Detectors Used in the Detector Assembly

Detectors received from Molectron show current responsivity at 10 Hz very close to the actual calculated value of 1.1×10^{-5} A/W (being 1.10 and 1.2×10^{-6}). The NEP (without offset) of the Molectron detector was determined to be 3.9 and 3.2×10^{-10} W, which was below the calculated value of 4×10^{-10} W (see SNR discussion in Subsection 3.3). Copies of the vendors' calibration work sheets are provided in Appendix C.

3.6 Mechanical Design

An important consideration in selecting the monochromator concept to be developed was our high level of confidence in our capability to design and build an extremely compact an d reasonably lightweight unit. We did not anticipate any mechanical or mechanical-optical design problems and we did not have any.

anticipate any mechanical or mechanical-optical design problems and we did not have any.

3.6.1 Optical Mounting

The optical design provides precise dimensions for locating all the optical elements. The mechanical design is directed toward retaining all the advantages of the precision of the optical design. This means that all optical elements are mounted without adjustment within a one-piece frame. The material for the frame should not be affected by temperature changes and the entire mechanical-optical structure should then be housed so as to isolate it from external stresses and environmental conditions.

This design philosophy has been carried out in the CDS monochromator design. An Invar* frame was machined from a solid block to provide a dimensionally stable support for the optics. The spherical seat for the collimating mirror was precision machined and lapped directly on the frame per the computerized ray trace. A beryllium-copper wave spring loads the mirror against its seat. The grating is located by two mounting surfaces that control the angularity and perpendicularity of the rulings. The grating is clamped against these surfaces and subsequently bonded into place. The entrance and exit slits are initially located at theoretical positions from the optical center line. After optimizing their location, the retaining screws are permanently tightened.

3.6.2 Housing Design

An aluminum housing is used to provide environmental protection and seal out all carbon dioxide from the optical path. The aluminum housing also provides the mounting interface for the source and detectors. Once the assembly is checked out for optical alignment and signal throughput, the back cover is electron beam welded. There are no internal parts that can get out of adjustment and no maintenance should be necessary throughout the life of the CDS.

---

*Low-expansion steel (see paragraph 3.8.4)

3.6.3 Sample Flow

The sample path is provided by the opening between the source window and the entrance slit and is 12 mm long. As the response of the CDS is almost instantaneous to a change in gas concentration, the sample flow is baffled to provide an averaging of the CO_2 concentration in the expired breath. This baffling provides protection of the windows exposed to the sample gas. Contaminants such as lint, hair, saliva, and desquamated epithelial cells are kept out of the sample path. Ample openings are provided so that gas diffusion can occur to achieve the necessary speed of response to increases in CO_2.

3.6.4 Structural Analysis

Due to the smallness and light weight of the components of the sensor assembly, no structural problems are anticipated. To illustrate the parameters and magnitudes involved, an analysis of the grating mounting and structure is presented. The grating is bonded to the main optics mounting frame. In order not to disturb the precise relationship of machined surface and grating plane, no bonding material is introduced in between. Instead, relief cuts into the contact area accommodate a minimum amount of epoxy that, in turn, anchors the grating to its mount after the grating has been precisely fixtured into location.

- Weight of grating: Density of material--2.5 g/cc
  Volume 1/2 cc
  Weight 1.25 g
- Contact area: a. 12.5 x 3.5 mm = 43.75 mm^2
  uncemented contact 2(3x3.5) = 21.00
  bonded area = 22.75 mm^2
- Bond strength: b. 365 lb/cm^2, or
  165 g/cm^2
- Bond strength for given area: $\frac{b}{a} = \frac{165}{22.75} = 7.25$ kG (16 lb)

This provides a safety factor of over 100 for the g forces exerted by the shuttle vibration specification.

It is of extreme importance that all optical elements of the monochromator assembly hold dimensional stability to about 150 millionths of an inch. As previously explained, original locations and dimensions are established by computerized ray tracing.

It is, therefore, very important to select a stable material that will at the same time have a very low thermal coefficient of expansion. We also have a very difficult weight target; thus, it is also necessary to machine all sections to minimum thicknesses without losing strength and introducing deformation during installation.

A most suitable metal covering all these requirements is Free Machining Invar 36. The material has the following pertinent physical characteristics:

- Density — 8.0 gm/cm^3 (0.291 $lb/in.^3$)
- Coefficient of thermal expansion — 25° to 100°C = 1.6 $cm/cm/°C \times 10^{-6}$
- Tensile strength — 4.5×10^5 kPa
- Yield — 2.8×10^5 kPa

To further enhance dimensional stability, the parts go through a heat treatment process before final touch-up; i.e., removal of no more than .0013 cm to final dimensions.

The material characteristics plus stabilization allow maintenance of sectional thicknesses that permit the manufacture of the components with equivalent or less weight than if they were made of aluminum and, of course, without the disadvantage of aluminum's rather large coefficient of thermal expansion.

3.6.5 Non-Metallic Materials

All non-metallic materials we expect to use are space-approved and/or have been used in actual space hardware such as the Backscatter Ultraviolet Spectrophotometer for Nimbus 4 and the Gas Chromatograph/Mass Spectrometer for the Mars Viking Lander.

- Optical components are fabricated from Pyrex (front surface mirror) and sapphire or germanium (lenses and windows).
- Plastic materials belong to the fluorocarbon TFE and polyimide family: Vespel (duPont) is used for insulating structural parts or precision spacers; Fluorocarbon (Teflon*) is used for insulating material on wires or for semi-resilient spacers.
- Ceramic (alumina) is present as a wafer substrate within the detector assembly. Mica mineral will be used for the source element substrate.
- Minute amounts of epoxy are used for retaining some of the optical components (see grating mount analysis). The epoxy presently considered is a Hysol No. 0151 formulation. The total amount is approximately 16 mm^3.

3.6.6 Size and Weight

The volume of the sensing element is 89.9 cm^3 (Figure 3-18). This is greater than the 20 cm^3 design objective. However, preliminary checks at NASA show this volume, based on dimensions of 87 x 40 x 25 mm (3.4 x 1.6 x 1 in.) can be placed within the spacesuit configuration being studied. A reduction in volume cannot be made without impairing sensor performance

The weight objective of 32 g as stated in the specification seems unlikely to be attained. The following is a calculated estimate of the unit by major components:

Optical base	- 26 g
Housing	- 18
Electronics	- 25 (cable and connector excluded)
Collimating mirror	- 4.5
Grating	- 2.5
Slits	- 2
Windows	- 5
Hardware	- 5
TOTAL	88.0 g

*A registered trademark of the duPont Company

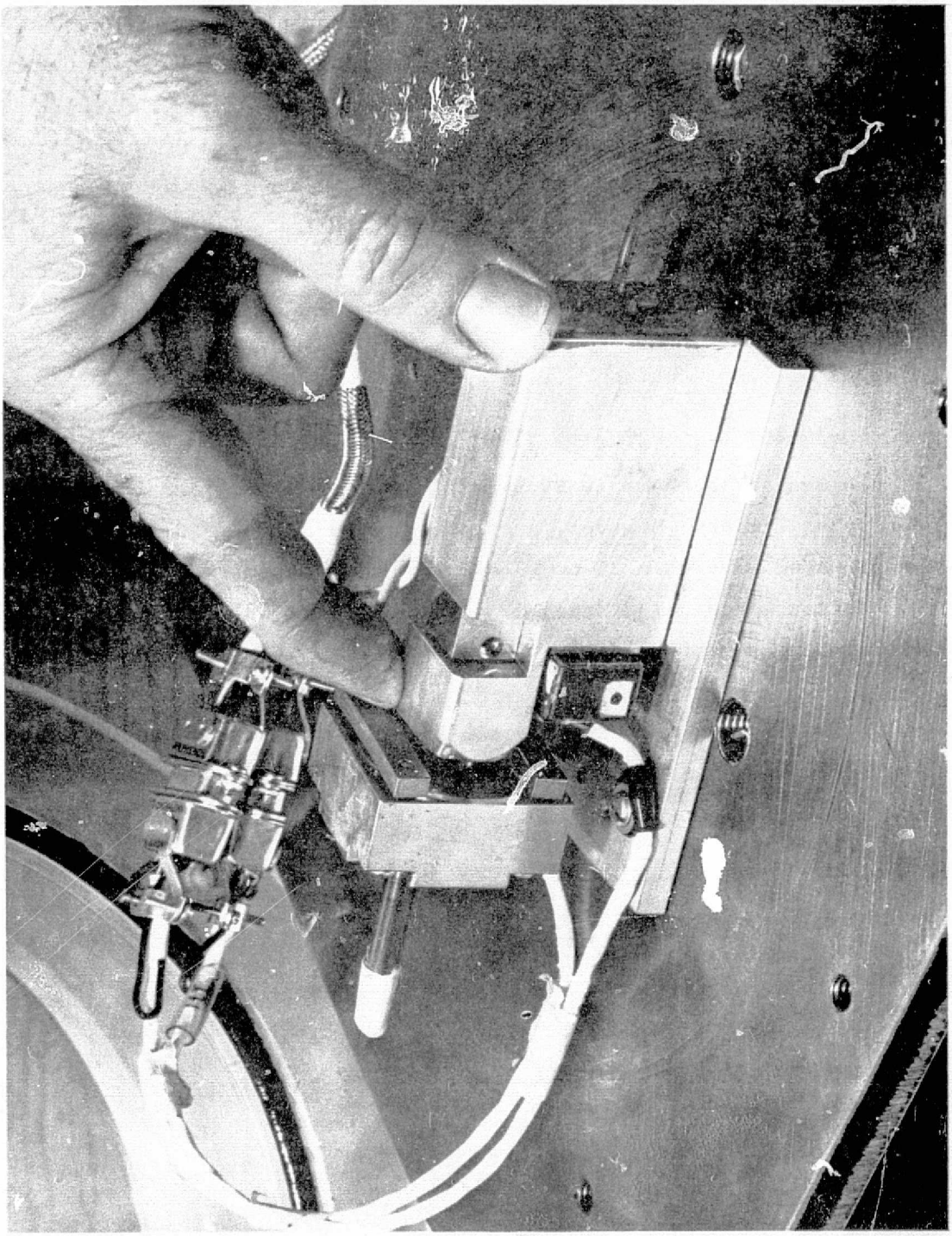

Figure 3-18. Sensing Element--CDS Breadboard

In reviewing the design of the total assembly and components, significant possible weight reduction cannot be achieved without jeopardizing overall performance and reliability, and/or incurring a substantial cost increase.

The actual weight of the breadboard sensing element is 120 g. This does not include the cables or any of the external electronics. For the breadboard assembly, the sensing element is the only part where effort was directed toward achieving minimum weight. There are some extra parts and weight in the breadboard that can be removed to reduce the weight to the expected value of 88 g.

3.7 Quality Assurance

The quality controls maintained on the CDS Program were commensurate with the objective of developing a measurement principle and fabricating and testing a breadboard system. While maintaining an overview of the design effort, purchase orders were reviewed, although neither Mil-Spec parts nor certifications were required. Close inspection of all fabricated parts was performed to ensure compliance with the drawing requirements.

The existing design does not appear to have any inherent deficiencies that would prevent the implementation of standard aerospace quality measures during continued development of flight-qualified hardware.

3.8 Reliability and Safety

The reliability and safety effort conducted during the CDS Program was directed toward verifying that the design approach allows for implementation of appropriate reliability and safety requirements during the flight development phase. The breadboard instrument has achieved this objective. Although further work is required to develop a reliable low power-high emissivity source and to package the electronics, these are reasonably straightforward problems compared to the monochromator development.

The potential safety problem of heat generation from the source has been given consideration and we are confident that the source finally selected for the sensor will not produce excessive housing temperatures.

4.0 FABRICATION PHASE (SOW Paragraph 3.2.3)

4.1 Purpose and Scope of Task

The objective of this phase was to prove the merits of the selected measuring concept by building a breadboard or prototype suitable for testing against the contract performance requirements. This phase would also disclose any problems with the machining or assembly processes used.

4.2 Results Obtained

No significant manufacturing problems were encountered in making our breadboard assembly. Beckman has considerable experience in manufacturing optical instruments for space application.

The monochromator involves critical machining tolerances in several areas. These were satisfactorily accomplished and the completed assembly did not need any adjustment.

No attempt was made to reduce the electronics to a high density package in this phase--this capability has been well demonstrated. It was more important to provide access to all portions of the electronic circuitry.

The fabrication phase has already shown that a flight package can be produced.

5.0 TEST PHASE (SOW PARA. 3.2.4)

5.1 Purpose and Scope

The Development Test Plan (see Appendix D) is in accordance with the requirements of paragraph 3.2.4.1 of the Contract Statement of Work. The plan and procedures detailing the conduct of the tests were designed to demonstrate the capability of the CDS to meet the performance requirements of paragraph 3.3 of the SOW.

5.2 Description of Test Specimen

The test specimen consisted of a sensing element and separate signal conditioning electronics. The overall system was arranged in a breadboard configuration. The sensing element was reduced in size to show that if development continued to flight-qualified hardware, it could be contained within the oral nasal area of the suit. It should be noted that this is not an optimized design. Laboratory equipment and commercial grade components and circuit elements have been used in some areas where there is no doubt that flight-qualified hardware can be developed.

The monochromator, the dual detector, and other assemblies critical to performance are detailed in the drawings accompanying the CDS breadboard.

5.3 Test Philosophy

The tests described and the resulting test data are intended to be integral elements of the design and development of the CDS. Sufficient testing has been performed to thoroughly verify performance, to surface and evaluate problem areas, and to define any additional development and design changes required to produce hardware meeting the design objectives.

5.4 General Test Requirements and Methods

5.4.1 Environment

Unless otherwise specified, testing was performed under laboratory ambient temperature and pressure conditions.

Many of the tests were performed with the CDS in a heavy-walled Lucite bell jar provided with a silicone vacuum greased, neoprene O-ring gasket and a 1.2-cm-thick, 31- x 31-cm steel baseplate. The internal volume of this bell jar was approximately 1.0 liter. Three ports were available for vacuum and purging connections. A 14-pin hermetic feed-through terminal mounted in the base provided electrical connections for the source and the detectors (see Figures 5-1 and 5-2).

Tests performed in the bell jar included the following: range, accuracy, specificity, and alarm point.

5.4.2 Adjustments and Repair

Early in the testing program it was determined that heat sinking of the source unit was required to prevent excessive drift in signal levels resulting from temperature rise produced by the 1.6-W source power conducted into the monochromator/detector assembly. Before heat sinking, a drift rate of approximately -4.5% of full scale per hour was observed. With the source block provided with a thin coating of thermal grease and clamped to the base plate, the drift rate was reduced to about -0.7% of full scale per hour.

During the course of the measurements a temperature sensitivity of the regulated laboratory power supply used to power the source drive was found to necessitate occasional readjustment of the source supply voltage. For measurement of P_{CO_2} with a reproducibility of ± 0.1 mm, control of the source supply to ± 0.005-V accuracy was found necessary.

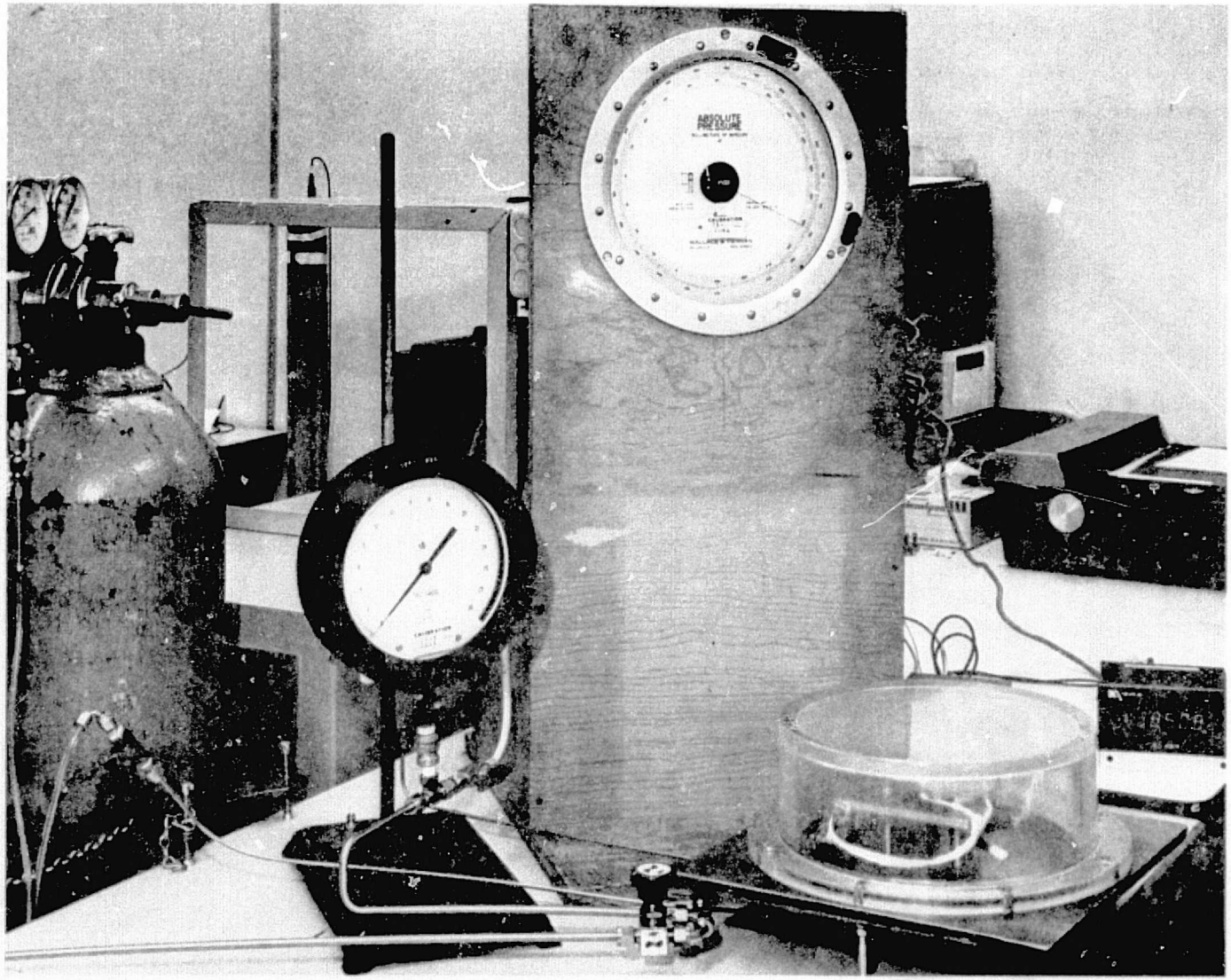

Figure 5-1. Laboratory Test of CDS in Bell Jar

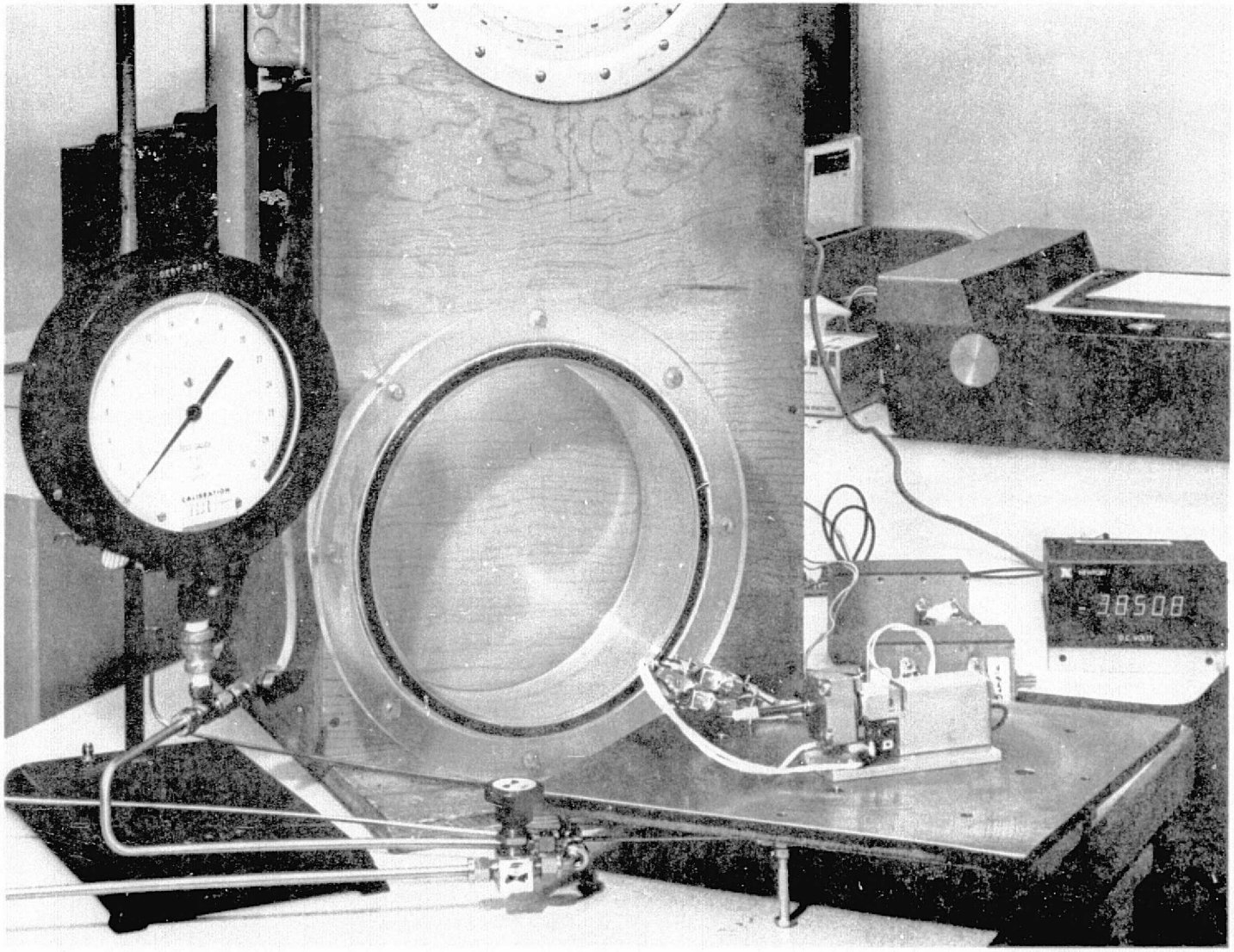

Figure 5-2. Laboratory Test of CDS on Bell Jar Baseplate--Cover Removed

5.4.3 Measurement and Test Equipment

During each test a record was made of all pertinent data. All measurements were performed with instruments and test equipment commensurate with the required precision and accuracy. The serial numbers and calibration data for each test instrument were recorded in the data log. The following test instruments were employed:

- Digital Multimeter: Systron-Donner Model 7004A
- Output Meter (Ratio): Newport 2000 AS-2, A3, E2 (U.S. Government Property ID No. STE-1224)
- Absolute Pressure Gauge: Wallace and Tiernan FA-129 0-800 mm ±0.17 full-scale accuracy
- Pressure Gauge: US Gauge type 18914 101-308 kPa (0-30 psig) ±0.25%

5.5 Testing

5.5.1 List of Tests

- Range
- Accuracy
- Response
- Specificity
- Switch Setting (Alarm Point)
- Power
- Voltage
- Operating Ambient
- Foreign Matter

5.5.2 Procedures

5.5.2.1 Range

The CDS was tested at 27.5 kPa (4.0 psia) over the range from 0 to 4.0 kPa (0 to 30 mmHg) P_{CO_2}. Additional tests at other total pressures (21.3, 37.8, and 127 kPa) extended the range covered to 18.6 kPa (140 mm) P_{CO_2}, as illustrated in Figure 5-3. Detailed data are presented in subsection 5.5.2.2.

5.5.2.2 Accuracy

The CDS was first calibrated with a series of mixtures of CO_2 in nitrogen. The mixtures used were all measured with one instrument, a Beckman Model LB-2

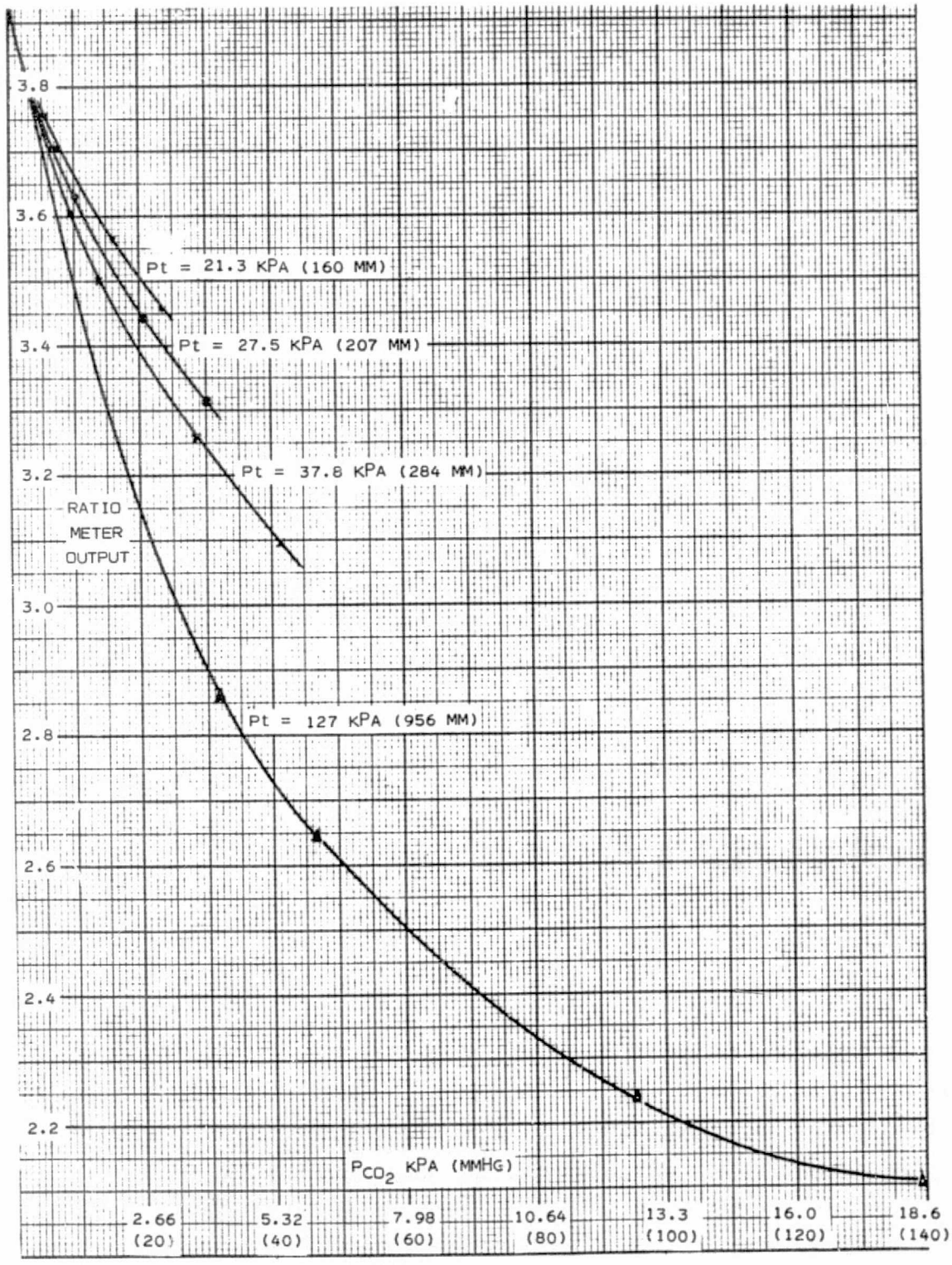

Figure 5-3. Range of Pressures Used in Testing CDS

Medical Gas Analyzer, to provide a common reference. The LB-2 was calibrated with an NBS standard reference material 1674, which is 7.01 ±0.07% CO_2 in nitrogen. The LB-2 is equipped with a linearizer and digital readout, and is accurate to ±0.1% CO_2.

The calibration gas mixtures were analyzed as follows:

Nominal CO_2 (%)	Analyzed CO_2 (%)
5.3	3.25
5.0	4.90
9.7	9.60
10.0	10.13

An additional mixture, required to provide 4.0 kPa (30 mmHg) P_{CO_2} at 28 kPa (207 mmHg) total pressure was blended to an estimated accuracy of ±0.2% at 14.5% CO_2. With these mixtures, the CDS was then calibrated over the P_{CO_2} range of 0 to 4.0 kPa (0 to 30 mmHg). This was done in the Lucite chamber (shown in Figure 5-1) at ambient temperature and at pressures of 21, 28, 38, and 128 kPa (3.1, 4.0, 5.5, and 18.5 psia).

In performing the tests, the values of both the sensing and reference channel dc signals were recorded in the data log in addition to the ratio meter output. An analog recording was made of the sensing channel output on expanded scale. The ratio meter output value is related to the sensing (S) and reference (R) signal values by the expression: Ratio = 4 S/R. Ratio meter output values for the complete range of ambient pressures and CO_2 calibration gas mixtures are shown in Table 5-1.

From this data, a series of drift-corrected calibration curves may be constructed. To present the data conventionally, the normalized difference in ratios between 0.0 kPa CO_2 and the various CO_2 levels has been graphed in Figure 5-4. These curves illustrate the effect of pressure broadening at a given CO_2 partial pressure. For example, at a P_{CO_2} of 1.33 kPa (10 mmHg) with the lowest system pressure of 21.3 kPa (3.1 psig) the output is 44% of full scale. However, with an increase in system pressure to 127 kPa (18.5 psia) the output is 81%. This is a basic, predictable effect, potentially compensatable, at least through the 21 to 38 kPa range of system pressure.

TABLE 5-1. RATIO METER READING OUTPUT VALUES

Elapsed Time (Min)	$\%CO_2$	P(kPa)	(kPa) P_{CO_2}	Meter Reading Ratio	Drift Correction	ΔRatio	Normalized* ΔRatio
0	0.0	0.1	0.0	3.934	-	-	-
4	0.0	127.0	0.0	3.932	-	-	-
11	0.0	37.8	0.0	3.933	0.001	-	0.0
34	3.25	127.0	4.13	2.855	0.001	0.078	174.0
38	3.25	37.9	1.23	3.603	0.001	0.330	53.3
41	3.25	37.5	0.89	3.706	0.001	0.227	36.7
44	3.25	21.3	0.69	3.758	0.001	0.175	28.3
60	0.0	0.6	0.0	3.933	0.001	-	0.0
66	4.90	127.0	6.24	2.642	0.001	1.291	209.0
69	4.90	37.9	1.85	3.499	0.002	0.433	70.0
71	4.90	27.5	1.34	3.631	0.002	0.301	48.6
73	4.90	21.3	1.04	3.704	0.003	0.227	36.7
92	0.0	0.3	0.0	3.930	0.004	-	0.0
98	10.1	127.0	12.8	2.275	0.004	1.655	267.0
100	10.1	37.8	3.83	3.253	0.004	0.677	109.0
101	10.1	27.5	2.79	3.439	0.004	0.491	79.3
102	10.1	21.3	2.15	3.560	0.004	0.370	59.8
141	0.0	0.1	9.0	3.929	0.005	-	0.0
151	14.5	127.0	18.5	2.103	0.005	1.826	295.0
154	14.5	37.9	5.49	3.092	0.005	0.837	135.0
159	14.5	27.5	3.99	3.310	0.005	0.619	(100.0)
162	14.5	21.3	3.09	3.452	0.005	0.477	77.0
199	0.0	0.1	0.0	3.928	0.006	0.000	0.0

*Δ Ratio is the difference in the signal ratio (4S/R) between the test P_{CO_2} value and the 0 kPa P_{CO_2} value. Normalized Δ Ratios are calculated on full scale being 3.99 kPa (30 mmHg) P_{CO_2} at 27.5 kPa (207 mmHg) total pressure.

For calibration at one pressure condition, the ratio output for one test series (≈1000 hr 7/17/75) has been plotted in Figure 5-5.

To determine the reproducibility of the output, two additional series of measurements were carried out at the same total pressure, 28 kPa (207 mmHg). The CO_2 partial pressure corresponding to these tests were then read from the calibration curve of Figure 5-5, and the results are shown in Table 5-2.

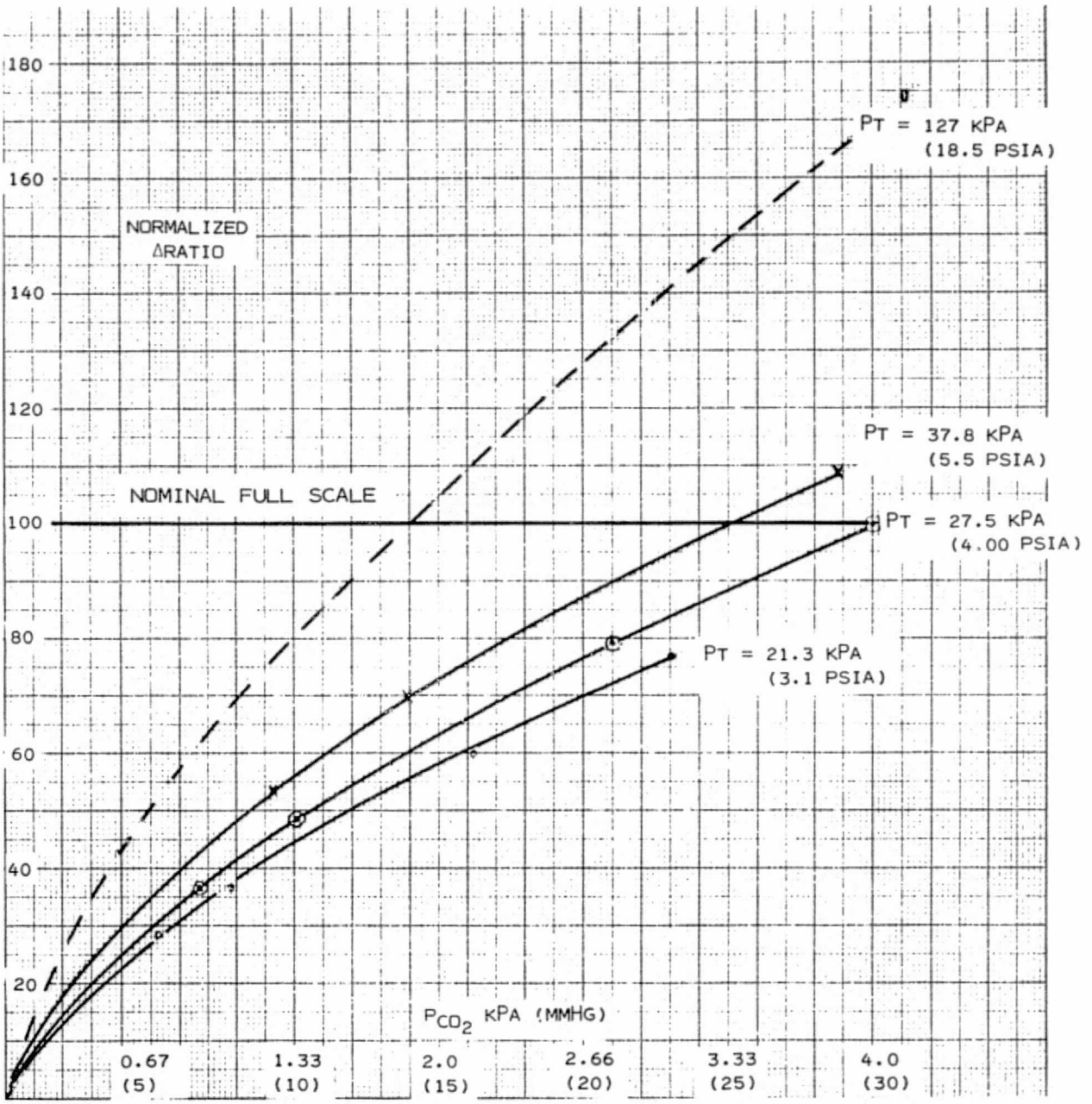

Figure 5-4. Normalized Difference in Ratios Between 0.0 kPa CO_2 and Various CO_2 Levels

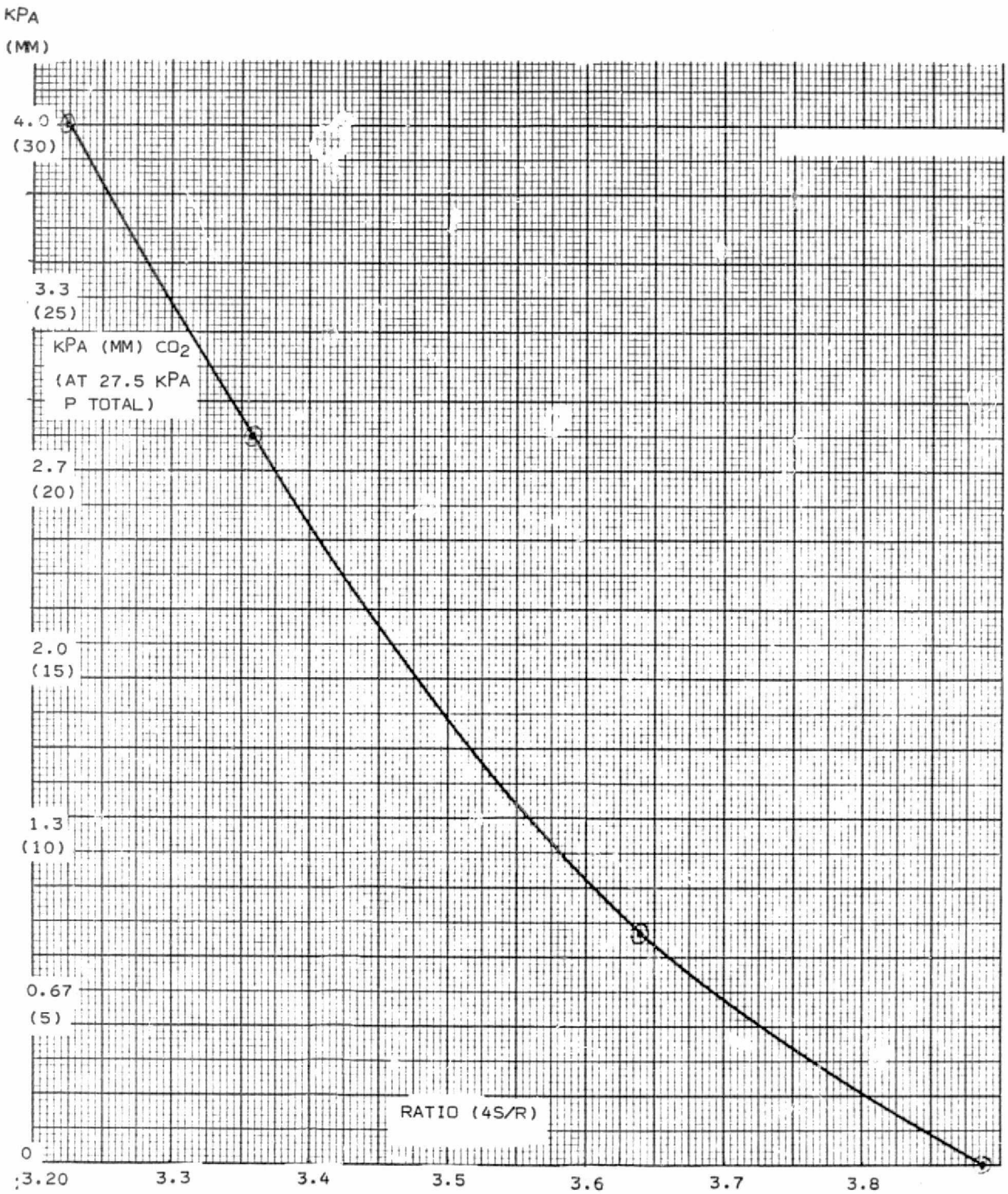

Figure 5-5. Ratio Output for One Test Series

TABLE 5-2. RATIO OUTPUTS FOR REPRODUCIBILITY TEST

$\%CO_2$	Calibration Gas		Ratio (=1000 hr 7/15)	Report 1600 hr 7/15			Report 0930 hr 7/16		
	kPa	(mm)		Ratio	kPa	($mmCO_2$)	Ratio	kPa	($mmCO_2$)
0.0	0.0	(0.0)	3.887	3.861	.08	(0.6)	3.873	.04	(0.3)
3.25	0.90	(6.75)	3.640	3.616	1.01	(7.6)	3.628	.96	(7.2)
10.1	2.80	(21.0)	3.359	3.330	3.03	(22.8)	3.346	2.90	(21.8)
14.5	3.99	(30.0)	3.223	-	-	-	-	-	-

Thus, without applying a correction for zero shift, the error at 1.3 kPa CO_2 (10 mmHg) P_{CO_2} was +0.24 kPa (1.8 mmHg) CO_2 at 6 hours after initial calibration, and +0.10 kPa (0.8 mmHg) CO_2 nearly 24 hours following calibration. If a zero correction is applied, these errors become +0.16 kPa (1.2 mmHg) and 0.08 kPa (0.5 mmHg), respectively. Additional reproducibility data are shown in Section 5.5.2.5.

After calibration, the accuracy of the CDS measurement was then tested. This was done with an independent test. The test was made with a 9.60% CO_2 in N_2 blend at a system pressure of 27.5 kPa (4.00 psia). The figures for calibration and measure[illegible] results are shown in Table 5-3.

TABLE 5-3. ACCURACY

Calibration Gas:						
$\%CO_2$	kPa	(mmHg)	4S/R			
0.0	0.0	0.0	3.873			
10.13	2.79	21.0	3.346			
3.25	0.895	6.72	3.628			
Test Gas:				Indicated kPa	P_{CO_2} (mmHg)	Δ %
(9.60)	(2.64)	(19.8)	3.363	2.66	20.0	1.0

5.5.2.3 Response

This test was run with the CDS mounted on the base plate and the Lucite cover removed. The gold-plated aluminum sample cell used throughout the tests occupied the sample path. This cell has a polished bore 4.7 mm ID and a path length of 12 mm. Two 3-mm-diameter sample ports were provided on opposite sides of the cell, one port near the source en d of the cell, the other near the monochromator housing.

The sensing channel output was recorded on a 25-cm Beckman Strip Chart Recorder. Scale expansion was applied, so that a 3.0-Vdc output was full scale (100 mV) and a 2.0-V output resulted in 0.0 mV at the recorder.

The output was allowed to stabilize on ambient air at the 2.95-V level; then 3.3% CO_2 was introduced at one of the sample cell ports. The time for complete response to this step change in CO_2 level was approximately 6 seconds. A 63% response occurred in 1.3 seconds, as shown in Figure 5-6.

5.5.2.4 Specificity

Testing was performed with the CDS mounted in the chamber as described in Subsection 5.5.2.2: Accuracy.

Following completion of the measurements tabulated in Table 5-1, the chamber was evacuated. Then 100% oxygen was admitted to a system pressure of 27.3 kPa (4.0 psia) and the output meter reading recorded.

Nitrogen was then admitted to a total pressure of 1 atmosphere before evacuating the chamber.

Nitrogen was purged through a gas scrubbing bottle containing distilled water for 30 minutes to remove dissolved CO_2. The nitrogen, saturated with water vapor at 25°C, was then admitted to the test chamber to a system pressure of 27.5 kPa (4.0 psia) and the output meter reading recorded.

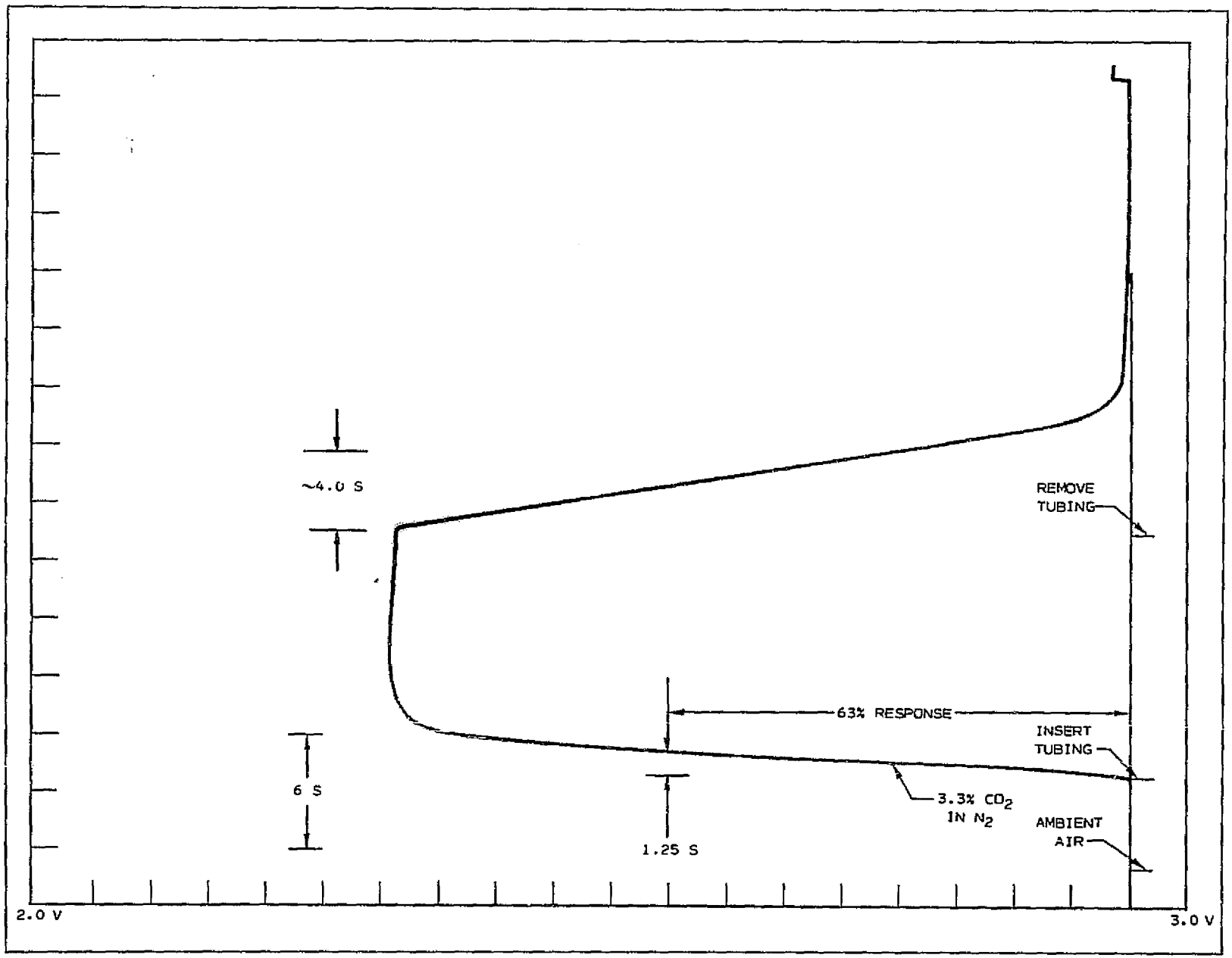

Figure 5-6. Response Test

The chamber was then evacuated and a test gas of 14.5% CO_2 in nitrogen admitted, to a system pressure of 27.5 kPa (4.0 psia). The P_{CO_2} was 4.0 kPa (30 mmHg). The output meter reading was recorded. Data from this series of measurements are presented in Table 5-4.

TABLE 5-4. DATA FROM SPECIFICITY TESTS

Test Gas	P_{CO_2}		P_{H_2O}		Ratio Output	Indicated CO_2	
	kPa	mm	kPa	mm		kPa	mm
N_2, evacuated	0.0	0.0	0.0	0.0	3.928	-	0.0
O_2	0.0	0.0	0.0	0.0	3.929	-	0.0
H_2O saturated N_2	0.0	0.0	0.86	6.6	3.915	.05	0.4
14.5% CO_2	4.0	30.0	0.0	0.0	3.307	4.0	30.0
N_2, evacuated	0.0	0.0	0.0	0.0	3.925	-	0.0

5.5.2.5 Switch Setting

This test provides data showing the system capability to resolve a change in P_{CO_2} of less than 0.5 kPa (4 mmHg).

The CDS was mounted in the test chamber as described in Subsection 5.5.2.2. The chamber was purged with nitrogen, then evacuated, and the output meter reading recorded. Then 4.9% CO_2 in N_2 was admitted to a system pressure of 27.5 kPa (4 psia) to provide a P_{CO_2} of 1.34 kPa, and the output meter reading recorded. System pressure was then reduced to 22.0 kPa to result in a P_{CO_2} of 1.08 kPa, and the output meter reading recorded. Then 4.9% CO_2 in N_2 was admitted to a system pressure of 33.0 kPa (1.6 kPa P_{CO_2}), and the output meter reading recorded. Pressure was then reduced back to 27.5 kPa for a repeat check on the 1.34 kPa P_{CO_2} output reading.

The test results include the effects of pressure broadening, since the total pressure, as well as the partial pressure of CO_2, was changed to produce the 1.34 ±0.26 kPa (10.1 ±2.0 mmHg) levels of P_{CO_2}.

Predicted normalized Δ ratio values for ±0.26 kPa (±2.0 mmHg) P_{CO_2} change at a constant total pressure of 27.5 kPa (207 mmHg) are 54.7 and 41.5, respectively, as determined from Figure 5-4. When these values are compared to observed normalized Δ ratio values of 59.3 and 38.1, respectively, the resulting errors in P_{CO_2} are found to be approximately -10% (at 8 mm) and +13% (at 12 mm). These errors are within the error band predicted in Section 5.6.4 of this report.

The test data are presented in Table 5-5.

The analog recording of Figure 5-7 indicates the relative signal-to-noise ratio for this ±0.27 kPa change in P_{CO_2}. A 0.27 kPa change in CO_2 partial pressure results in an output level change of about 20 times the system noise level.

Additional testing to determine the repeatability of switching at the alarm point was performed as described in the following paragraphs.

The CDS was mounted in the bell jar with the source block clamped to the base plate. One and one-half hours after applying power, a series of measurements were undertaken at 27.5 kPa (207 mmHg) total pressure. An initial calibration was performed with 0, 3.25%, 4.90%, 10.1%, and 14.5% CO_2. Between successive gas samples, the bell jar was evacuated to 0.13 kPa, partially filled to 13 kPa with the next gas mixture to be tested, and re-evaluated.

Following calibration, a series of ten cycles between 0 and 1.35 kPa (0 and 10.1 mmHg) P_{CO_2} was completed. Sensing and reference channel signal values were recorded, on expanded scale, on 100 mV strip chart recorders, with a 3.00 V signal corresponding to 100 mV and a 2.00 V signal reading 0 mV. The source supply voltage was controlled to ±0.03%. Testing occurred over a period of 7 hours. After completion of the repeatability measurements, a second calibration series was performed. Signal ratios (4S/R) corresponding to the Newport Output Ratio Meter readings were then calculated from the sensing and reference signal values.

TABLE 5-5. DATA FROM SWITCH SETTING TESTS

System Pressure		P_{CO_2}		Meter Reading	Δ	Normal-ized Δ	Indicated* CO_2		Error in P_{CO_2}**		
kPa	(mm)	kPa	(mm)				kPa	(mm)	kPa	(mm)	%
0.0	0.0	0.0	0.0	3.925	.000	0	0	0	-	-	-
27.5	206.8	1.34	10.1	3.623	.302	(48.8)	1.34	10.1	-	-	-
22.0	165.4	1.07	8.1	3.689	.236	38.1	0.97	7.3	-.10	-.80	- 9.9
33.0	248.0	1.60	12.1	3.558	.367	59.3	1.82	13.7	+.22	+1.6	+13.2
27.5	206.5	1.34	10.1	3.622	.303	48.8	1.34	10.1	-	-	-

* Indicated kPa P_{CO_2} were determined by reference to Figure 5-4 (27.5 kPa curve)
**Pressure Reading

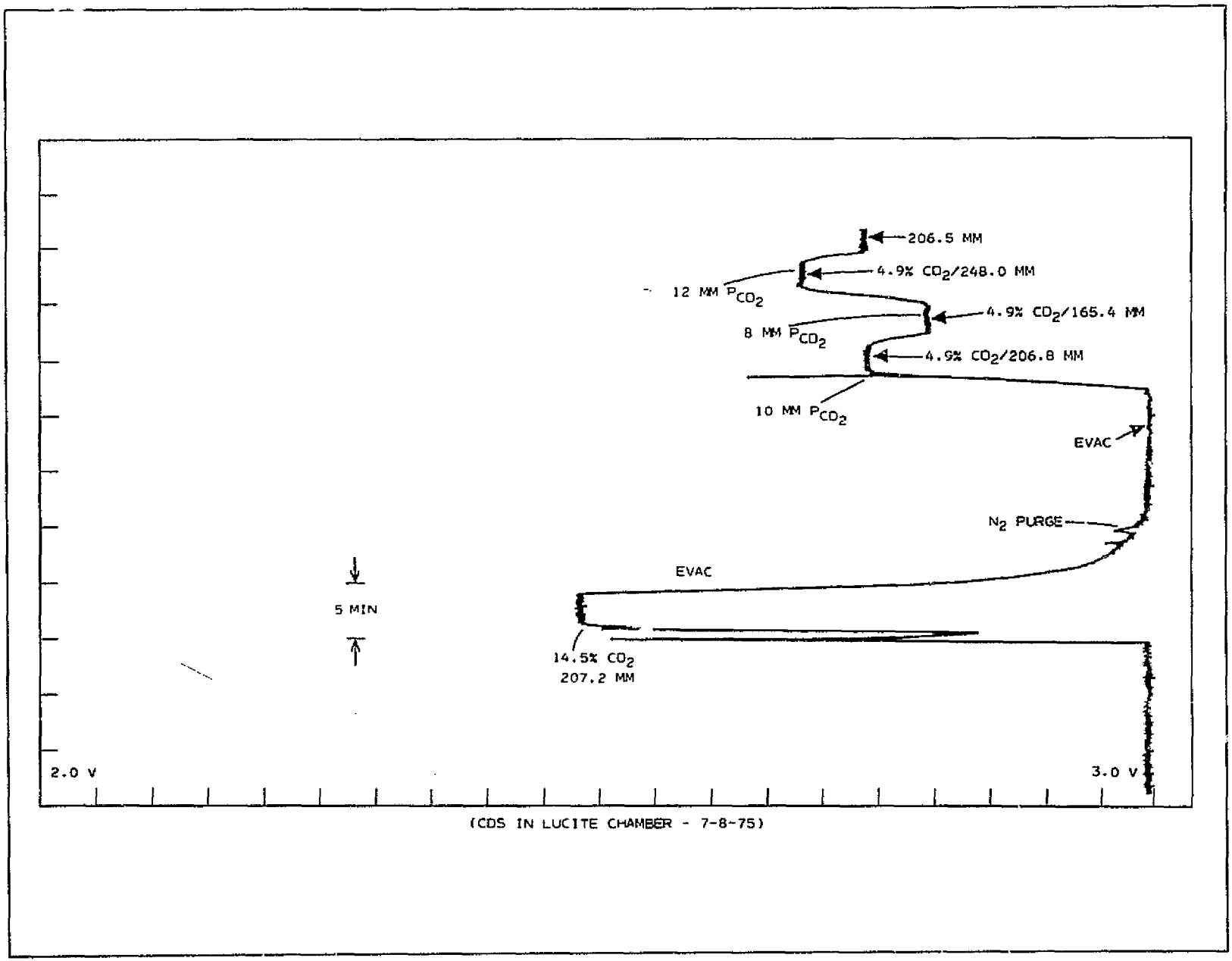

Figure 5-7. Relative Signal-to-Noise Ratio for ±0.27 Change in P_{CO_2}

The test data are summarized in Table 5-6, below.

TABLE 5-6. CALIBRATION AND REPRODUCIBILITY DATA AT 27.5 kPa (207 mmHg)

P_{CO_2} kPa	P_{CO_2} mm	Number of Measurements	Ratio (4S/R) Mean Value	Standard Deviation	SD IN P_{CO_2} kPa	SD IN P_{CO_2} mm
0.0	0.0	13	3.909	.0052	.009	.065
0.89	6.73	2	3.643	N/A	N/A	N/A
1.35	10.1	12	3.555	.005	.03	.20
2.79	21.0	2	3.344	N/A	N/A	N/A
3.99	30.0	2	3.203	N/A	N/A	N/A

For the repeatability measurements, the signal ratios measured at 1.35 kPa P_{CO_2} have a mean value of 3.555, with a standard deviation of 0.0051, corresponding to 0.027 kPa (0.2 mmHg) P_{CO_2}. This shows that the random error of the measurement in this critical region, at the 95% confidence level, is only 10% of the signal expected and thus no difficulties are expected in meeting the alarm switching criteria. At 0 kPa, the mean ratio value is 3.909, with a standard deviation of 0.0052. At this CO_2 level, the standard deviation amounts to 0.009 kPa (0.065 mmHg) P_{CO_2}.

Thus, the standard deviation at the 1.35 kPa (10 mmHg) P_{CO_2} level is 1/10 the ±0.27 kPa (±2 mmHg) P_{CO_2} level change required for alarm level sensitivity.

5.5.2.6 Power

During the testing period, readings were recorded of the power supply voltages and currents indicated by the power supply panel meters. The stated power consumption of the Newport output ratio meter was noted. The data are shown in Table 5-7.

TABLE 5-7. POWER SUPPLY VOLTAGES AND CURRENTS

Power Supply	Volts (DC)	Amperes	Calculated Watts
Nominal 10 Vdc for Source	+4.8 Vdc (Avg)	0.38	1.82
+5 V for Timing Circuit	+5.0	0.12	0.60
+ and -10 V for Electronics	+10 -10	0.003 0.005	0.03 0.05
Total (excluding output meter)			2.50 W
Newport output ratio meter: 115 Vac, 60 Hz, 0.1A, 11.5 W			

In a flight model system, the Newport ratio meter would be replaced by an integrated ratio circuit, offering a major reduction in power consumption. The miniaturized source would also consume less power than the commercial source employed in the breadboard instrument.

5.5.2.7 Voltage

This test was conducted in conjunction with the accuracy test described in paragraph 5.5.2.2. After the output meter reading of 1.34 kPa (10.1 mmHg) P_{CO_2} was recorded, power supply levels for the signal processing electronics were adjusted to determine the effect of non-standard power supply conditions on instrument calibration. The test data indicate that the output meter reading is insensitive to supply voltage variations within the ratings of the operational amplifiers, provided that sufficient supply voltage is maintained to accommodate the complete 10-Hz waveform without clipping in the post amplifier. Data are presented in Table 5-8.

TABLE 5-8. OUTPUT METER READINGS FOR VARIOUS SIGNAL PROCESSING SUPPLY VOLTAGES

Signal Processing Supply Voltages	Output Meter Readings
+10/-10 Vdc	3.620
+14/-14 Vdc	3.620
+10/-9.18 Vdc	3.740*
+10/-9.72 Vdc	3.626**
+7/-10 Vdc	3.620

* Severe clipping of reference signal negative peak

** Clipping of reference signal negative peak

The useful range of signal processing supply voltages could be readily extended from ±7 to ±15 V by lowering the source supply voltage to reduce signal amplitudes, at some sacrifice in the signal-to-noise ratio.

The effect of source voltage variation is shown in Table 5-9. Again, operation of the source at a voltage above about 4.3 Vdc, average (supply voltage above about 9.7 Vdc), results in clipping of the negative peak of the reference signal at a signal processing supply voltage of +10/-10 Vdc.

TABLE 5-9. EFFECT OF SOURCE VOLTAGE VARIATION

Source (Vdc, Avg)	Source Supply (Vdc)	Sensing Signal (Vdc)	Reference Signal (Vdc)	Output Ratio (0 kPa CO_2
3.40	7.791	1.558	1.583	3.935
3.60	8.191	1.848	1.877	3.941
3.80	8.638	2.167	2.196	3.947
4.00	9.067	2.494	2.524	3.951
4.20	9.487	2.832	2.865	3.958
4.30	9.695	3.005	3.037	3.958
4.40	9.923	3.206	3.213	3.984
4.50	10.124	3.373	3.296	4.093
4.60	10.329	3.556	3.358	4.235

With reference to Figure 5-5 (adjusted for zero shift), a change in source supply voltage from 7.79 to 9.69 V produced a change in output ratio of 0.023, corresponding to approximately 0.07 kPa (0.5 mmHg) CO_2.

5.5.2.8 Operating Ambient

The optics portion of the analyzer was mounted inside the temperature-controlled chamber (Forma Scientific Co.). The electronics assemblies and power supplies were located outside the chamber. The CDS temperature tests were conducted over an 18-hour period, using the following temperature cycle programs:

°C	(°F)	Hours
23.9	75	1
5.5	42	1-1/2
28.9	84	3
38.3	101	1-1/2
49.4	121	1-1/2
28.9	84	2-1/2
5.5	42	3
21.7	61	1-1/2
28.9	84	2-1/2

An expanded scale analog recording was made of the sensing channel output. In addition, reference channel and ratio outputs were measured during the initial and final 1-1/2-hour periods of the test. During most of the test period, nitrogen was flowing at 1.5 liters per minute through the housing surrounding the sensor. The response to 3.31 kPa (24.9 mm) P_{CO_2} was measured near the beginning and end of the test period at 5.5 and 28.9°C. The test results are presented in Table 5-9

The sensing channel response to CO_2 at levels near 0 kPa P_{CO_2} is approximately 0.225 Vdc/kPa. The cause of the observed hysteresis has not been identified; however, the extreme value of error over the temperature range of 5.5 to 49.4°C for this test series was only ±.16 kPa (±1.2 mm P_{CO_2}). However, the temperature test results are inconclusive and must be repeated with a source more closely approaching the flight configuration.

TABLE 5-10. TEMPERATURE TEST DATA

	Time	Chamber Temp (°C)	kPa (P_{CO_2})	Sensing Channel (Vdc)	Ratio Output	ΔRatio 3.3% CO_2	Normalized ΔRatio
7/9	1705	5.5	3.3	2.023	3.007	-	-
	1752	5.5	0.0	2.695	3.962	0.955	1.015
	2105	28.9	0.0	2.710	-	-	-
	2230	38.3	0.0	2.718	-	-	-
	2355	49.4	0.0	2.727	-	-	-
7/10	0240	28.9	0.0	2.678	-	-	-
	0500	5.5	0.0	2.650	-	-	-
	0725	28.9	0.0	2.725	-	-	-
	0830	28.9	0.0	2.715	3.956	0.941	1.000
	0.859	28.9	3.3	2.030	3.015	-	-

Pressure — These tests were performed in the bell jar as described in Subsection 5.5.2.2. The first test was performed as outlined in the test plan. A test series was performed in which the total pressures (P_t) were adjusted to produce the same P_{CO_2} values--0.67 and 4.0 kPa (5.0 and 30.0 mmHg)--for several different total pressures. The results are shown in Table 5-11.

TABLE 5-11. PRESSURE TEST DATA FOR THE SAME P_{CO_2} VALUES FOR DIFFERENT TOTAL PRESSURES

$\%CO_2$	P_t (kPa)	P_{CO_2} (kPa)	Ratio Output	ΔRatio	Normalized ΔRatio
3.3	20.1	0.67	3.806	0.157	25.0
4.9	13.6	0.67	3.827	0.136	21.7
10.1	6.7	0.67	3.854	0.109	17.4
3.3	121	3.99	2.918	1.045	166
4.9	81.3	3.99	3.059	0.904	144
10.1	39.9	4.02	3.235	0.728	116
14.5	27.5	3.99	3.335	0.628	(100)
0.0	0.0	0.0	3.963	0.000	0

These tests illustrate the pressure broadening effects. Normalized Δ Ratio is calculated as described in Section 5.5.2.2.

Foreign Matter — This test was carried out to determine the effects of foreign matter. Baseline signal and ratio measurements were made over a 48-hour period at the start of tests. Repeat measurements were performed at 170 and 192 hours after start. At this time the power was turned off and the source assembly removed to permit cleaning the sample cell and windows. No visible evidence of contamination was observable. After cleaning, the sample cell and source were mounted, and the sensor was powered and allowed to stabilize for two hours. Measurement of signals and signal ratio confirmed that disassembly, cleaning, and reassembly resulted in a change of less than 0.04 kPa equivalent P_{CO_2}. The test results are graphed in Figure 5-8.

Additional measurements before and after cleaning showed a negligible change in response to CO_2; at 0.89 (6.7 mmHg) P_{CO_2} the response changed by less than 0.01 kPa (0.1 mmHg).

As indicated by the test data, there has been a signal loss in both channels over the 215-hour period of the test program. The most likely explanation is a deterioration of source output resulting from evaporation of tungsten from the source onto the inner surface of the source window. As the 170- to 215-hour readings indicate, this trend appeared to slow down with continued operating time.

5.6 Discussion of Test Results

5.6.1 Accuracy Test

Drift corrections have been applied to adjust the ratio data for changes resulting mainly from temperature change. Further development of the CDS would include electronic temperature compensation to correct for temperature sensitivity.

As is shown from the calibration curves for the range of system pressures, the CDS accuracy improves as the pressure and P_{CO_2} are lowered. At the pressure

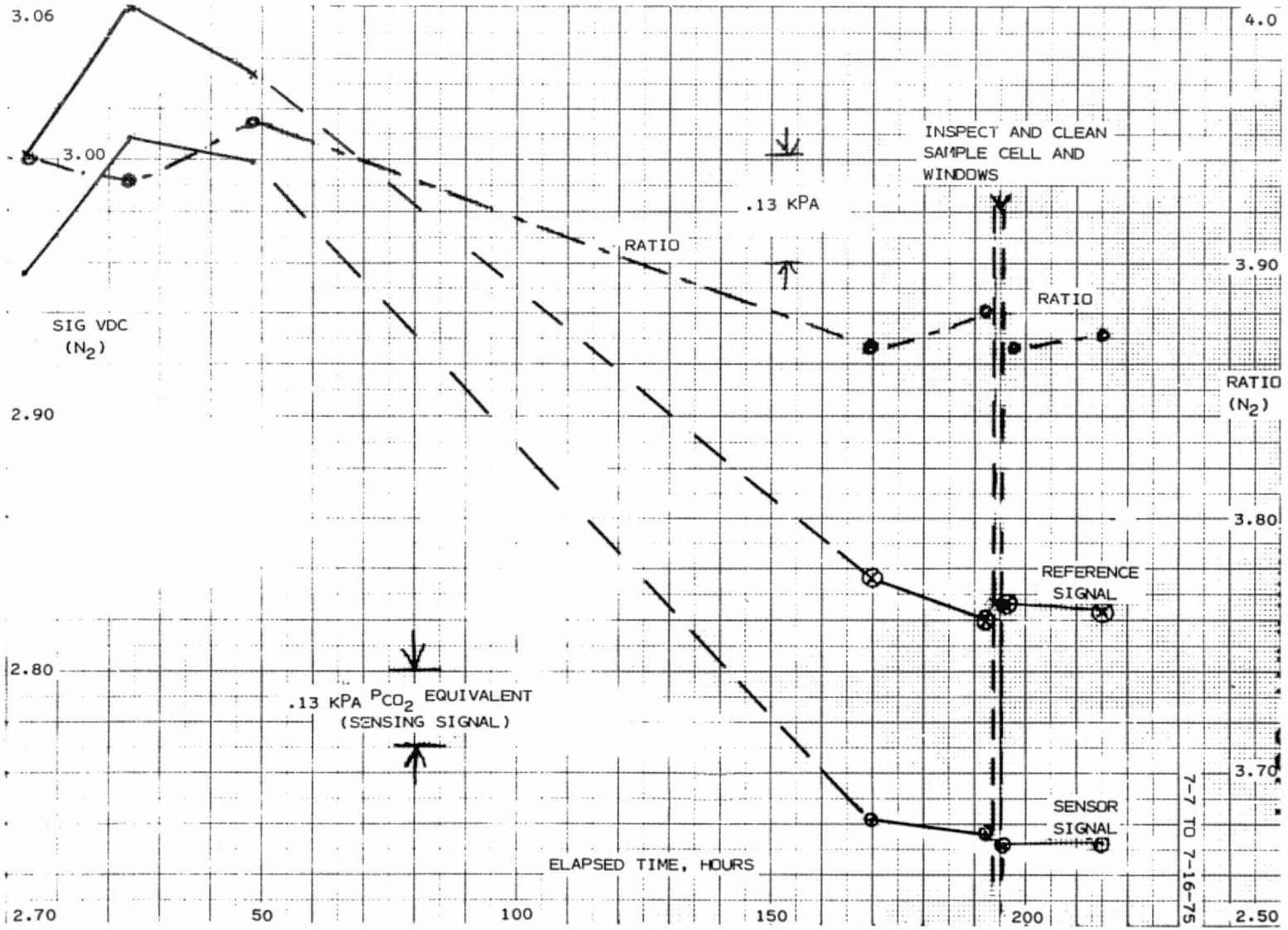

Figure 5-8. Foreign Matter Test Data

and concentration of greatest concern, i.e. the alarm point, the requirement of ±5% accuracy can be met. The data for the accuracy measurement at 2.666 kPa (20 mmHg) P_{CO_2} shows a difference of only 0.027 kPa (0.2 mmHg) from the actual value of 2.639 kPa (19.8 mmHg). This is only 1% error in the reading, or 0.67% of full scale. Over the normal operating range of pressures, compensation might not be needed, particularly since the pressure effect is completely predictable and a calibration curve could be provided for an extended pressure range.

After further development of the CDS, an improved accuracy determination should be made. This would require the use of two complete sets of gas blends, with CO_2 contents determined by an independent method capable of measurement to ±0.05% CO_2 accuracy. One set of standards would be employed in the CDS calibration; the second set would then be analyzed, CO_2 contents determined from the calibration data, and values compared to the "correct" values.

As discussed previously (see Foreign Matter), there has been a downscale drift in response with time, apparently resulting from a deterioration in source output. This drift could be automatically corrected by employing the reference signal to readjust the source power for constant output by means of suitable circuitry.

5.6.2 Specificity

The grating monochromator inherently provides the maximum specificity possible with an infrared measurement. The monochromator does have to be optimized to achieve the best response. The optical design was compromised in the breadboard by using a 1x3-mm entrance slit instead of 1x1. However, as seen from the test data, less than 0.5% interference resulted from the contaminant gases tested.

All the tests for calibration and accuracy were made with CO_2 in N_2. Ideally it should be done in O_2, as there is a difference in the self-broadening coefficient of the gases. However, the difference is only 6% and N_2 was considered satisfactory for breadboard testing.

5.6.3 Operating Ambient Temperature

This is an area in which more detailed testing should be carried out, although the observed temperature effects over the range of 5.5° to 49.4°C accounted for a change in P_{CO_2} of less than ±0.133 kPa (1 mmHg).

To provide additional data, the tests would be repeated over a period of several days, with analog recording of sensing and reference channel outputs, sensor temperature, source voltage, and a source of the flight configuration.

5.6.4 Pressure

The pressure response of the system follows the theoretical dependence of total absorption of the 2350 cm^{-1} CO_2 band with absorber concentration and total pressure. In Figure 5-9, the CDS data of Subsection 5.5.2.2 has been replotted in terms of atm-cm CO_2 at four total pressures versus the normalized Δ ratio value. These curves are similar to those presented in Figure 14 of AF CRL-255, "Infrared Absorption by Carbon Dioxide," by D.E. Smith, D. Gryvnak, and D. Williams. These curves are also similar to those of Burch, *et al.*, reproduced as Figure A-3, page 1-8, of the CDS Concept Study Data Package (IR-2679-101). As a further test of the theory generated in the Concept Study Report, the total pressure effect predicted by the error function given in equation (6), page 1-9 of the Concept Study Report may be compared to the experimental results. The theoretical equation should be completely valid for small pressure changes about a given value, and only approximate for changes of 10% or more in total pressure. The comparison is facilitated by the data presentation of Table 5-12, from which it may be seen that the theory adequately predicts the observed changes in P_{CO_2} due to relatively large percentage changes in total pressure. It is particularly significant that the range in indicated P_{CO_2} for the 21 to 38 kPa (3.1 to 5.5 psia) range of total pressure is only 1.13 to 1.60 kPa (8.5 to 12.7 mm), when the true value is 1.33 kPa (10 mm). The CDS is capable, therefore, of providing usable alarm point accuracy without total pressure compensation for a limited range such as 21 to 38 kPa (3 to 5.5 psia). The agreement with theory is sufficiently precise to permit accurate compensation if it is required.

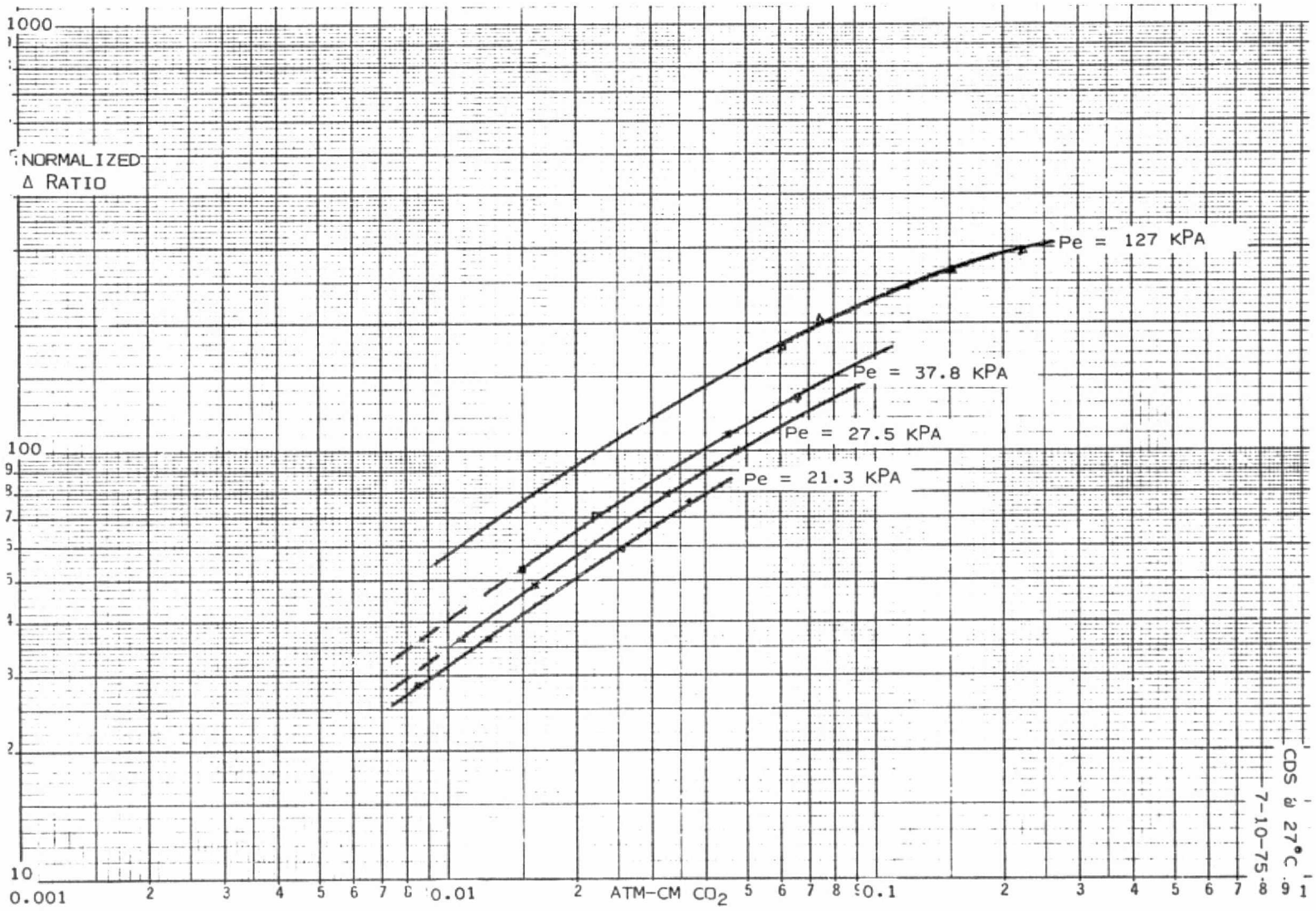

Figure 5-9. Atm-CM CO_2 at Four Total Pressures Versus the Normalized Δ Ratio Value

TABLE 5-11. COMPARISON OF OBSERVED TO PREDICTED EFFECTS OF TOTAL PRESSURE VARIATIONS UPON INDICATED P_{CO_2}

Calibration Total Pressure (kPa)	Operating Total Pressure (kPa)	Partial Pressure of CO_2 (kPa)	Theoretical Effect as % of Indicated P_{CO_2}	Observed Effect as % of Indicated P_{CO_2}	Indicated P_{CO_2} kPa	Indicated P_{CO_2} mm	Error in Indicated P_{CO_2} kPa	Error in Indicated P_{CO_2} mm	Observed Error as % of Full Scale P_{CO_2}
27.5	37.8	1.33	$\leq$ +18.8	+26	1.69	12.6	+.36	+2.6	+9.0
27.5	21.3	1.33	$\leq$ -11.3	-15	1.13	8.5	-.20	-1.5	-5.0
27.5	37.8	2.66	$\leq$ +18.8	+17.5	3.12	23.5	+.46	+3.5	+11.7
27.5	21.3	2.66	$\leq$ -11.3	-16.0	2.23	16.8	-.43	-3.2	-10.7
27.5	37.8	0.67	$\leq$ +18.8	+16	0.77	5.8	+.10	+0.8	+2.7
27.5	21.3	0.67	$\leq$ -11.3	-8	0.61	4.6	-0.6	-0.4	-1.3

6.0 HARDWARE AND DOCUMENTATION DELIVERY (SOW Paragraph 3.2.5)

6.1 Purpose and Scope of Task

The breadboard assembled and used for the development tests was required to be delivered to NASA-JSC. An "as-built" drawing package that defines the breadboard was also required.

6.2 Results

A working breadboard was delivered per the contract requirements. The breadboard is suitable for continued tests and evaluation at NASA.

A drawing package was also delivered. The drawing package includes specification control drawings as well as the detail parts and assembly drawings.

APPENDIX A

TEST DATA

CARBON DIOXIDE SENSOR TEST DATA

TITLE: RANGE (Ref paragraph 4.2.1)

Performance Requirement: The CDS shall be capable of measuring P_{CO_2} between 0 and 30 mmHg.

TEST CONDITIONS

Output shall be recorded with the system at 4.0 psia. Data shall be taken at the time of test for accuracy, paragraph 4.2.2.

TEST DATA

Nominal mmHg P_{CO_2}	Actual pCO_2	Output (Newport Ratio Meter)
0	0	3.934
5	6.8	3.707
10	10.1	3.633
20	20.7	3.444
30	30.0	3.316

DATA BY C. H. Beebe

DATE 7/10/75

CARBON DIOXIDE SENSOR TEST DATA

TITLE: ACCURACY (Ref. paragraph 4.2.2)

Performance Requirement: Accuracy shall be ±5% of full scale or better at normal operating conditions.

TEST CONDITIONS

Ambient Temp, 27-28 °C (80-82°F)

Tag Analysis, $\%CO_2$	Nominal Value
0	0
3.3	5
5	10
10	20
14.5	30

*Calc P_{CO_2} @ Sys Pressure

TEST DATA

Newport Ratio Meter Output at System Pressure

3.1 psia (160 mmHg)		4.0 psia (207 mmHg)		5.5 psia (284 mmHg)		18.5 psia (956 mmHg)	
Actual* P_{CO_2}	Output	P_{CO_2}	Output	P_{CO_2}	Output	P_{CO_2}	Output
0	3.937	0	3.935	0	3.933	0	3.932
5.3	3.759	6.8	3.707	9.4	3.604	31.6	2.856
7.8	3.707	10.1	3.633	13.9	3.501	46.9	2.643
16.0	3.565	20.7	3.444	28.4	3.257	95.1	2.279
23.2	3.458	30.0	3.316	41.3	3.097	138.7	2.108

DATA BY CH Beebe

DATE 7/10/75

CARBON DIOXIDE SENSOR TEST DATA

TITLE: RESPONSE (Ref paragraph 4.2.3)

Performance Requirement: Time for a 63% response to a step change in CO_2 partial pressure from 2.5 mmHg to 25 mmHg *shall not exceed one minute at normal operating conditions.*

TEST CONDITIONS	TEST DATA (Include copy of Recorder Chart) (TUBING WITH 3.3% CO_2 inserted and removed)	
Ambient temp, 28 °C	inserted	removed
Record analog output of sample signal level		
1 - Equilibrated output, low concentration (ambient air)	94.7 MV	94.7 MV
2 - Equilibrated output, high concentration (24.9 mm P_{CO_2})	30.9 MV	30.9 MV
Total change in output	63.8 MV	63.8 MV
Time to reach 63% of change of output	≃1.25 SEC.	≃4.0 SEC

DATA BY C H Beeke

DATE 7/10/75

CARBON DIOXIDE SENSOR TEST DATA

TITLE: SPECIFICITY (Ref paragraph 4.2.4)

Performance Requirement: The CDS shall be specific for CO_2 with no more than 0.5 percent change in either zero or span occurring due to exposure to oxygen, nitrogen, or water vapor at any concentration, or any combination. The zero or span shall not change more than 0.5% as a result of exposure to trace contaminants normally found in a closed ecological system.

TEST CONDITIONS

The same test setup as in paragraph 4.2.2 shall be used. Nominal pressure of 4.0 ±1.5 psia

System Pressure	Sample Gas
4.0 psia (207 mmHg)	O_2
	N_2 (100% R.H.)
	30 mm CO_2 plus water vapor
	30 mm CO_2 (dry)

TEST DATA

Sensor Newport Ratio Meter Output

Test	Baseline		Δ	NORMALIZED Δ
3.929	3.928	(N_2/VAC.)	+.001	–
3.915	3.926	(N_2/VAC.)	-.011	-1.
3.307	3.925	(N_2/VAC.)	.618	99.
3.310	3.929	(N_2/VAC.)	.619	(10

DATA BY C H Beebe

DATE 7/10/75

CARBON DIOXIDE SENSOR TEST DATA

TITLE: SWITCH SETTING (Ref paragraph 4.2.5)

Performance Requirements: The switch shall close when the average inspired CO_2 level reaches 10 ±.0 mmHg as indicated by the telemetry output. The switch shall remain closed as long as the CO_2 level is above the set point. The switch shall open when the level drops below the set point.

TEST CONDITIONS

This test shall be conducted in conjunction with paragraph 4.2.2, Accuracy

TEST DATA

	Sys Press	%CO_2	Calc P_{CO_2}	Output (in V from Signal Channel) ↓	RATIO METER OUTPUT
Output at 10 mmHg P_{CO_2}	207.0	4.9	10.1	-2.746	3.623
Output at 8 mmHg P_{CO_2}	165.4	4.9	8.1	-2.802	3.689
Output at 12 mmHg P_{CO_2}	248.0	4.9	12.1	-2.691	3.558
Rpt 10 mm CO_2	206.5	4.9	10.1	-2.745	3.622

DATA BY C H Beebe

DATE 7/13/75

CARBON DIOXIDE SENSOR TEST DATA

TITLE: POWER (Ref paragraph 4.2.6)

Performance Requirement: Power consumption of the CDS shall be less than three watts. (10 watts max for breadboard)

TEST CONDITIONS

Data may be taken during any of the performance tests

- Supply Voltage
- Current
- Calculated Power

TEST DATA

(Sum of Power Supplies)

SOURCE: 4.3V AVE. X .38A AVE. = 1.64 WATTS

+10V: .003 A = .03

-10V: .005A = .05

+5V: .120 A = .60

2.32 W

NEWPORT RATIO METER 115V AC / .1 A = 11.5 W.

DATA BY CH Beebe

DATE 7/10/75

CARBON DIOXIDE SENSOR TEST DATA

TITLE: VOLTAGE (Ref paragraph 4.2.7)

Performance Requirements: To establish allowable voltage variations to the CDS

TEST CONDITIONS	TEST DATA	NEWPORT RATIO METER OUTPUT
Record supply voltage (AMPLIFIERS, ETC., EXCLUDING SOURCE)	+10 / −10 v.	
Record equilibrated output at nominal ~~30~~ 10 mmHg P_{CO_2}, 4 psia		3.620
Increase supply voltage to obtain 5% increase in output	+14 / −14 v.	3.620
Decrease supply voltage to obtain 5% decrease in output	+10 / −9.184 v.	3.740

(CLIPPING STARTS ON ±10 V AC SIG at supply voltage less than −10 V)

SOURCE VOLTAGE (AVE.)	
4.30	3.624
4.20	3.620
3.97	3.617
3.50	3.598
4.45	3.679
4.54	3.794

DATA BY C H Beebe

DATE 7/10/75

Note: Clipping can be prevented at lower supply voltages by operating at lowered source voltages to reduce signal levels.

CARBON DIOXIDE SENSOR TEST DATA

TITLE: OPERATING AMBIENT (Ref paragraph 4.2.8)

Performance Requirements: The CDS shall be designed to perform within the following environmental requirements:

Temperature	40°F to 110°F
Pressure	3.1 psia to 18.5 psia (4.0 ±1.5 psia normal)
Relative Humidity	0% to 100%
Gas Composition	100% oxygen

Additional requirements of fungus, salt fog, accoustical noise, and gravity will not be tested for with the CDS Breadboard.

TEST CONDITIONS

Temperature Cycling

Ambient temp 28 °C (82 °F)
Ambient press 755 mmHg
Percent CO_2 3.3 / 0.0 Calc P_{CO_2} 24.9 / 0.0
Output, Ambient temp
Output, °C (40°F)
Output, °C (110°F)

Pressure

Data can be obtained during the accuracy test
Output at 4.0 psia nominal (5 mm P_{CO_2}
Output at [illegible] psia nominal ([illegible] mmP_{CO_2} 2.5PSIA/35mm
Output at 5.5 psia nominal (6.5 mmP_{CO_2}
Output at 4.0 psia nominal (30 mmP_{CO_2}
Output at [illegible] psia nominal ([illegible] mmP_{CO_2} 2.5PSIA/18.9mm
Output at 5.5 psia nominal (31.5 mmP_{CO_2}

For relative humidity, see Data Sheet, Specificity
For 100% Oxygen, see DataSheet, Specificity

TEST DATA

T°C	°F		NEWPORT RATIO METER OUTPUT N_2	NEWPORT RATIO METER OUTPUT 3.3% CO_2	SENSING CHANNEL SIG VDC N_2	SENSING CHANNEL SIG VDC 3.3% CO_2
4.4	40	(530PM)	3.959	3.009	2.692	2.00[illegible]
28.9	84	OVERNITE RUN	—	—	2.707	—
49.4	121	OVERNITE RUN	—	—	2.718	—
28.9	84	OVERNITE RUN	—	—	2.668	—
5.6	42	OVERNITE RUN	—	—	2.641	—
28.9	84	(0830AM)	3.953	3.016	2.702	2.012
		6.8 mm P_{CO_2}	—	3.696		
		4.3	—	3.795		
		9.3	—	3.600		
		30.0	—	3.311		
		18.6	—	3.556		
		41.3	—	3.087		

DATA BY CH Beebe
DATE 7/10/75

CARBON DIOXIDE SENSOR TEST DATA

TITLE: FOREIGN MATTER (Ref paragraph 4.2.9)

Performance Requirements: Foreign matter, such as dust, smoke, water, saliva, and hair shall not degrade the performance or life of the CDS

TEST CONDITIONS	TEST DATA (Newport Ratio meter output)
Baseline output from 10 mm P_{CO_2}, para 4.2.2	3.633
Comparative output at 10 mm P_{CO_2} after all testing completed	3.639
Comparative output at 10 mm P_{CO_2} after cleaning sample path windows	3.618

DATA BY C.H Beebe

DATE 7/16/75

E PAYSON
GN EOLE
24MAR26

PRE AMPLIFIER TEST

BREAD BOARD #1
(UNMARKED FET)

THE FOLLOWING TESTS WILL BE PERFORMED TO EVALUATE THE PRE AMPLIFIER ASSY (BREAD BOARD)

P#

1. POWER CONSUMPTION
2. DC OFFSET
3. FREQUENCY RESPONSE
4. TRANSIENT RESPONSE
5. LINEARITY
6. NOISE

BASIC SCHEMATIC

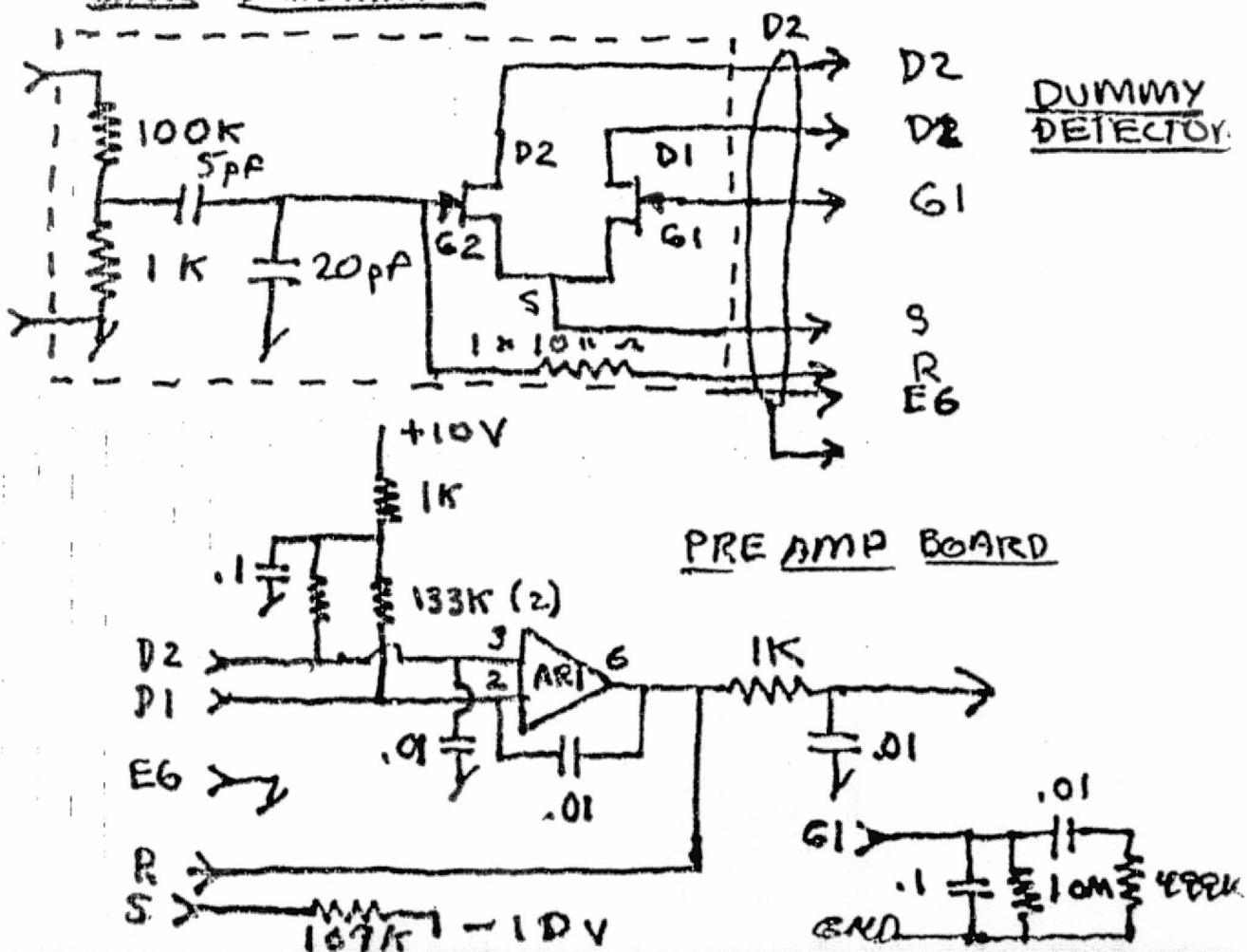

E PAYSON
GN COLE
24 MAR 75

POWER CONSUMPTION

PURPOSE TO MEASURE POWER DRAWN BY THE PREAMP / DETECTOR BOX WITH THE POWER SUPPLIES SET FOR + 2 ~~M~~ − 10 VOLTS.

+ SUPPLY		ΔV	R	P
V_{IN}	10.057	88 mV	220 Ω	3.52×10^{-5} W
$V_{(7)}$	9.969			

− SUPPLY				
V_{IN}	10.092	87 mV	220 Ω	3.44×10^{-5} W
V_4	10.005			

TEST CONDITIONS:

1. INPUT SHORTED (AC)
2. DUMMY LOAD BOX CONNECTED

DC OFFSET 25°C AMBIENT

TEST CONDITIONS

1. INPUT SHORTED (AC)
2. + 10.05 V
   − 10.09 V
3. NO SPECIAL SHIELDING

	V_o
TAGGED FET	−22.5 mV
PLAIN FET	+1.2 mV

JOB NO. 1361-2679 OSCILLOSCOPE MODEL 545A ENGINEER E PAYSON

ATP NO. _____ TECHNICIAN G N COLE

CONTRACT _____ SERIAL NO. BREADBOARD 1 DATE 24 MAR 75

TEST CONDITIONS

VERT .5 / 5 /DIV

HORIZ 50 mS /DIV

LOAD NONE

INPUT SINE WAVE

TEMP 25°C °C

PROBE 1X / 1X

CH1

CH2

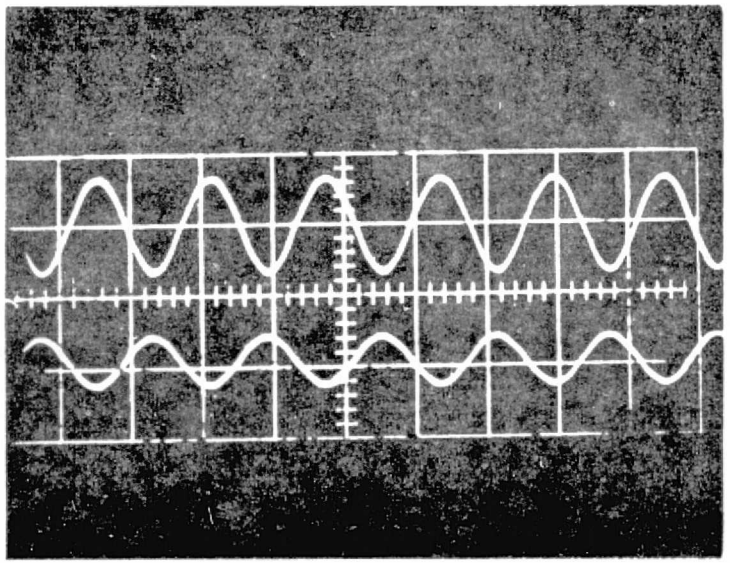

DESCRIPTION SINE WAVE RESPONSE AT 13 HZ.

SINE WAVE – 13 Hz

NOTE: IN THE FOLLOWING DIAGRAMS THE PREAMP/DUMMY DETECTOR AND FET WILL BE INDICATED BY THE FOLLOWING SYMBOL:

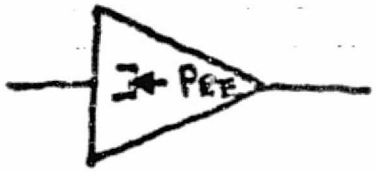

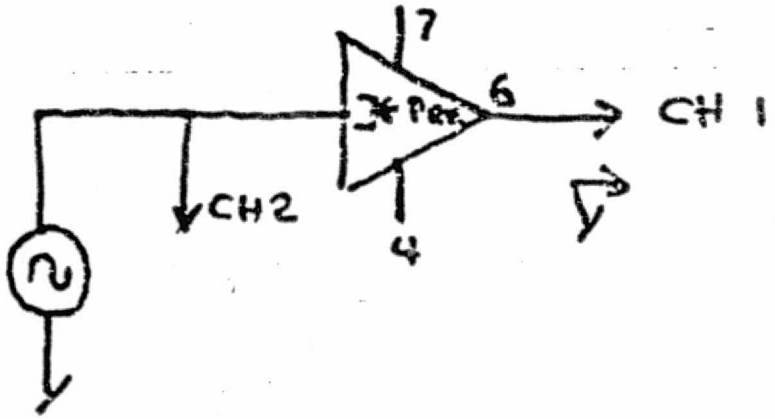

$V_7 = +10.00$ V DC
$V_4 = -10.00$ V DC

JOB NO. 1361-2679 OSCILLOSCOPE MODEL 545A

ATP NO. _____

CONTRACT _____ SERIAL NO. BREADBOARD 1

ENGINEER E PAYSON

TECHNICIAN G N COLE

DATE 24 MAR 75

CH1

CH2

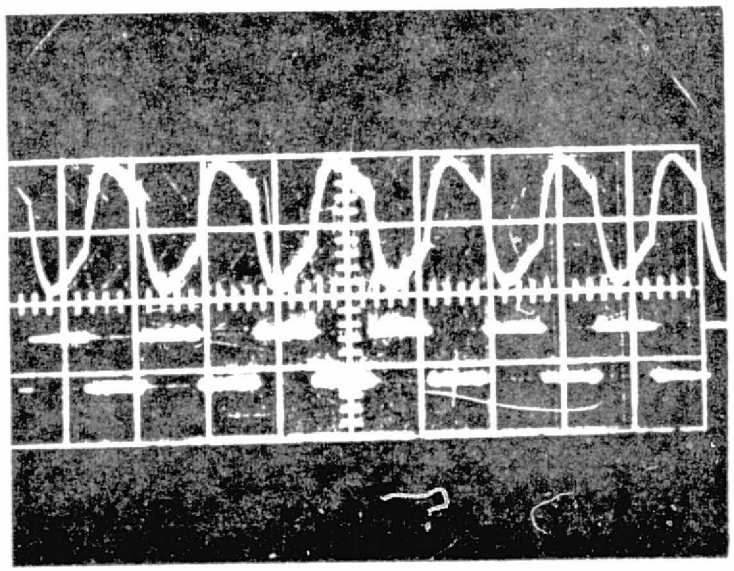

DESCRIPTION SQUARE WAVE RESPONSE
13 HZ INPUT

TEST CONDITIONS

VERT .5 1 5 /DIV

HORIZ 50 MS /DIV

LOAD NONE

INPUT SQ WAVE

TEMP _____ °C

PROBE _____

SQUARE WAVE RESPONSE

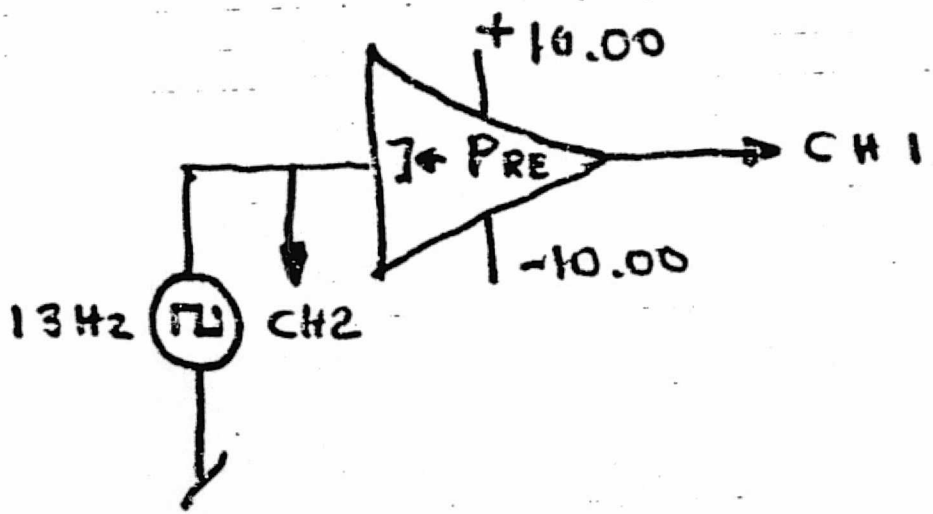

JOB NO. 1361-2679 OSCILLOSCOPE MODEL 545A ENGINEER E PAYSON

ATP NO. _____ TECHNICIAN G N COLE

CONTRACT _____ SERIAL NO. BREAD BOARD 1 DATE 24 MAR 75

CH 1

CH 2

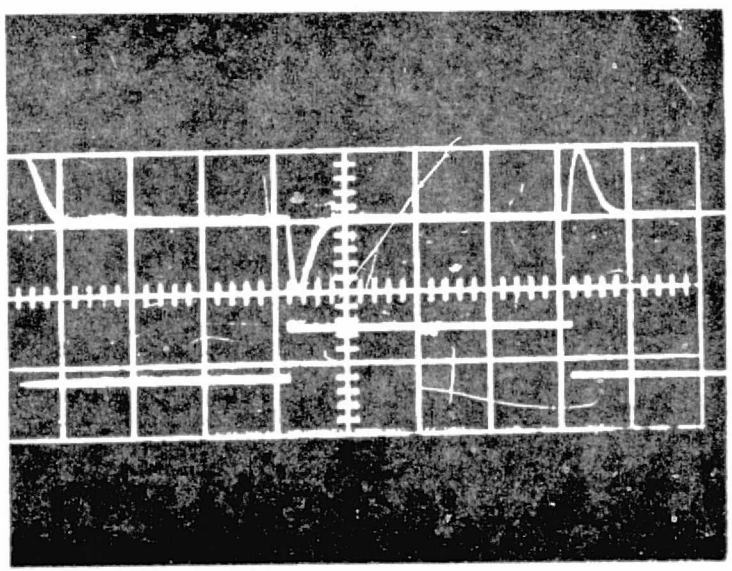

DESCRIPTION TRANSIENT RESPONSE
1.0 Hz

TEST CONDITIONS

VERT .5 / 5 /DIV

HORIZ .1 S /DIV

LOAD NONE

INPUT SQ WAVE

TEMP _____ °C

PROBE 1X / 1X

TRANSIENT RESPONSE TEST

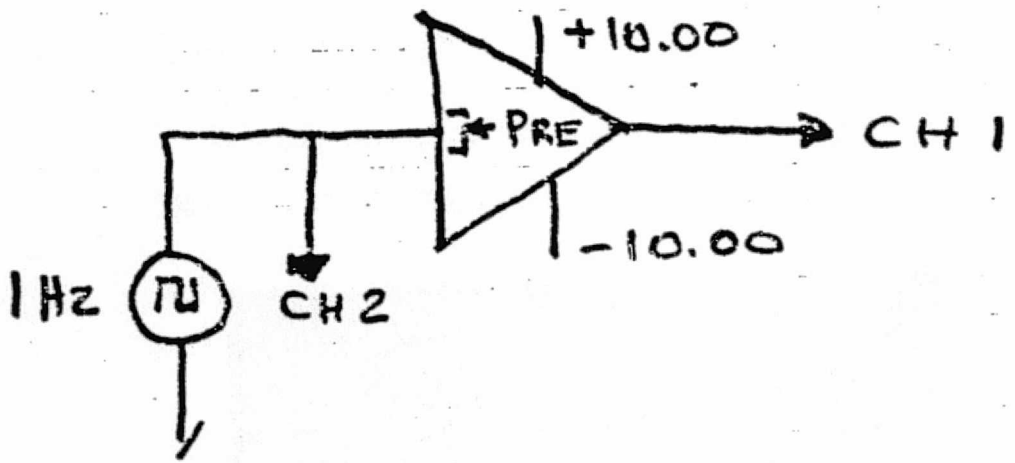

JOB NO. 1361-2679 OSCILLOSCOPE MODEL 545A ENGINEER E PAYSON

ATP NO. _____ _____ TECHNICIAN G N COLE

CONTRACT _____ SERIAL NO. BREAD BOARD 1 DATE 24 MAR 75

CH1

CH2

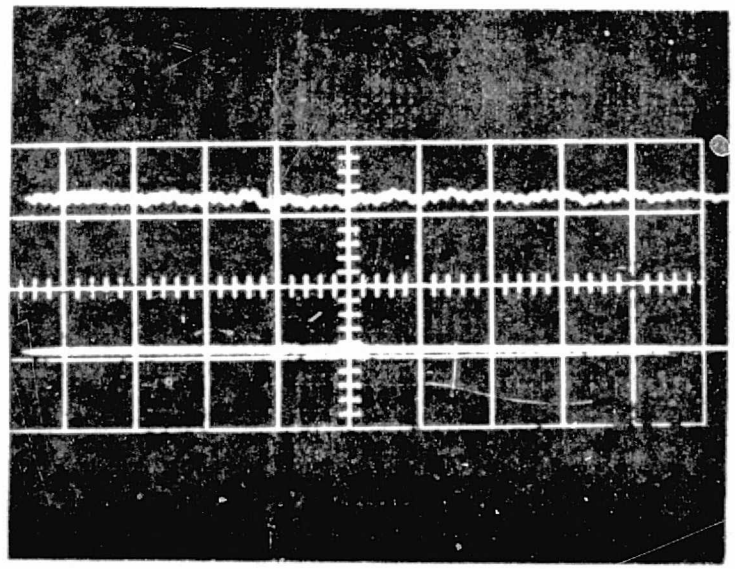

DESCRIPTION NOISE

TEST CONDITIONS

VERT 5mV /GND /DIV

HORIZ .1S /DIV

LOAD NONE

INPUT SHORTED

TEMP _____ °C

PROBE 1X / GND

NOISE TEST

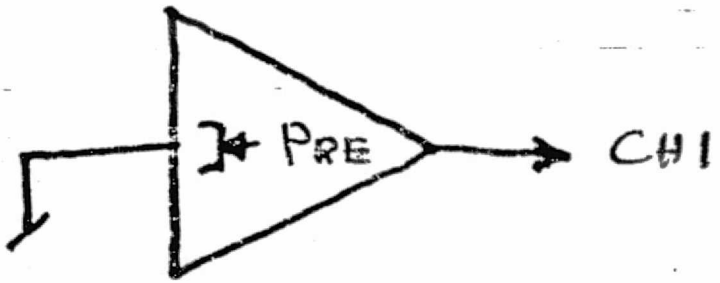

CH2
SET TO SAME GAIN
AS CH 1.

(SCOPE PREAMP IS QUIET AT 5 mV/DIV)

JOB NO. 1361 2679 OSCILLOSCOPE MODEL 545A

ATP NO. _____

CONTRACT _____ SERIAL NO. BREADBOARD 1

ENGINEER E PAYSON

TECHNICIAN G N COLE

DATE 24 MAR 75

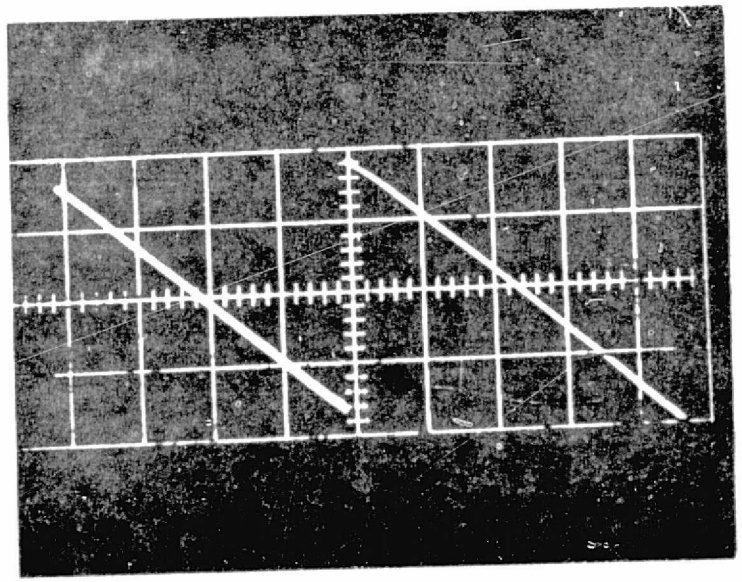

DESCRIPTION LINEARITY

LEFT SIDE HI LEVEL 2V /DIV VERT

RIGHT SIDE LO LEVEL .1V /DIV VERT

12 Hz INPUT

TEST CONDITIONS

VERT SEE BELOW /DIV

HORIZ EXT INPUT /DIV

LOAD NONE

INPUT SINE WAVE

TEMP _____ °C

PROBE 1X

LINEARITY TEST

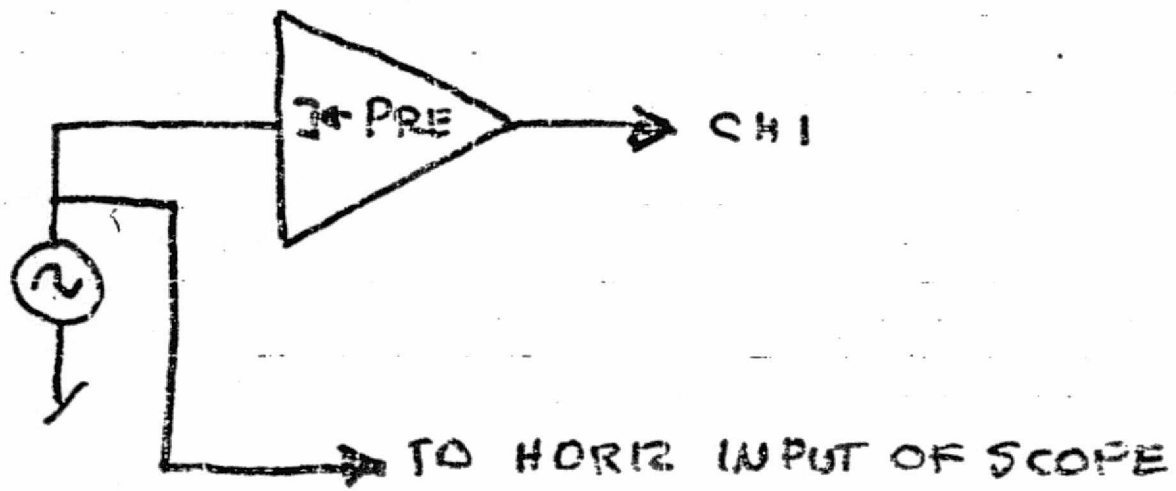

JOB NO. 1361 2679 OSCILLOSCOPE MODEL 545A

ATP NO. _____

CONTRACT _____ SERIAL NO. BREADBOARD 1

ENGINEER E PAYSON

TECHNICIAN G N COLE

DATE 24 MAR 75

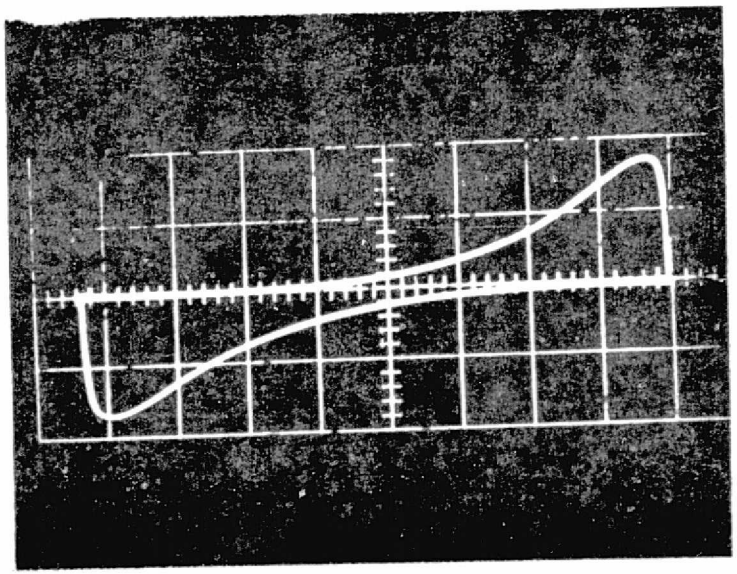

DESCRIPTION TRANSIENT RESPONSE
LOW LEVEL 50 mV / cm

TEST CONDITIONS

VERT 50 mV /DIV

HORIZ EXT INPUT /DIV

LOAD NONE

INPUT SQ WAVE

TEMP _____ °C

PROBE 1 X

EXPANDED TRANSIENT TEST

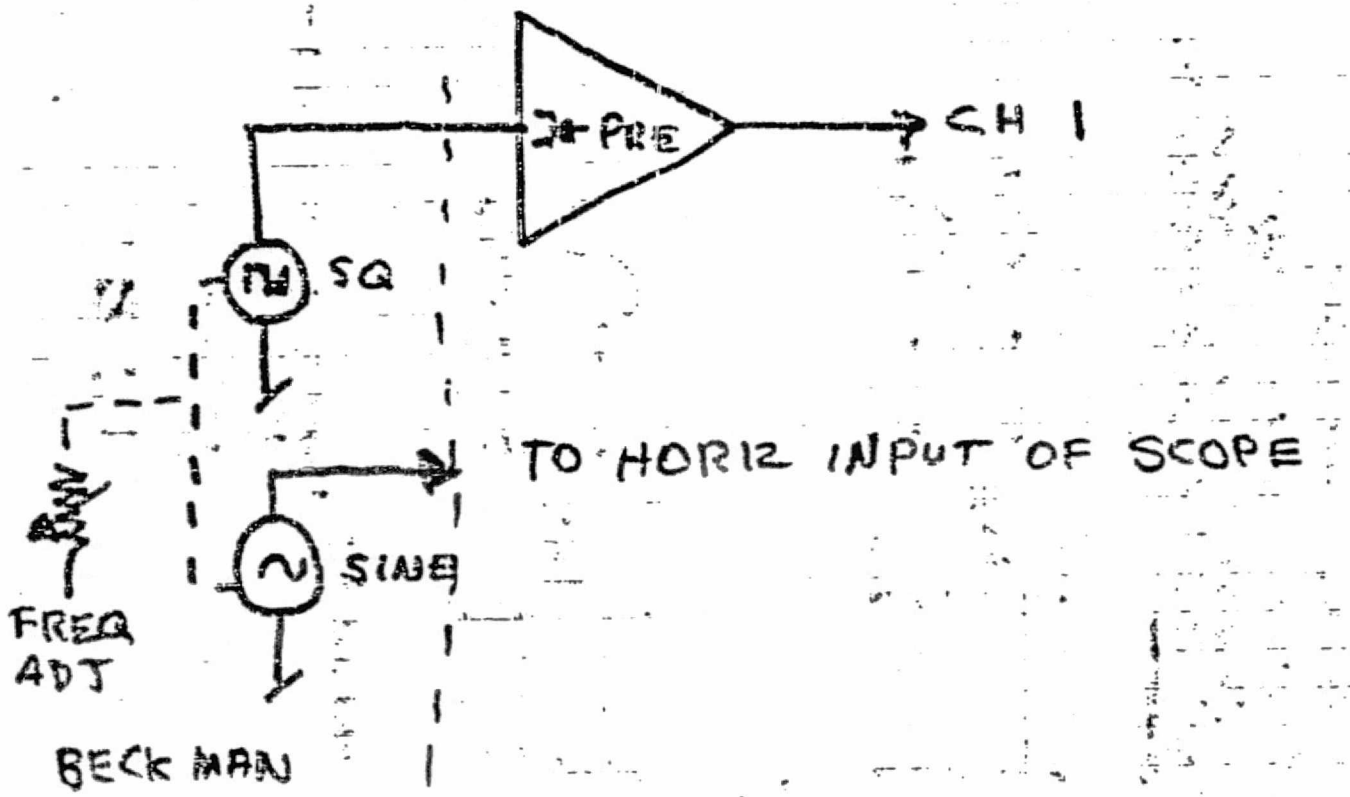

POST AMPLIFIER TESTS

GN COLE
E PHYSMN
4 MAR 75

PURPOSE: THE FOLLOWING TEST WILL BE PERFORMED TO EVALUATE THE POST AMPLIFIER (BREAD BOARD) ASSY.

	P. #s
1. DC OFFSET	5-3
2. FREQUENCY RESPONSE	7-8
3. TRANSIENT RESPONSE	
4. GAIN & FREQ	
5. POWER CONSUMPTION	
6. LINEARITY	13-14

TEST EQUIPMENT USED:

1. ± 6 - 10V DC SUPPLIES
2. DC MA METER
3. BECKMAN 9010 FUNCTION GEN.
4. TEKTRONIX 585A
5. H P 400A AC VOLTMETER
6. DIGITAL VOLT METER

BASIC SCHEMATIC:

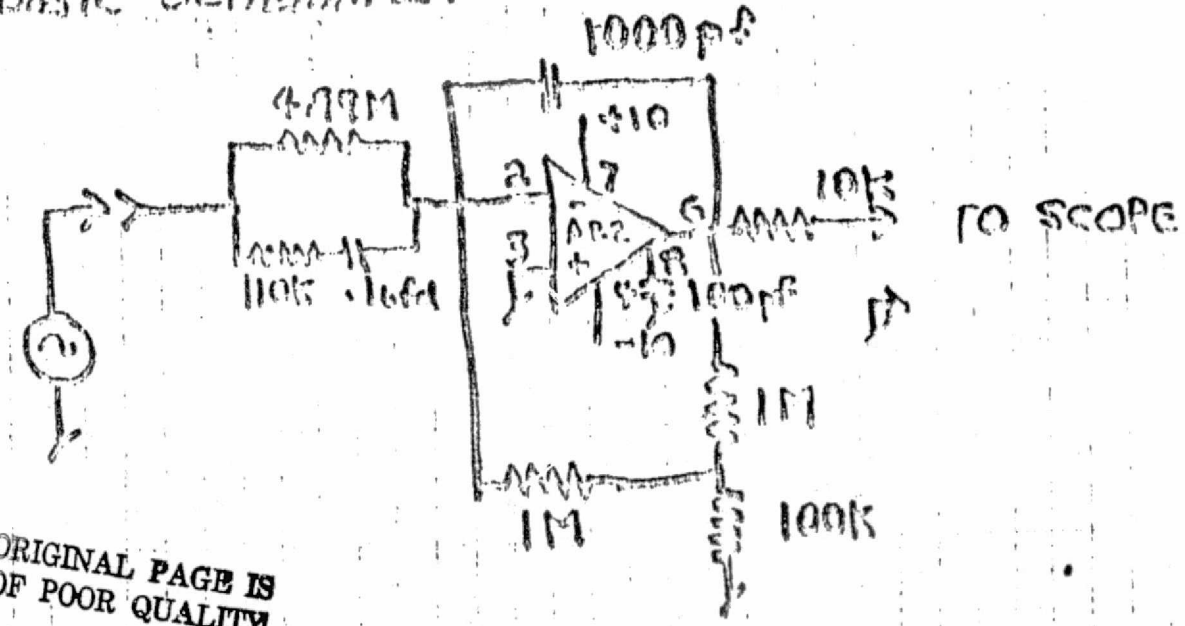

THE FOLLOWING VOLTAGES WERE TAKEN AT AR2 UNDER THE FOLLOWING CONDITIONS

1. + SUPPLY +10.00V
2. − SUPPLY −10.00V
3. INPUT SHORTED

PIN #	VOLTAGE
1.	NC
2.	.0000
3.	.0000
4.	−9.93
5.	NC
6.	+12.6 mV
7.	+9.93
8.	+.0706

NOTE: UNLESS OTHERWISE SPECIFIED THE SYMBOL:

WILL BE USED TO INDICATE THE CIRCUIT SHOWN ON PAGE 1. (ONE).

C M COLE
E PARSON
4 MAR 75

DC GAIN

DC INPUT	DC OUTPUT
0.000V	+ 12.6 MV
+1.000V	-2.398 V
-1.000V	+2.423 V

POWER CONSUMPTION

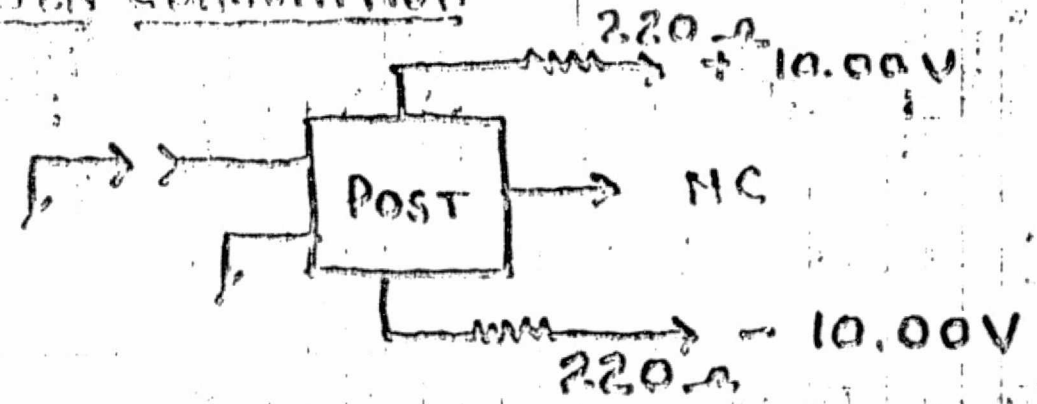

INPUT	VDROP	IDC AMPS	POWER
+10.00V	.0683	3.09×10^{-4}	3.09 mW
-10.00V	.0686	3.11×10^{-4}	3.11 mW

FREQUENCY RESPONSE

G M CALC
E PAXTON
4 MAR 86

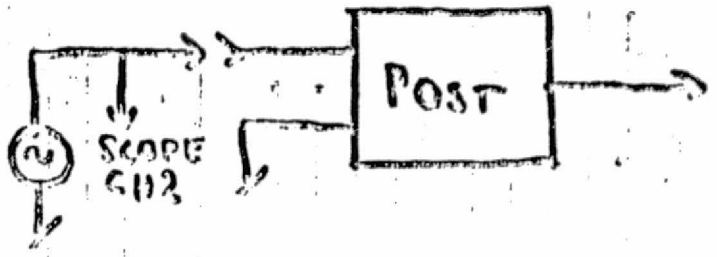

FREQ	INPUT VOLTS	OUTPUT VOLTS	VOUT - VIN
1 Hz	.15 P-P	2.2 V P-P	14.667
5 Hz		4.6	30.67
10 Hz		7.6	50.67
15 Hz		8.0	53.33
20 Hz		9.0	60.67
25 Hz		6.3	42.0
30 Hz		5.8	38.67
60 Hz		3.2	21.33
80 Hz		2.2	14.67
192 Hz		1.5	10.0
1493 Hz	.15 P-P	.16 V P-P	1.0

VOUT · VIN⁻¹

VOUT MAX 8.1 V P-P AT 14.5 Hz 54

NOISE TO BE TAKEN IN SHIELD ENVIRONMENT

WIDE BAND		FILTERED	
_____	P-P	_____	P-P
_____	RMS	_____	RMS

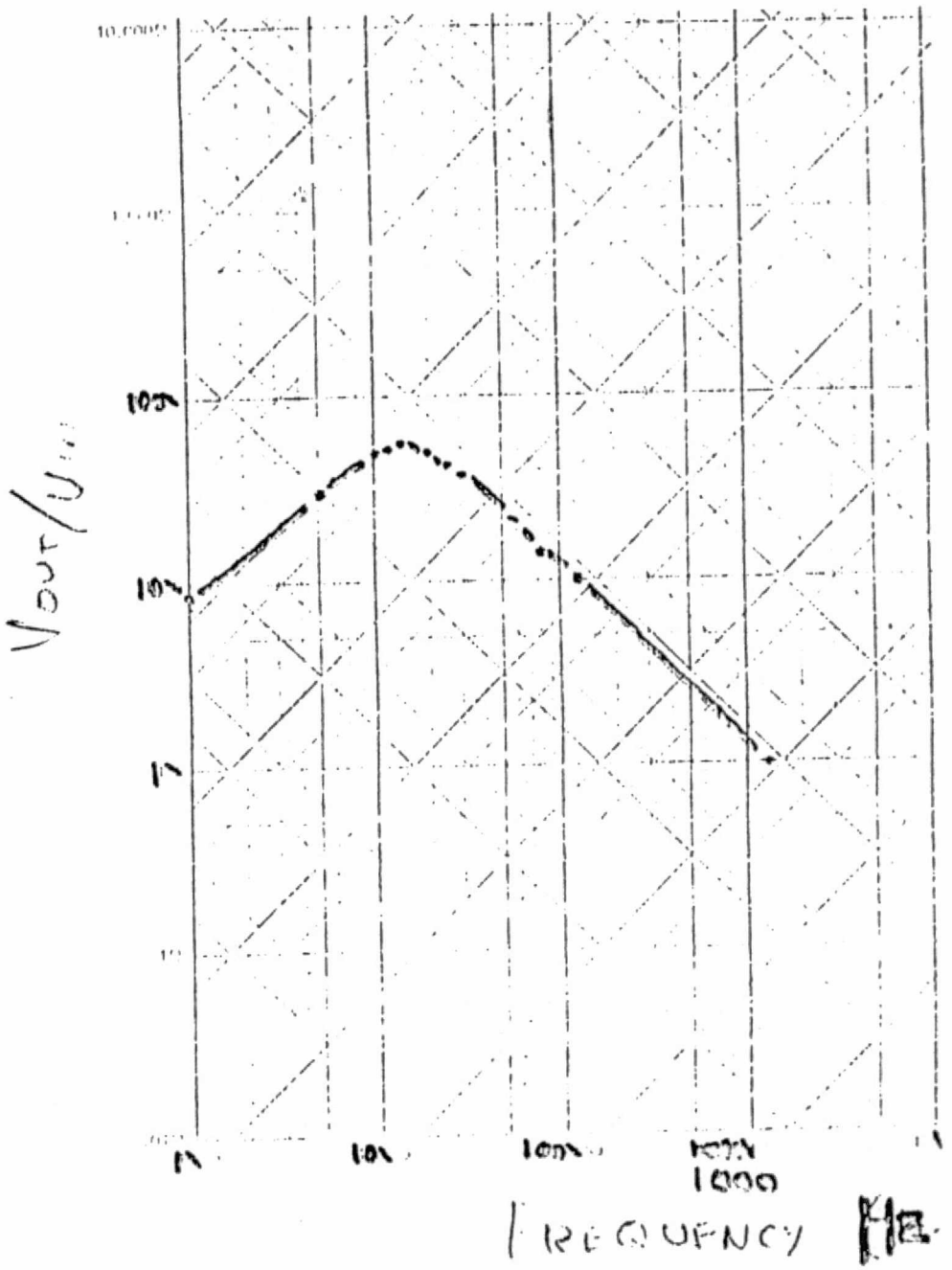

VOUT: VIN=1 / FREQUENCY

JOB NO. 1361-2679 OSCILLOSCOPE MODEL T35

ATP NO. _____

CONTRACT _____ SERIAL NO. POST AMP #1 BREAD BOARD

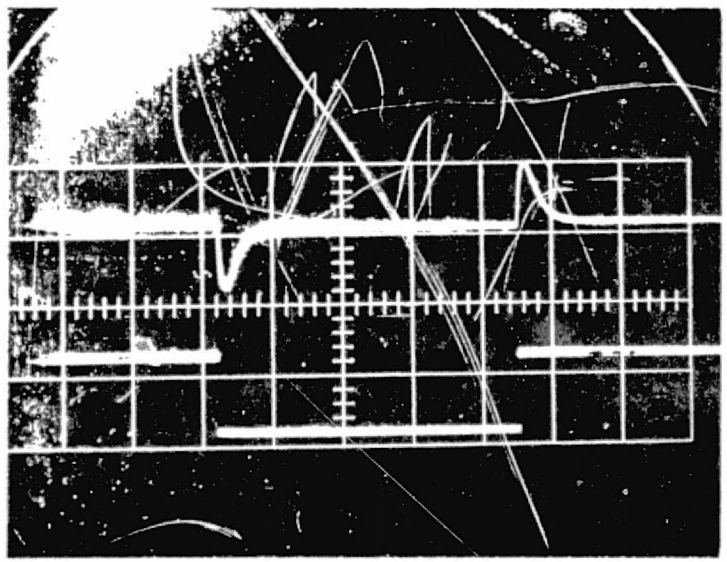

ENGINEER E PAYSON

TECHNICIAN G N COLE

DATE 5 MAR 75

TEST CONDITIONS

VERT 10V / 50 MV /DIV

HORIZ .1 SEC /DIV

LOAD NONE

INPUT SQ WAVE

TEMP 25°C °C

PROBE X1 OUTPUT
X10 INPUT

TRANSIENT RESPONSE

1.1 Hz

GAIN CALC
SEE PAGE 27
SEE PAGE 28

TRANSIENT RESPONSE

FREQUENCY 100. 1.1 Hz

V_{in} 50 mV p-p

V SUPPLY ± 10.00 V

S. N. Cole
E. Payson
5 MAR 75

SQUARE WAVE RESPONSE

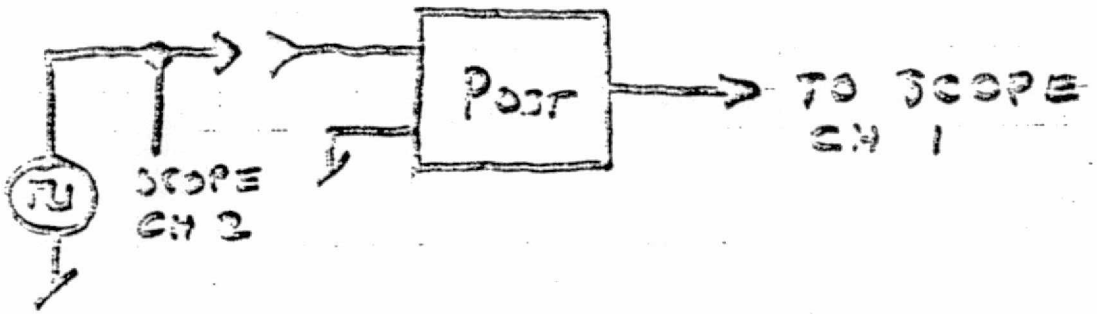

FREQUENCY INPUT

1K Hz AT 50 mV p-p

SUPPLY + 10.00 V
- 10.00 V

JOB NO. 1361-2679 OSCILLOSCOPE MODEL T35

ATP NO. _____

CONTRACT _____ SERIAL NO. POST AMP

ENGINEER E PAYSON

TECHNICIAN G N COLE

DATE 5 MAR 75

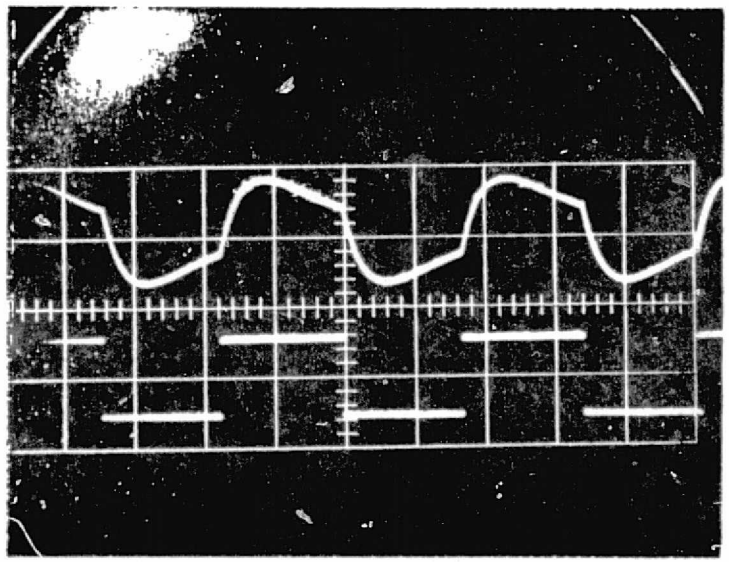

TEST CONDITIONS

VERT 10V / 50mV /DIV

HORIZ 20 mS /DIV

LOAD NONE

INPUT SQ WAVE

TEMP _____ °C

PROBE SQ WAVE RESPONSE

14 Hz

#2

JOB NO. 1361-2675 OSCILLOSCOPE MODEL

ATP NO. _____ 545A

CONTRACT _____ SERIAL NO. POST AMP 1 BREADBOARD

ENGINEER E PAYSON

TECHNICIAN G N COLE

DATE 5 MAR 75

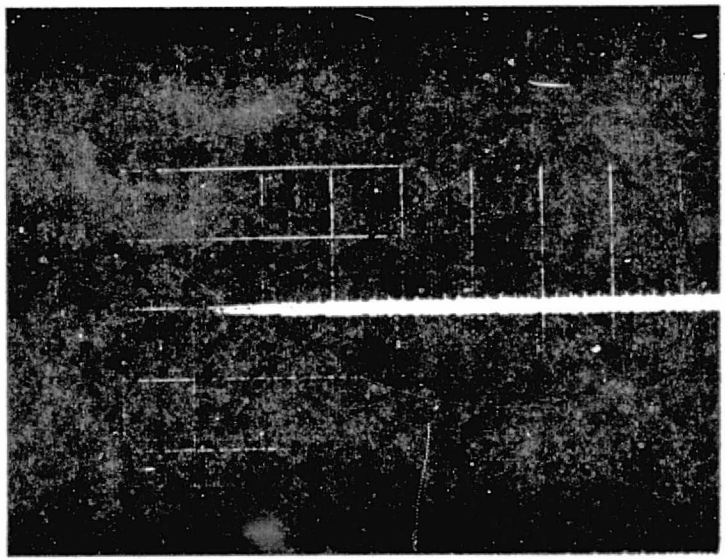

TEST CONDITIONS

VERT .005 V /DIV

HORIZ 10 mS /DIV

LOAD NONE

INPUT SHORTED

TEMP _____ °C

PROBE x1

NOISE

#3

NOISE

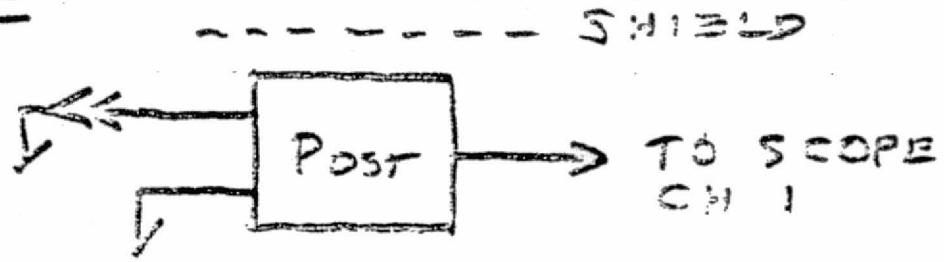

SUPPLY +10.00 V
-10.00 V

JOB NO. 1361-2679 OSCILLOSCOPE MODEL

ATP NO. _____ 545A

CONTRACT _____ SERIAL NO. POST AMP 1 BREAD BOARD

ENGINEER E PAYSON

TECHNICIAN G N COLE

DATE 5 MAR 75

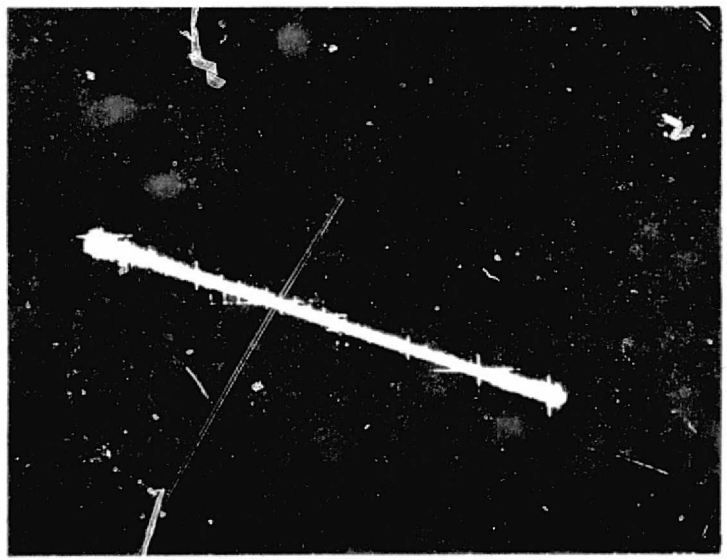

TEST CONDITIONS

VERT 5V /DIV

HORIZ EXT /DIV

LOAD NONE

INPUT SINE

TEMP _____ °C

PROBE LINEARITY

14 HZ INPUT

#4

G. N COLE
E. PAYSEN
SMD: 75

LINEARITY

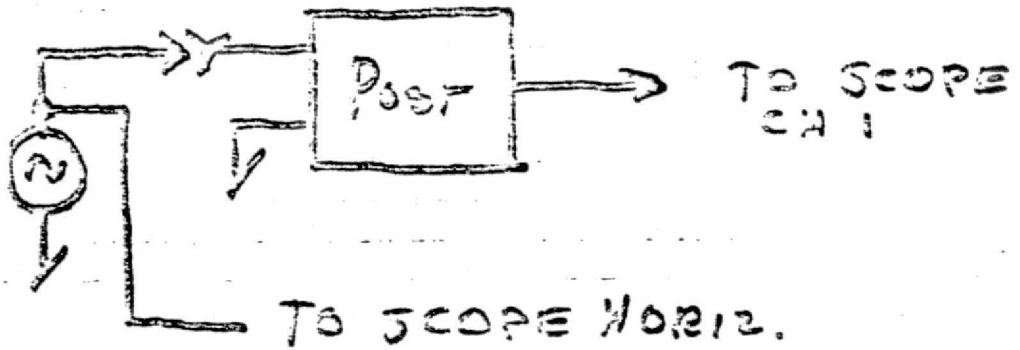

ADJUST FREQUENCY FOR ZERO PHASE SHIFT BEFORE TAKING PICTURE.

SUPPLY +10.00 V
-10.00 V

JOB NO. 1361-2679 OSCILLOSCOPE MODEL

ATP NO. _____ 545A

CONTRACT _____ SERIAL NO. POST AMP #1 BREAD BOARD

ENGINEER E PAYSON

TECHNICIAN G N COLE

DATE 5 MAR 75

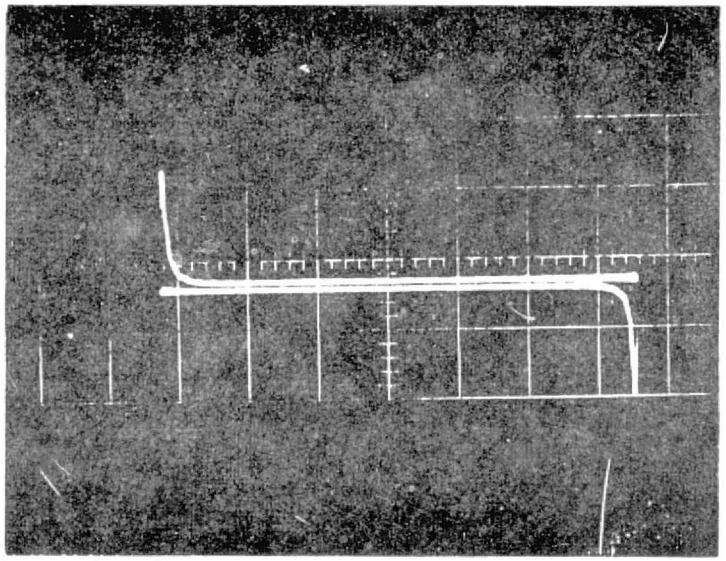

DESCRIPTION TRANSIENT RESPONSE 1 HZ

TEST CONDITIONS

VERT 5V /DIV

HORIZ EXT /DIV

LOAD _____

INPUT SQ WAVE

TEMP _____ °C

PROBE _____

#5

TRANSIENT RESPONSE

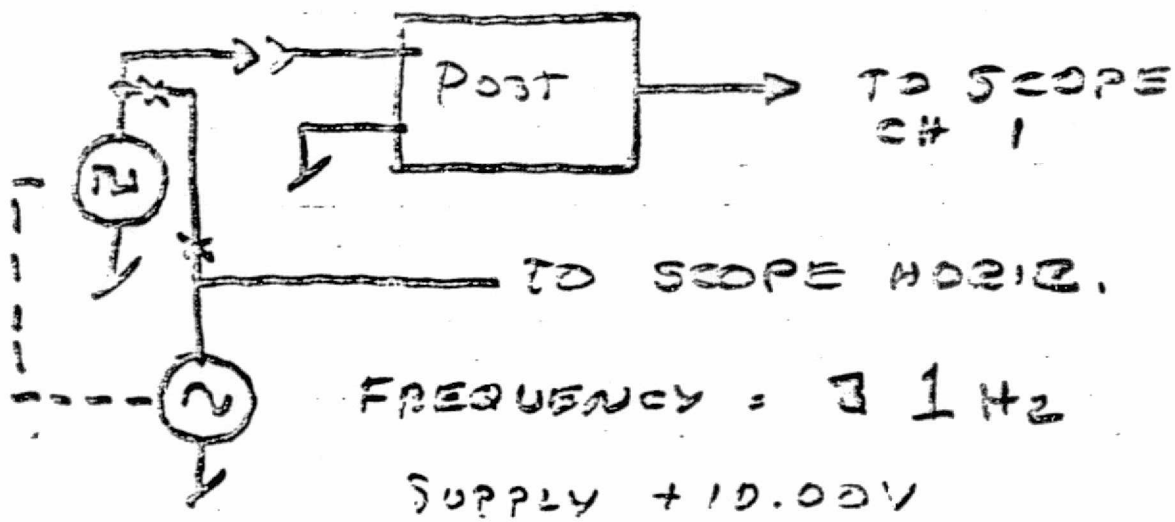

JOB NO. 1361-2679 OSCILLOSCOPE MODEL

ATP NO. _____ 545A

CONTRACT _____ SERIAL NO. POST AMP #1 BREAD BOARD

ENGINEER E PAYSON

TECHNICIAN G N COLE

DATE 5 MAR 75

TEST CONDITIONS

VERT 5 V /DIV

HORIZ EXT /DIV

LOAD _____

INPUT SQ WAVE

TEMP _____ °C

PROBE _____

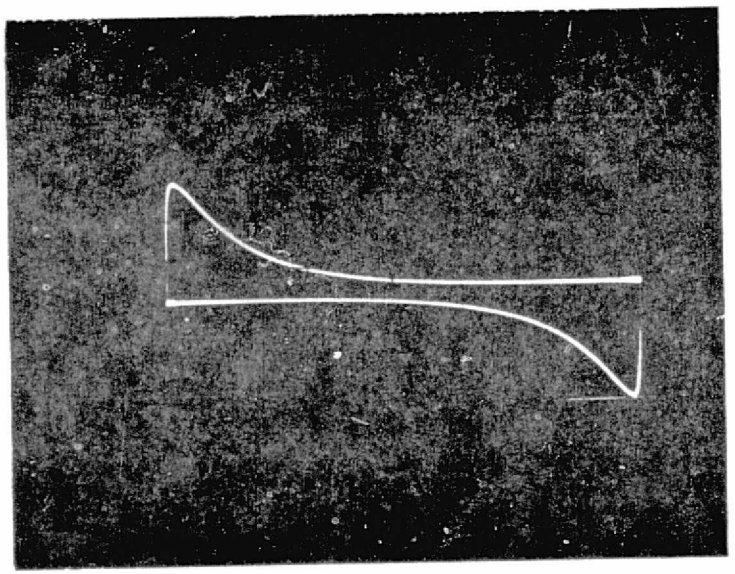

DESCRIPTION TRANSIENT RESPONSE
4 Hz

#6

TRANSIENT RESPONSE

SAME AS P 15

FREQUENCY = 3 Hz

JOB NO. 1361-2679 OSCILLOSCOPE MODEL

ATP NO. _____ 545A

CONTRACT _____ SERIAL NO. POST AMP #1 BREAD BOARED

ENGINEER E PAYSON

TECHNICIAN G N COLE

DATE 5 MAR 75

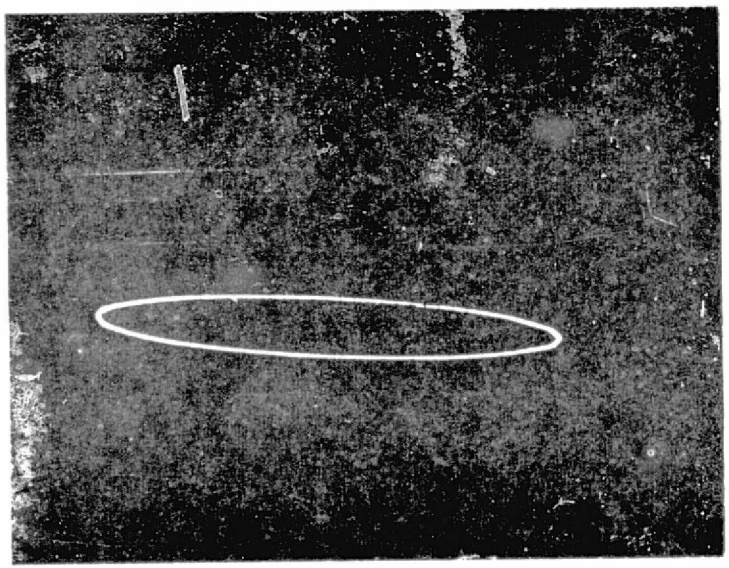

DESCRIPTION 3 HZ SINE FREQ/PHASE RESPONSE

TEST CONDITIONS

VERT 5V /DIV

HORIZ EXT /DIV

LOAD _____

INPUT SINE WAVE

TEMP _____ °C

PROBE _____

#7

PHASE / FREQUENCY RESPONSE

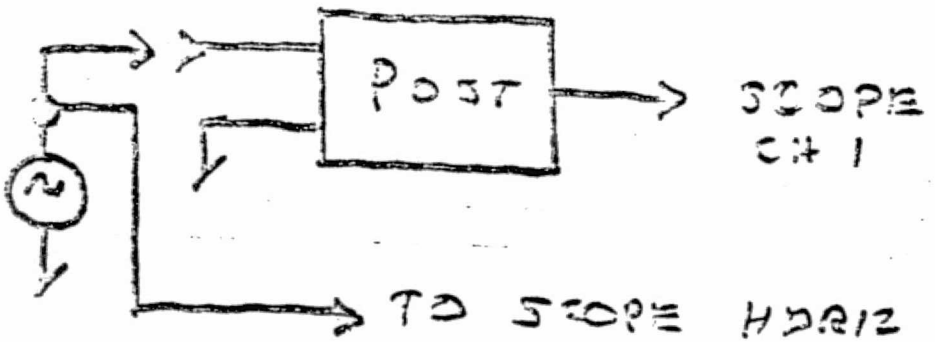

SUPPLY +10.00 V
-10.00 V

FREQUENCY 3 Hz SINE

FREQUENCY RESPONSE DATA

BREAD BOARD #1
PRE AMP

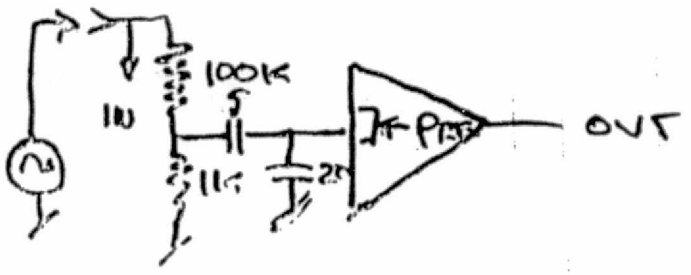

~~V_{IN}~~ V_{OUT}

$V_{IN}' = V_{IN}/\approx 500$

F	V_{IN}	V_{OUT}	$V_{OUT} \cdot V_{IN}^{-1}$ dB
1	$1V_{P-P}$	32 mV_{P-P}	
3		80	
5		110	
7		140	
8		150 mV	
9			
10		160 mV	
11			
12		150	
13			
14		140	
15		130	
17		120	
19		115	
20		90	
25		80	
30		424	
50		2.8	
100			
2	$1V_{P-P}$	50	

DEMOD TEST .1 - .1-3R

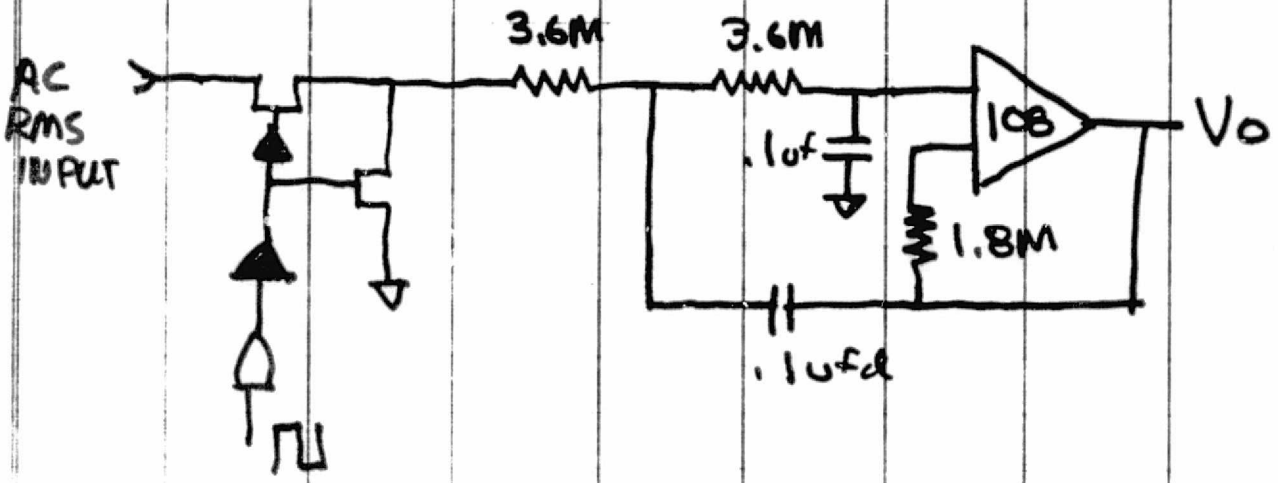

PURPOSE: 1. TO MEASURE OUTPUT WITH RESPECT TO INPUT FREQUENCY.
$V_{IN} = K \cdot 1V_{RMS}$

2. TO MEASURE OUTPUT RIPPLE WITH RESPECT TO INPUT FREQUENCY.
$V_{IN} = K = 1V_{RMS}$

EQUIPMENT TEK 535A - D PLUG IN
BECKMAN 9010
SD DUM
±15V SUPPLIES

DEMOD .1-.1-3R

DC OUTPUT VS FREQUENCY

F_{IN}	DVM	V_{IN}	V_{O} DC
10 Hz	1.089	3V P-P	.5176
20 Hz		1.004	.4700
30 Hz		1.004	.4678
50 Hz		1.003	.4661
100 Hz		1.001	.4647
500 Hz		1.001	.4641
1000 Hz		1.002	.4640

AC RIPPLE OUTPUT VS FREQUENCY

F_{IN}		V_{IN}	V_{O} AC (10^{-3} V)
10 Hz	1.089	3V P-P	1.26
20 Hz		1.004	.59
30 Hz		1.004	.53
50 Hz		1.003	.57
100 Hz		1.001	.79
500 Hz		1.001	3.07
1000 Hz		1.002	6.14

	DC OUT VS FREQUENCY		D_{COUT}	A_{COUT} (10^{-3})
(RETAKE)	10 Hz	1.001	.4762	1.3

G N COLE
E PAYSON
18 FEB 75

DEMOD TEST .69 - .068

PURPOSE: TO MEASURE OUTPUT SENSITIVITY TO INPUT FREQUENCY.
FREQUENCY RANGE: 10-1000 Hz
VOLTAGE INPUT: 3.V P-P

TEST SET UP:-

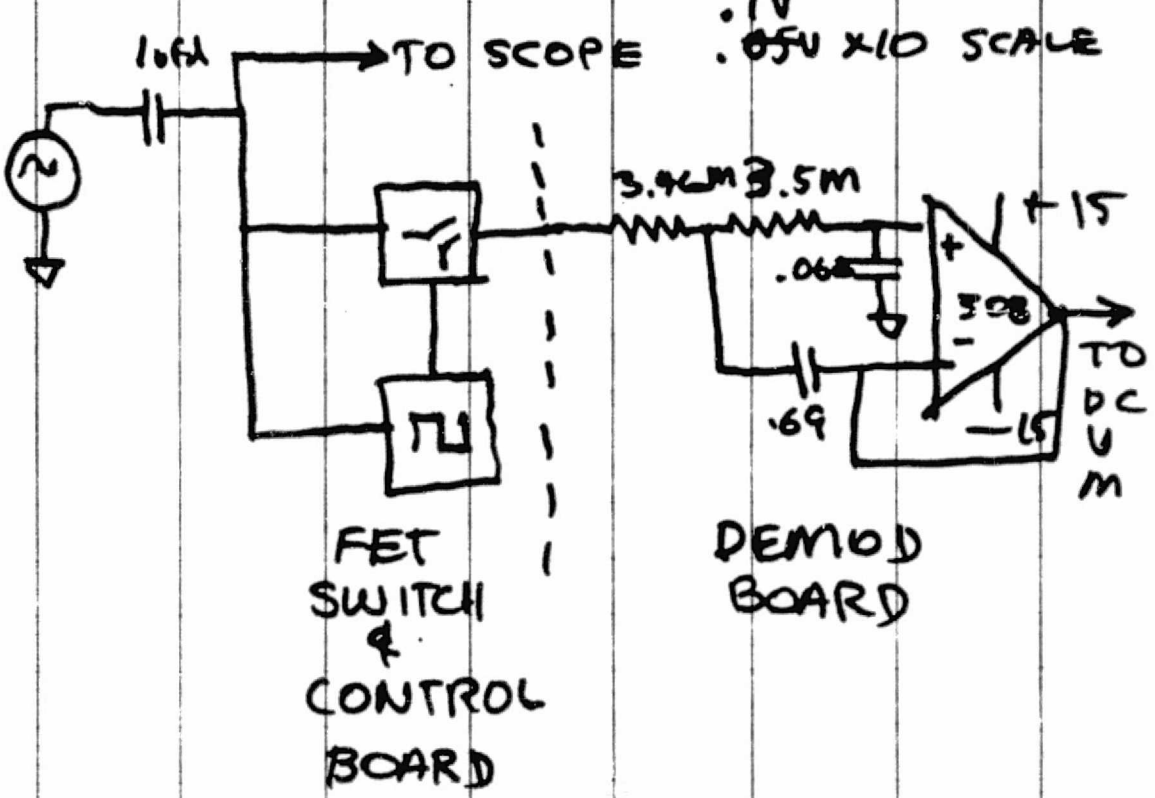

EQUIPMENT:

TEK 535A - D
BECKMAN 9010
SD DVM
±15V SUPPLIES

G N COLE
E PAYSON
18 FEB 75

DEMOD .69-.068

RESPONSE: DC OUTPUT VS. FREQUENCY

	INPUT VOLTS RMS	DC OUTPUT
10 Hz	1.0	-.530
20 Hz	1.0	-.520
30 Hz	1.0	-.516
50 Hz	1.0	-.513
70 Hz	1.0	-.510
100 Hz	1.0	-.507
200 Hz	1.0	-.501
300 Hz	1.0	-.501
400 Hz	1.0	-.501
500 Hz	1.0	-.5020
1000 Hz	(3V P-P)	-.5025

RESPONSE: AC RIPPLE RMS VS FREQ

10 Hz	11.5V ~~P~~ V P P	. ~~.00~~ .14
20 Hz	15V P-P	. ~~.44~~ .22
30 Hz	15V	. ~~.34~~ .13
50 Hz	15V	. ~~.30~~ .13
70 Hz	15V	. ~~.30~~ .13
100 Hz	15V	. .13
200 Hz	15V	. .13
300 Hz	15V	. .13
400 Hz	15V	. .13
500 Hz	15V	. .13
1000 Hz	15V	. .13
	INPUT P-P	AC AN OUT SD DVM $\times 10^{-3}$

AMBIENT DC NOISE $.13 \times 10^{-3}$ V AT OUTPUT WITH BECKMAN 9010 TURNED OFF.

AC Response Low Freq

	V_{IN} P-P	V_{OUT} P-P
Hz		
1 Hz	180 mV	40 mV
3 Hz	400 mV	10 mV
6 Hz	200 mV	6 mV
10 Hz	1100 mV	3 mV

G COLE
E PAYSON
[redacted]-18-19-FEB75

OVEN TEST DEMOD

.69-.069

PURPOSE: TO TEST OFFSET AND STABILITY OVER 0-50°C RANGE

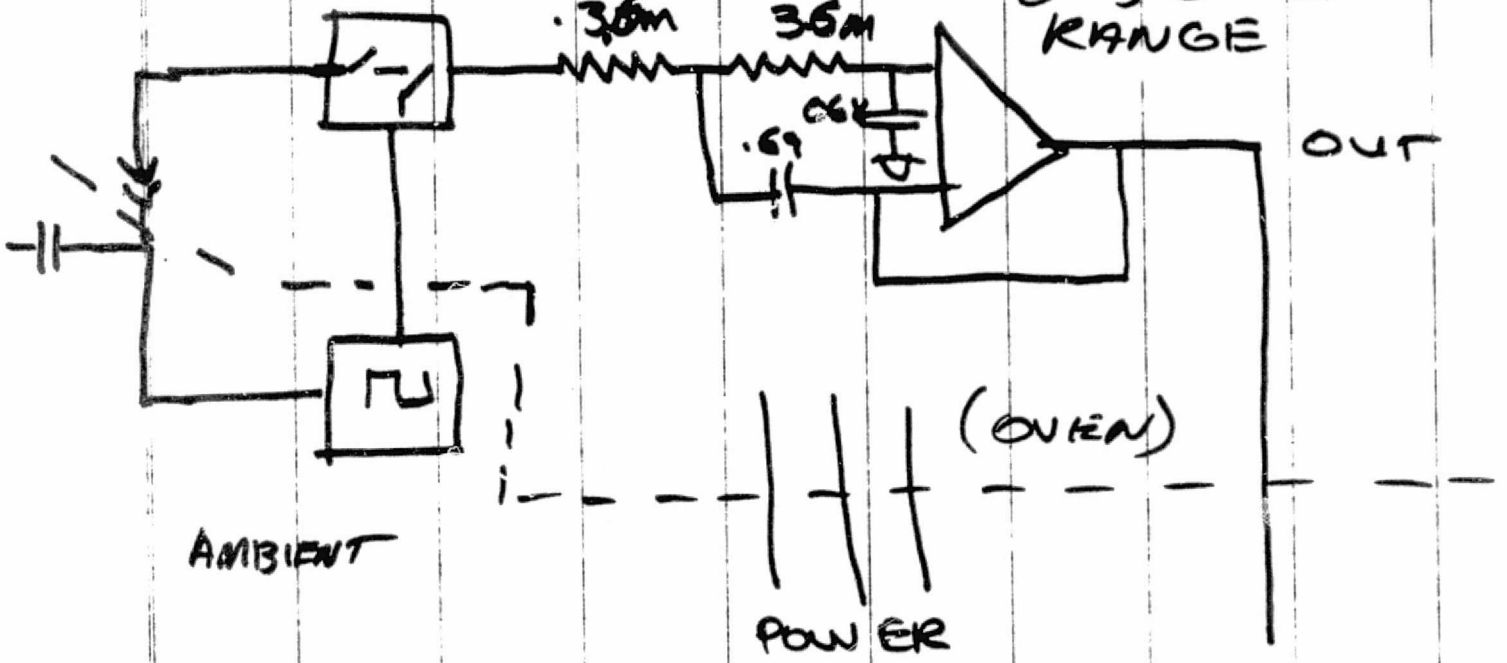

TEST EQUIPMENT
TEK 535A - DPLUG IN
BECKMAN 9010
±15V SUPPLIES
S.D. DVM -
OVEN 0-50°C ± 1°C

DATA:

INPUT SHORTED (SWITCHER ON)

T °C	DC OUTPUT mV	AC RIPPLE 10^{-3}
25 °C	16.2	0.1
15 °C	22.0	0.12
5°	22.3	0.10
25°	15.4	0.02
35°	13.9	.07
45°	11.0	.07
25°	17.2	0.1

INPUT OPERATING 1V RMS - 3V PP

T °C	DC OUTPUT 5	10	100	AC	RIPPLE 10^{-3} 5	10	100
25	.528	.512	.483	1.02	.26	.1	
15	.529	.508	.481	1.1	.24	.1	
5	.544	.517	.489	1.0	.32	.0	
25	.514	.501	.473	1.01	.24	.01	
35	.534	518	482	105	.28	.05	
45	.580	.503	.469	1.00	.26	.09	
25	534	504	470	1.05	.25	.1	

SUSPECT THIS DATA AS I AM NOT ABLE TO JUDGE 3V P-P ON SCOPE WITH ENOUGH ACCURACY

Human Test Jig #312

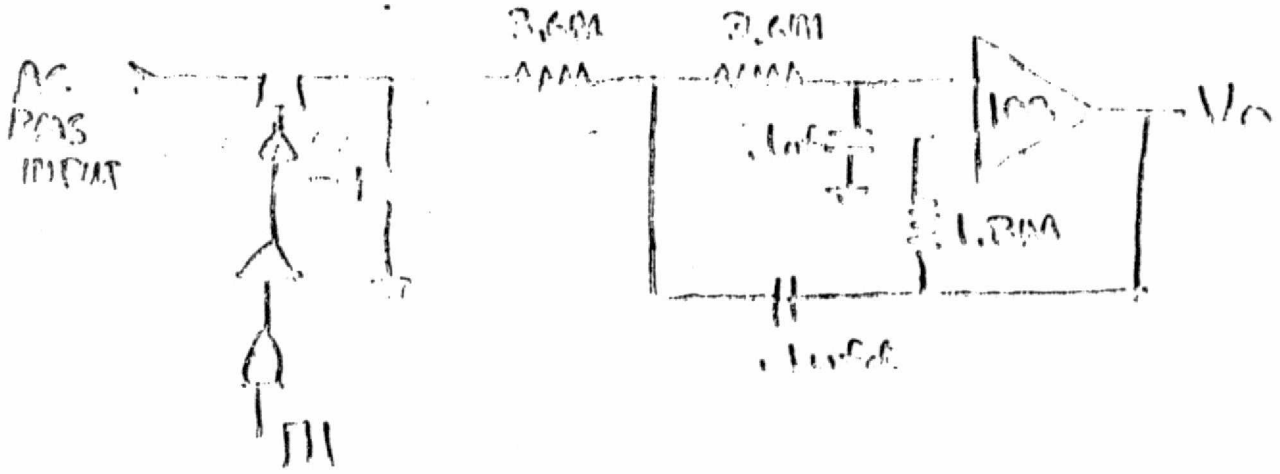

Purpose: 1. To Measure output with respect to input frequency.
Vin = K = 1V RMS

2. To Measure output ripple with respect to input frequency.
Vin = K = 1V RMS

Equipment: TEK 5854 - 2 Plug In
Programmable
5 D Runs
Test Supplies

- 2 -

Demod 1:1-BR

DC Output vs Frequency

f_m	Pin	V_{in}	V_{DC}
10Hz	1003	3V p-p	.5176
20Hz		1.004	.4700
30Hz		1.004	.4678
50Hz		1.003	.4661
100Hz		1.001	.4647
500Hz		1.001	.4641
1000Hz		1.002	.4640

DC Ripple Output vs Frequency

f_m		V_{in}	V_{DC} (ripple)
10Hz	1003	3V p-p	1.26
20Hz		1.004	.59
30Hz		1.004	.53
50Hz		1.003	.57
100Hz		1.001	.79
500Hz		1.001	3.07
1000Hz		1.002	6.14

				(10^{-3})
	DC out vs	Frequency	Power	Amount
(Reduce)	10Hz	1.001	.4762	1.3

Demod Test Jig

Purpose: To measure output sensitivity to input frequency.
Frequency Range: 10-1000 Hz.
Voltage input: 3.V P-P

Test Set up:

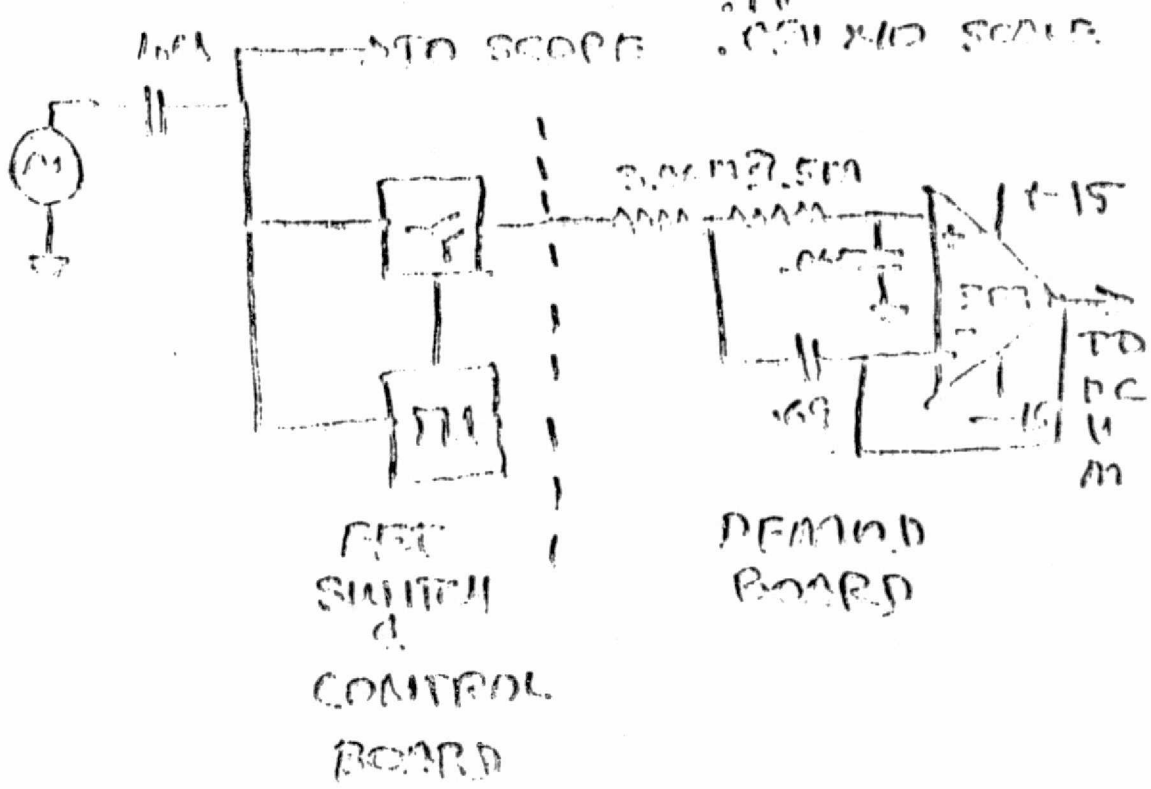

Equipment:

Tek 535A - P
Rectron 2010
S.D. DVM
±15V Supplies

Demod .69 - .063

Response: DC output vs. Input Volts p-p

	Input Volts p-p	DC output
10 Hz.	1.0	-.530
20 Hz.	1.0	-.520
30 Hz.	1.0	-.516
50 Hz.	1.0	-.513
70 Hz.	1.0	-.510
100 Hz.	1.0	-.507
200 Hz.	1.0	-.501
300 Hz.	1.0	-.501
400 Hz.	1.0	-.501
500 Hz.	1.0	-.500
1000 Hz.	(3M p-p)	-.500

Response: DC ripple vs. Input

	Input p-p	DC ripple
10 Hz.	15V p-p	.[illegible]
20 Hz.	15V p-p	.[illegible]
30 Hz.	15V	.[illegible]
50 Hz.	15V	.[illegible]
70 Hz.	15V	.[illegible]
100 Hz.	15V	.13
200 Hz.	15V	.13
300 Hz.	15V	.13
400 Hz.	15V	.13
500 Hz.	15V	.13
1000 Hz.	15V	.13

ORIGINAL PAGE IS OF POOR QUALITY

Input p-p

DC ripple

Ambient DC noise .15 mV p-p at output with precision pots turned CCW.

AC Response Low Pass

Hz	V_{in} P-P	V_{out} P-P
1 Hz	180 mV	410 mV
3 Hz	200 mV	10 mV
6 Hz	200 mV	6 mV
10 Hz	1100 mV	3 mV

Quad Temp Runner

.69 - .069

Purpose: To test offset and stability over 0-500°C range

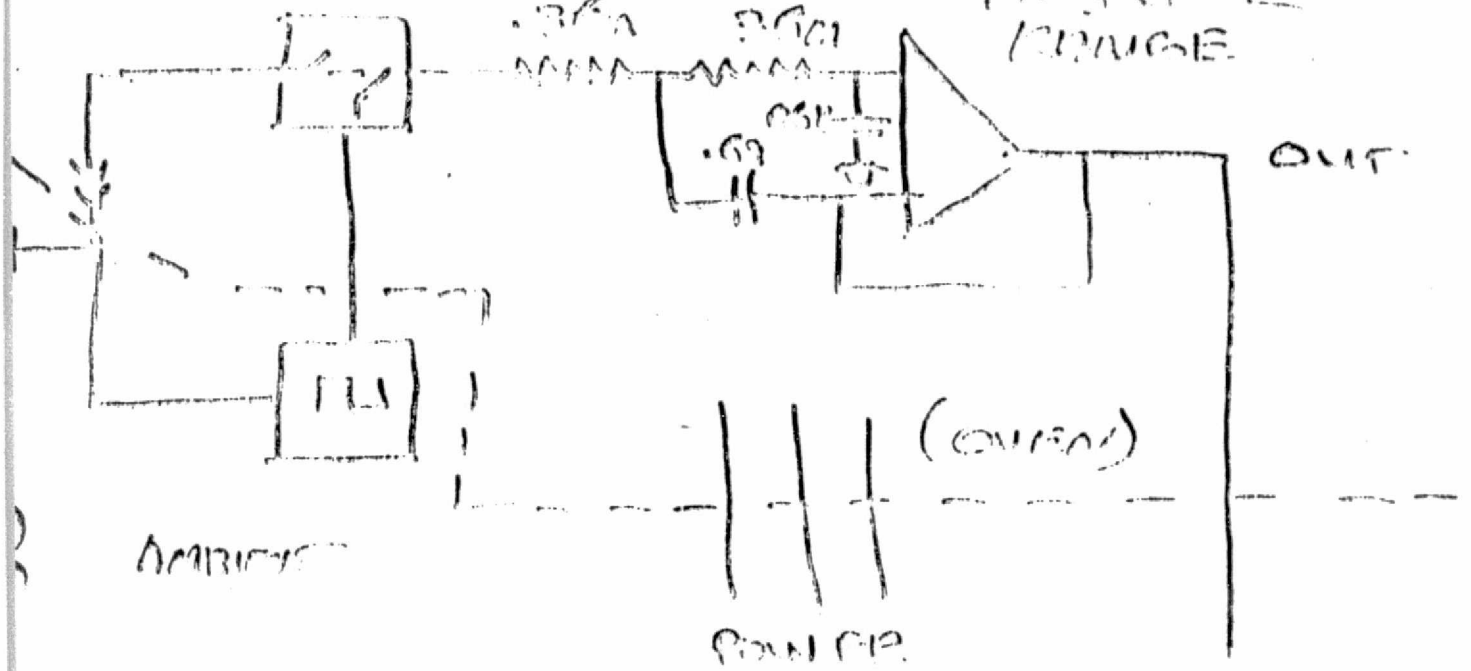

Test Equipment:

Heat Gun - Range in
Burning Bird
+ 15V Supplies
D.V.M.
Oven 0 - 500°C +/- 1°C

Data:

Input Specified
(Supplied by)

T °C	DC output mV	AC Ripple
25°C	16.2	0.1
15°C	22.0	0.12
5°	22.3	0.10
25°	15.4	0.03
35°	13.9	.07
45°	11.0	.05
25°	12.2	0.1

Input Operating [illegible] - SUPP

T °C	DC output 5	10	100	AC	Ripple (0	
25	.528	.512	.483	1.02	.20	.1
15	.529	.503	.481	1.1	.24	.1
5	.544	.517	.479	1.0	.32	.0
25	.514	.501	.477	1.01	.24	.01
35	.534	.518	.483	1.05	.28	.05
45	.540	.508	.481	1.03	.24	.03
25	.534	.501	.480	1.05	.25	.01

Subtract this data as!
Do not come to surge
[illegible] [illegible]

APPENDIX B

DESIGN NOTES

Beckman INSTRUMENTS, INC.	DESIGN NOTES	DN
TITLE Half Wave Filter	ANALYSIS	SHT 1 OF 7
	ORIGINATOR S & P	REV
	DATE 1-16-75	APPR

I. Transfer Function (No offset Voltage)

Fig 1

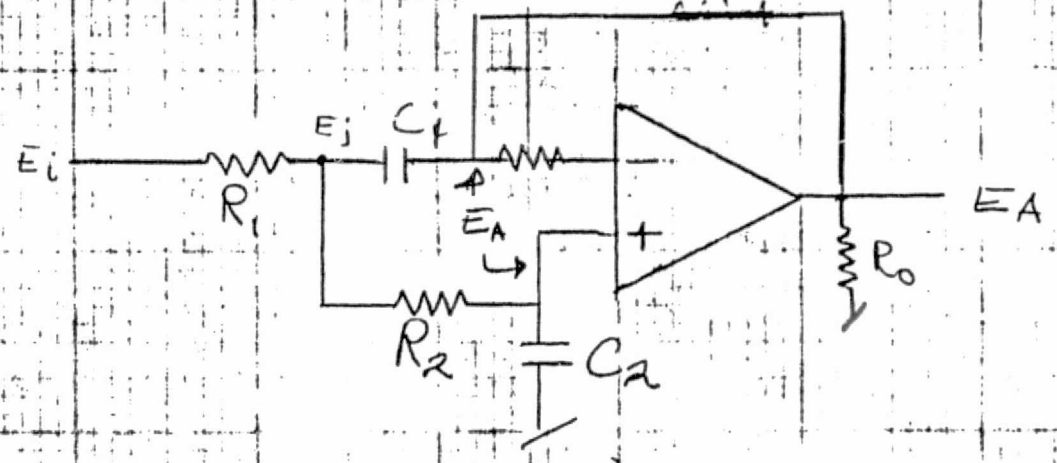

A) $$\frac{E_i' - E_j}{R_1} + \frac{E_A - E_j}{R_2} + \frac{E_A' - E_j''}{1/SC_1} = 0$$

for $R_1 = R_2$

$$E_A = \left[\frac{2 + SC_1R}{1 + SC_1R}\right] - \frac{E_i}{1 + SC_1R}$$

B) $$\frac{E_j - E_A}{R_2} - E_A(SC_2) = 0$$

C) $$(E_j - E_A)(SC_1) - \frac{E_A}{R_o} = 0$$

from B

$$E_j = E_A + E_A SC_2R_2$$

$$E_j = E_A[1 + SC_2R]$$

Substitute Into A)

$$E_A = \frac{E_A[1+SC_2R][2+SC_1R]}{1+SC_1R} - \frac{E_i}{1+SC_1R}$$

$$E_A\left[\frac{1+SC_1R-(2+2SC_2R+SC_1R+S^2C_1C_2R)}{1+SC_1R}\right] = \frac{-E_i}{1+SCR}$$

$$\frac{E_A}{E_i} = \frac{-1}{-1-2SC_2R-S^2C_1C_2R^2}$$

Gives

Eq 1 $$\frac{E_A}{E_i} = \frac{1/R^2C_1C_2}{S^2+2S/C_1R+1/R^2C_1C_2}$$

$$S = j\omega = j2\pi f$$

II Wave Equation

Assumption: Input wave approximates a sin wave

Fourier ½ wave equation

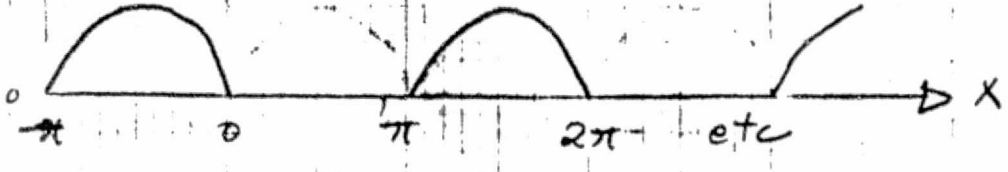

$$f(x) = \sin x, \quad \text{for } 0 < x < \pi$$

$$0, \quad \text{for } -\pi < x < 0$$

Beckman INSTRUMENTS, INC.	DESIGN NOTES	DN
TITLE	ANALYSIS	SHT 3 OF 7
Half Wave Equat. [Filter]	ORIGINATOR LLP	REV
	DATE 1-16-75	APPR

Fourier Equations

$$a_0 = \frac{1}{\pi}\int_{-\pi}^{\pi} f(x)\,dx$$

$$a_n = \frac{1}{\pi}\int_{-\pi}^{\pi} f(x)\cos nx\,dx$$

$$b_n = \frac{1}{\pi}\int_{-\pi}^{\pi} f(x)\sin nx\,dx$$

where

$$F(x) = \frac{a_0}{2} + \sum_{n=1}^{\infty}\left[a_n \cos nx + b_n \sin nx\right]$$

Now For $-\pi < x < 0$

$a_n = 0$
$b_n = 0$
$a_0 = 0$
} since $f(x) = 0$

Now For $+0 < x < \pi$

$$a_0 = \frac{1}{\pi}\int_0^{\pi} \sin(x+\pi) = -\frac{1}{\pi}\left[\cos x\right]_0^{\pi} = \frac{2}{\pi}$$

$\sin x$ or $\sin x$.

$$a_n = \frac{1}{\pi}\int_0^{\pi} f(x)\cos nx\,dx$$

from $\sin x \cos nx = \dfrac{\sin x(1+n) + \sin x(1-n)}{2}$

$$a_n = \frac{1}{\pi}\int_0^{\pi} \frac{\sin(1+n)x + \sin(1-n)x}{2}\,dx$$

$$= \frac{1}{2\pi}\left[\frac{-\cos(1+n)x}{1+n} + \frac{\cos(1-n)x}{1-n}\right]_0^{\pi}$$

$$= \frac{-1}{2\pi}\left[\frac{\cos(1+n)\pi}{1+n} + \frac{\cos(1-n)\pi}{1-n} - \left(\frac{1}{1+n} + \frac{1}{1+n}\right)\right]$$

$$a_n = \begin{cases} n \text{ odd} & \frac{1}{1+n} + \frac{1}{1-n} - \left[\frac{1}{1+n} + \frac{1}{1-n}\right]; \text{ Gives } a_n = 0 \\ n \text{ even} & \frac{-1}{1+n} - \frac{1}{1-n} - \left[\frac{1}{1+n} + \frac{1}{1-n}\right]; \frac{2}{\pi(1-n)^2} \end{cases}$$

$$a_n = \frac{2}{\pi(1-n)^2} \quad \text{for } n \text{ even}$$

$$b_n = \frac{1}{\pi}\int_0^{\pi} \sin x \sin nx\,dx$$

From $\sin x \sin nx = \dfrac{\cos(1-n)x - \cos(1+n)x}{2}$

$$= \frac{1}{2\pi}\left[\frac{\sin(1-n)x}{1-n} - \frac{\sin(1+n)x}{1+n}\right]_0^{\pi} = 0$$

Except for b_1

$$b_1 = \frac{1}{2}$$

ORIGINAL PAGE IS OF POOR QUALITY

Beckman INSTRUMENTS, INC.	DESIGN NOTES	DN
TITLE	ANALYSIS	SHT 5 OF 7
Half wave Eq. [Filter]	ORIGINATOR LZP	REV
	DATE 1-16-75	APPR

Refering to pg 3 for $f(x)$

$$f(x) = \frac{1}{\pi} + \frac{1}{2}\sin x - \frac{2}{3\pi}\cos 2x - \frac{2}{15\pi}\cos 4x - \frac{2}{105\pi}\cos 6x - \ldots$$

For voltage Transfer wave Equation

Eq 2
$$u(t) = \frac{E}{\pi} + \frac{E}{2}\sin \omega t - \frac{2E}{\pi}\left[\frac{1}{3}\cos 2\omega t + \frac{1}{15}\cos 4\omega t + \ldots\right]$$

III Input vs output Filter

A) Refer pg 1 fig 1.

$R_1 = R_2 = 3.79$ MΩ

$C_1 = C_2 = .1$ μfd

$\omega = 2\pi f = 20\pi$; for $f = 10$ Hz

B) Assumption:

① It is obvious from Eq 2 how fast this equat. drops of therefore I will approximate this equation by the 1st three terms

Eq 3
$$u(t)^* = \frac{E}{\pi}\left[1 + \frac{\pi}{2}\sin \omega t - \frac{2}{3}\cos 2\omega t\right]$$

Beckman INSTRUMENTS, INC.	DESIGN NOTES	DN
TITLE Half Wave Eq. [Filter]	ANALYSIS	SHT 6 OF 7
	ORIGINATOR EZP	REV
	DATE 1-16-75	APPR

Substituting Eq 3 into Eq. 1 we obtain
let M(wt) be new Txfer function

$$M(\omega t) = \frac{E_0}{\pi}\left[1 + \frac{\pi}{2}\sin\omega t \left\{ \frac{\frac{1}{R^2C_1C_2}}{-\omega^2 + j\omega\left(\frac{2}{C_1R}\right) + \frac{1}{R^2C_1C_2}} \right\} - \frac{2}{3}\cos 2[\omega t] \left\{ \frac{\frac{1}{R^2C_1C_2}}{-[2\omega]^2 + j\,2\omega\left(\frac{2}{C_1R}\right) + \frac{1}{R^2C_1C_2}} \right\}\right]$$

c) Using Values III A we can simplify
*Simplifications Relate to [w] or [2w]

$$w^2 = 3948$$

$$j\omega\frac{2}{C_1R} = j\,331$$

$$\frac{1}{R^2C_1C_2} = 6.96$$

D) let Eq 1 For our purposes

$$\frac{E_A}{E_L} \cong \frac{-1}{w^2 R^2 C_1 C_2} = \begin{cases} -.00176 & \text{For } w = 20\pi \\ -.0004408 & \text{For } 2w = 40\pi \end{cases}$$

Beckman INSTRUMENTS, INC.	DESIGN NOTES	DN
TITLE Half wave Eq. Filter	ANALYSIS	SHT 7 OF 7
	ORIGINATOR LLP	REV
	DATE 1-16-75	APPR

E.) To Find output voltage

$$M(\omega t) = \frac{E_0}{\pi}\left[1 + \frac{\pi}{2}\sin 20\pi t\,(.00176) - \frac{2}{3}\cos 40\pi t\,(.0004408)\right]$$

① @ $M(\omega t)_{MAX}$ " $t = 0, 2\pi \ldots$

$$= \frac{E_0}{\pi}\left[1.000293\right] = \boxed{.31840\ E_0}$$

② @ $M(\omega t)_{MIN}$ $t = \pi/2, \frac{5\pi}{2}, \ldots$

$$= \frac{E_0}{\pi}\left[.997235\right] = \boxed{.31742\ E_0}$$

F) This Relates to a ripple of

$\boxed{.30570}$

APPENDIX C

DETECTOR PERFORMANCE DATA SHEETS

P1-40/70, P2-40, P4-40/70 CALIBRATION WORK SHEET

Date 6/6/75

P.O. No. _____

Name Carlos Roundy

Customer Beckman

Model No. P14-7102

Serial No. 2 Element B

Wavelength of source (λ) 632.8 nm

Optics used (effect on R_V) _____

Resistor feedback (___) load (✓) 10" ohms

Bandwidth (-3db pts) _____, Risetime (10-90%) _____

f (Hz)	~~Pin (mW)~~	Vout (mV)	R_V (V/W)	E_n uV/√Hz	NEP (W/√Hz)
1					
3					
10	7.5uW	7.8	1040	.40	3.8×10^{-10}
40					
100					
300					
1K					